Preparación y caracterización de espumas multifuncionales a base de nanocompuestos de poliolefinas.

Memoria realizada por: Marcelo de Sousa Pais Antunes

Dirigida por: Profesor José Ignacio Velasco Perero

Memoria presentada para optar al grado de Doctor por la Universidad Politécnica de Cataluña

UNIVERSITAT POLITÈCNICA DE CATALUNYA

Departament de Ciència dels Materials i Enginyeria Metal.lúrgica

Centre Català del Plàstic

Marcelo de Sousa Pais Antunes
Terrassa, Julio de 2010

4.4. Espumas de polipropileno cargado con hidróxido de magnesio.

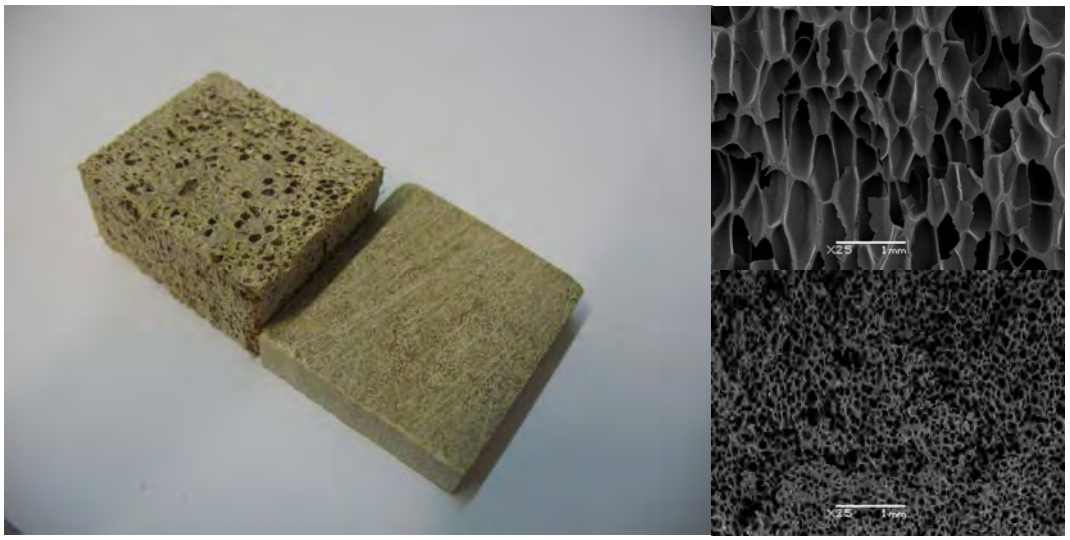

4.4.1. Justificación y objetivos.

Una de las principales características de los materiales plásticos de base poliolefínica reside en su pobre resistencia al fuego, limitando sus aplicaciones en sectores como el de la construcción o automoción, donde se han venido implementando normativas cada vez más estrictas. Así, y debido a las limitaciones impuestas a los sistemas halogenados retardantes de llama comúnmente empleados en matrices de poliolefina [20], se ha vuelto a considerar la estrategia de incorporar altos contenidos de refuerzos inorgánicos como hidróxidos metálicos (hidróxido de aluminio o magnesio), que se descomponen endotérmicamente liberando agua, de esa manera limitando la propagación de la llama por un mecanismo combinado de absorción de calor y extinción de la misma [21]. De entre estos dos hidróxidos, el de magnesio presenta la ventaja de una superior temperatura de descomposición (≈ 340 ºC frente a los 200 ºC del hidróxido de aluminio – véase sección 3.1.3 del capítulo 3), permitiendo su incorporación por técnicas de mezclado en fundido en polipropileno (punto de fusión en torno a los 160-165 ºC y temperaturas de procesado cercanas a los 200 ºC). Sin embargo, y debido a su menor eficacia como retardante de llama frente a los sistemas halogenados mencionados anteriormente, se necesitan de muy elevados porcentajes de estos hidróxidos para poder llegar a alcanzar los valores mínimos requeridos por las normativas. Esta situación conlleva a dificultades de procesado y muchas veces costes superiores debido a la necesidad de tratar superficialmente las partículas o de usar aditivos de proceso tales como lubricantes.

Teniendo en cuenta que es la fracción volumétrica de polímero la que contribuye a la combustibilidad del composite, se podría usar la espumación como estrategia de disminución de la misma en conjunto con la incorporación de elevados porcentajes de refuerzos minerales [22], al mismo tiempo que posibilitaría una reducción de costes asociados a su procesado, ya que se ha demostrado con anterioridad que la espumación promueve una superior dispersión de las partículas presentes en el material, de esa manera incrementando su funcionalidad.

Por todo ello, y considerando las características de las espumas de PP presentadas en la presente memoria de tesis, esto es, espumas rígidas de densidad media-alta pensadas sobre todo para aplicaciones de tipo estructural, se creyó conveniente estudiar el efecto que tendría sobre las mismas la incorporación de elevados

porcentajes de hidróxido de magnesio (50 y 70% en peso) con el objetivo de desarrollar nuevos materiales que fueran simultáneamente ligeros (controlando el grado de expansión de la fracción polimérica) y altamente cargados (para incrementar su resistencia al fuego) para aplicaciones donde pueda resultar interesante la combinación de ambas características, como por ejemplo en el sector de la construcción.

Tal como para las demás espumas en base PP analizadas hasta este momento, el estudio de estas espumas con elevados porcentajes de hidróxido de magnesio (50 y 70% en peso) ha sido llevado a cabo considerando una primera publicación donde se incluyen los principales resultados de la preparación de los compuestos, posterior espumación química por compresión e influencia tanto del proceso como de la presencia de los elevados porcentajes de hidróxido en la estructura celular final. En particular, y considerando en determinados casos la formación de estructuras celulares altamente anisotrópicas para los superiores grados de expansión, se analizó en detalle la microestructura de las espumas (características cristalinas y morfología de los compuestos espumados) y su influencia en el comportamiento térmico-mecánico-dinámico y de resistencia al fuego.

En la publicación incluida en la sección anterior y titulada *Heat transfer of mineral-filled polypropylene foams* se extiende la caracterización de estos materiales celulares al estudio de la conductividad térmica. En particular, la estructura celular altamente anisotrópica de algunos de estos materiales induce una orientación preferencial de las partículas de hidróxido, con interesantes consecuencias en las propiedades finales de conductividad térmica, con las espumas presentando considerables anisotropías térmicas.

4.4.2. Resumen de los trabajos y conclusiones.

El artículo titulado ***Characterization of highly filled magnesium hydroxide-polypropylene composite foams***, aceptado para publicación en la revista **Journal of Cellular Plastics**, se centra en el estudio de los efectos combinados de la espumación química por compresión y presencia de elevados porcentajes de partículas inorgánicas micrométricas en la microestructura y respectivas propiedades térmico-mecánico-dinámicas y comportamiento frente a la llama de espumas de PP con elevados porcentajes de hidróxido de magnesio, en particular un 50 y un 70% en peso.

Los principales resultados recopilados en esta publicación pueden subdividirse en el estudio de la estructura celular y microestructura de los compuestos celulares, caracterización de las propiedades térmico-mecánico-dinámicas y resultados preliminares sobre su comportamiento al fuego, al haber sido ideadas para aplicaciones donde se requiere, junto con las ventajas de ligereza y buen balance de propiedades específicas, una buena resistencia al fuego.

En lo que toca a la caracterización de la estructura celular, las espumas con superiores porcentajes de hidróxido no sólo presentan tamaños de celda considerablemente más pequeños (≈ 180 μm) que las de 50% (tamaños de celda cerca de 4 veces superiores), sino igualmente una estructura celular más isotrópica e independiente del grado de expansión. Por el contrario, la estructura celular de las espumas con un 50% de hidróxido resultó crecientemente anisotrópica al expandir cada vez más el material, alcanzando valores del grado de anisotropía (*AR*) superiores a 3 para las espumas de densidad relativa 0.17 (0.211 g/cm^3).

En vista a la anisotropía celular generada durante la espumación, especialmente para las espumas con un 50% de $Mg(OH)_2$ de elevado grado de expansión, se evaluaron tanto las orientaciones de las partículas como de la fracción cristalina de la matriz polimérica por difracción de rayos-X. Tanto si se considera la orientación de las partículas de hidróxido como la del cristal α-PP del polímero, las espumas presentan anisotropías crecientes en la dirección de crecimiento de la espuma al introducir superiores fracciones de gas (superiores grados de expansión). Esta combinación de anisotropía tanto de las partículas como de los cristales de polímero resultó en propiedades térmico-mecánico-dinámicas dependientes de la dirección, observándose un incremento de la diferencia entre ambas direcciones al aumentar el grado de anisotropía celular.

La caracterización preliminar del comportamiento al fuego de estos materiales celulares y respectivos sólidos de partida mostró resultados interesantes debidos a la espumación, con las espumas presentando una superior extinción de la llama que los sólidos respectivos debido a la combinación de los elevados porcentajes de refuerzo mineral y estructura celular, ésta útlima actuando como una capa intumescente protectora.

Aunque preliminares, se trató de analizar la posible influencia de la estructura celular y orientación preferencial de las partículas en el comportamiento frente a la llama de las espumas por termogravimetría. Se observaron pequeñas diferencias de estabilidad térmica entre las dos configuraciones consideradas, las espumas presentando una estabilidad térmica ligeramente superior en la dirección axial de crecimiento que en la radial, indicando que la estructura celular y orientación de las partículas afecta a la estabilidad térmica a elevada temperatura.

A los resultados recopilados en este artículo hay que añadir el análisis de la conductividad térmica presentado en conjunto con el de las espumas de PP reforzado con MMT en la publicación *Heat transfer of mineral-filled polypropylene foams* (ver sección 4.3). En esta publicación se demuestra cómo la anisotropía celular y cristalina de las espumas inducida por el proceso de espumación y la presencia de las partículas resulta en propiedades de transporte del flujo de calor anisotrópicas, con valores de conductividad considerablemente superiores en la dirección de orientación de las celdas/partículas, esto es, en la dirección de crecimiento de la espuma (dirección axial), que en la dirección radial.

En primer lugar hay que destacar los elevados valores de conductividad térmica obtenidos para los sólidos de referencia y en particular para el compuesto con el 70% en peso de hidróxido ($\approx$ 1 $W.m^{-1}.K^{-1}$, 4 veces superior a la conductividad del PP, 0.26 $W.m^{-1}.K^{-1}$), resultando posteriormente en espumas con conductividades térmicas considerablemente superiores a la ya referida conductividad del PP. Por ejemplo, para una densidad relativa de 0.47, las espumas de PP con 70% en peso de hidróxido presentan una conductividad de aproximadamente 0.45 $W.m^{-1}.K^{-1}$.

Aunque las espumas de PP con hidróxido de magnesio presenten una evolución de la conductividad térmica con la densidad relativa que se puede considerar típica de los materiales celulares, con la conductividad disminuyendo al incrementar la fracción de gas (menores densidades relativas), como se puede observar por los resultados presentados en la fig. 4.3.2 de la anterior sección de resultados, existen diferencias importantes para las espumas del 50% de menor densidad relativa, directamente relacionadas con la anisotropía celular generada durante el proceso de espumación y que induce una orientación preferencial de las partículas de hidróxido en la dirección de expansión. Así, y con el objetivo de elucidar posibles anisotropías térmicas debidas a

esta estructura celular y orientación preferencial de las partículas, se realizaron medidas de la conductividad térmica de las espumas de PP con hidróxido en el modo anisotrópico del conductivímetro, esto es, determinando por separado las contribuciones a la conductividad térmica en la dirección axial (dirección de crecimiento, λ_{axial}) y radial (λ_{radial}) de la espuma. Tal como se aprecia en la fig. 4.4.1 y se comenta en la publicación ya referida, y si se define la anisotropía térmica como el cociente entre las contribuciones axial y radial ($\lambda_{axial}/\lambda_{radial}$), se observa como ésta sube al espumar el material, esto es, al disminuir la densidad relativa, alcanzando un máximo de 2.5 para la espuma más ligera (λ_{axial} = 0.217 $W.m^{-1}.K^{-1}$ y λ_{radial} = 0.086 $W.m^{-1}.K^{-1}$).

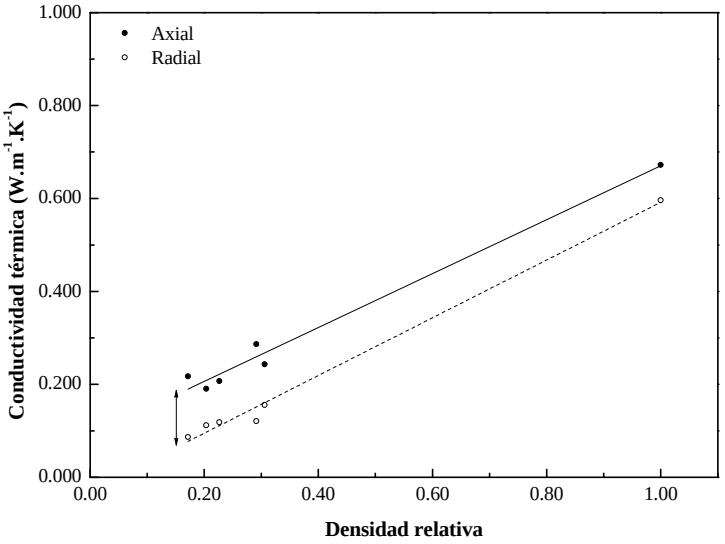

Figura 4.4.1. Comparativa entre las componentes axial y radial de la conductividad térmica en función de la densidad relativa para las espumas de PP con 50% de $Mg(OH)_2$.

Los resultados combinados de caracterización de la estructura celular y microestructura y morfología de los compuestos, junto con el análisis de sus propiedades térmico-mecánico-dinámicas, comportamiento frente al fuego y por último conductividad térmica, abren buenas perspectivas para el desarrollo de materiales celulares con un comportamiento ignífugo y propiedades reguladas en función del grado de expansión.

4.4.3. Artículos publicados.

4.4.3.1. *Characterization of highly filled magnesium hydroxide-polypropylene composite foams*.

Characterization of highly filled magnesium hydroxide-polypropylene composite foams

M. Antunes[1*], L. Haurie[2], J.I. Velasco[1]

[1]Centre Català del Plàstic. Departament de Ciència dels Materials i Enginyeria Metal.lúrgica. Universitat Politècnica de Catalunya. C/Colom 114. E-08222 Terrassa, Barcelona, Spain.

[2]EPSEB, Departament de Construccions Arquitectòniques II. Universitat Politècnica de Catalunya. Av. Dr. Marañon, 44-50, E-08028 Barcelona, Spain.

[*]Marcelo.Antunes@upc.edu; Phone: (+34)937837022; Fax: (+34)937841827

ABSTRACT: Magnesium hydroxide filled polypropylene foams were prepared by a compression-moulding chemical foaming process and studied considering the foaming effects and particle's influences on the microstructure (cellular structure and induced particle and polymer orientations), dynamic-mechanical and flame retardancy of the polypropylene composites. Two load percentages, 50 and 70 wt.% of magnesium hydroxide, as well as different foam densities, were considered. Results are discussed in terms of the observed anisotropy-induced cellular and particle and crystal orientations and their effects on the direction-dependent dynamic-mechanical and flame behaviour results. Preliminary flame retardancy characterization of the several solid and foamed composites showed interesting results due to foaming, foams globally exhibiting a higher extinguishability than the respective solid composites.

KEYWORDS: Polypropylene foams, magnesium hydroxide, thermo-mechanical properties, flame retardancy.

INTRODUCTION

One of the key challenges regarding plastic materials lies on the development of increasingly lightweight components with improved specific properties [1-2]. One possible strategy considers the foaming of the polymer base material by incorporating a blowing agent, ultimately combining the weight reduction with fillers that add particular characteristics, such as higher stiffness, thermal stabilization and thermal conductivity, among others, at the same time maintaining the low density of the composite material by controlling the expansion of the base matrix. Due to a good properties-cost balance, rigid polypropylene (PP) foams possess a high level of interest in sectors such as the automotive or construction. Alongside the production and foaming of these materials and final thermal and mechanical properties, the improvement of their flame retardancy is still required for certain applications. Typically, as a possible solution to the arrival of increasingly more demanding environmental restrictions, limiting the use of halogen-based flame retardant systems such as the common PP flame retardant aliphatic bromine compounds [3], one of the most used strategies for the flame retardancy of polyolefins lies on the addition of high inorganic filler amounts [4]. Among them, the most commonly used due to the combined low cost-flame retardancy efficiency are calcium carbonate and magnesium and aluminium hydroxides. For instance, magnesium hydroxide endothermally liberates water at around 340 ºC, delaying ignition, diluting the combustible gases and inhibiting oxygen from aiding to the combustion of the polymer [5]. None the less, the need of adding increasingly higher amounts of these inorganic fillers, not as efficient as the brominated flame retardants, to meet with the new flame retardancy requirements in sectors such as construction, results in processing difficulties, and thus in higher costs due to particle surface modification or the need of processing additives such as lubricants.

Although the fire retardant behaviour of PP composites has been considerably studied [6-7], limited work has been dedicated to the characterization of foamed PP with improved flame retardancy, mainly due to PP's high flammability, making it hard to comply with UL 94 V-0 rating [4]. Foaming these highly-filled polymer-based composite materials comes as a possible solution to these problems, not only allowing

to reduce the volume fraction of plastic, thus limiting the combustibility effect of the base polymer and processing costs, but has also been shown to add to a better dispersion of the fillers, even at high filler amounts, increasing its functionality efficiency [8-9]. In this sense, this work considers the development and characterization of rigid PP foams with an improved flame retardant behaviour by incorporating different amounts of magnesium hydroxide, results being compared with similar expansion ratio-produced unfilled PP foams.

EXPERIMENTAL

Materials and Compounding

First of all, and previous to foaming, the different PP-Mg(OH)$_2$ composites were melt-compounded using a co-rotating twin-screw extruder (Collin Kneter 25X36D, L/D=36) at a temperature that never surpassed 180 ºC. Three different PP homopolymer (Sabic PP 513A)-based formulations, with 0, 50 and 70 wt.% of magnesium hydroxide (Magnifin H-5 KV from Martinswerk), respectively referred for now on as PP, PP-50Mg and PP-70Mg, were prepared by adding *in-situ* the filler in the form of powder (density = 2.38 g/cm^3, specific BET surface area = 2.0-5.0 m^2/g and particle size, d_{90} = 2.4-4.4 μm) to the extruder during the melt-compounding stage. In all cases, 1.5 phr (parts per hundred of resin) of azodicarbonamide (ADC), Porofor ADC/M-C1, supplied by Lanxess Energizing Chemistry, with a density of 1.65 g/cm^3 and average particle size of 3.9 ± 0.6 μm, were added as chemical blowing agent. Stearic acid (0.2 phr) was used as lubricant.

Foaming Process

Once water-cooled, pelletized and dried, the extruded composites were foamed using a one-step compression-moulding foaming process in a hot-plate press (IQAP-LAP PL-15). The composite pellets were initially placed into a circular steel mould (diameter of 74 mm and thickness of 3.5 mm) and heated at 175 ºC applying a constant pressure. The resulting discs were cooled under pressure in the press using recirculating water. Once

prepared, the solid discs were allowed to foam by thermal decomposition of the ADC at a typical temperature of 200 ºC. The foamed PP-$Mg(OH)_2$ composites showed a final expansion ratio (*ER*), defined as the ratio between the density of the solid base polymer composite and the density of the foam, i.e., the reverse of relative density, between 2 and 6. Specimens were directly cut from the foamed composite materials in order to analyze their crystalline characteristics and dynamic-mechanical and flame retardant properties.

Testing Procedure

Density of the several solids and foams was measured according to standard procedures (ISO 845). The ash content of the composite materials was determined as the mean value of three different specimens according to ISO 3451, with the effective $Mg(OH)_2$ content being calculated considering a loss on ignition (1200 ºC) due to the endothermal decomposition of magnesium hydroxide of 31 wt.%.

The cellular structure of the foams was observed using a JEOL JSM-5610 scanning electron microscope (SEM). Samples were prepared by fracturing at low temperature and sputter depositing a conductive thin layer of gold. Both the average cell size (ϕ) and cell density were obtained from low-magnification micrographs using the intercept counting method [10]. Two different cell sizes were determined: ϕ_{VD} (VD: Vertical Direction), and ϕ_{WD} (Width Direction). The aspect ratio (*AR*), defined as the ratio between the highest and smallest cell sizes ($AR = \phi_{VD}/\phi_{WD}$), was determined for the several composite foams using a representative cell population. Schematics showing specimen configurations and the most characteristic cellular structure parameters are presented in fig. 1. High-magnification SEM micrographs were used to assess the morphology of the foamed composites.

Both polypropylene as well as magnesium hydroxide's crystalline characteristics were analyzed by means of wide angle X-ray scattering (WAXS). A Bruker D8 diffractometer with CuKα radiation (λ = 0.154 nm) operating at 45 kV and 40 mA was used. Scans were taken from 1 to 60º with a rotation step of 0.033º and a step time of 0.06 s. In order to study possible crystal and particle anisotropies, a set of two

measurements were done for each sample, pointing the X-Ray beam parallel (P, fig. 1(c)) and perpendicular (N, fig. 1(d)) to the foam's surface.

Dynamic mechanical analysis (DMA) was used to measure possible direction-dependent dynamic-mechanical response of the several foamed composites as well as to study the viscoelastic behaviour of the polypropylene matrix and how the foaming process and presence of magnesium hydroxide may affect it. The DMA equipment (TA Instruments Q800 Dynamic Mechanical Analyzer, DMA) was calibrated according to the standard procedure. The storage modulus (*E'*), loss modulus (*E''*) and loss tangent (*tan* δ) were obtained in a three-point bending configuration using a span length of 50.00 mm. As with WAXS, two configurations, parallel (P) and perpendicular (N), respectively shown in fig. 1(a) and (b), were considered. Experiments were performed at a frequency of 1 Hz from -20 to 150 °C and heating rate of 2 °C/min using liquid nitrogen as cryogenic fluid. A static strain of 2 % and dynamic of 0.02 % with a preload force of 0.01 N and force track of 120 % were chosen. Test specimens were prepared in a prismatic shape with a nominal length of 55.00 ± 0.10 mm, width of 13.00 ± 0.10 mm and thickness of 3.00 ± 0.05 mm in the case of the solids and 3.50 ± 0.10 mm for the foamed samples.

The flame retardancy behaviour of the several solid and respective foamed composites was characterized by means of the dripping test using an electrical radiator according to UNE 23725-90 and measuring the minimum oxygen concentration required to sustain burning (limiting oxygen index, LOI) according to ISO 4589. In the case of the LOI experiments, prismatic-shaped test specimens similar to the ones used in DMA (55 × 13 mm^2, 3 mm thick) were employed.

An adapted thermogravimetric analyzer (for now on known as *macro-TGA*) was also used to acquire a first notion of possible flame behaviour differences between the two main specimen configurations due to induced anisotropies and preferential particle orientation. Thermogravimetric analysis (TGA) was performed using a Nabertherm 1100 ºC muffle furnace coupled with a Gram Precision ST-510 precision balance in air flow at a heating rate of 3 ºC/min from 25 to 1000 ºC.

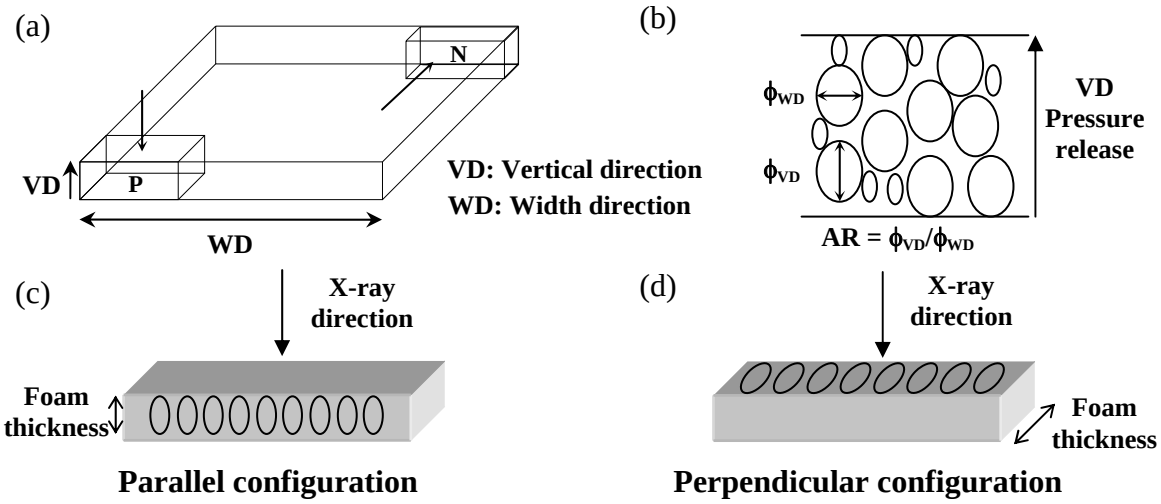

Figure 1. (a) Schematic showing specimen configurations and (b) characteristic cellular structure parameters; (c) parallel (P) and (d) perpendicular (N) specimen configurations.

RESULTS AND DISCUSSION

Foaming Behaviour and Cellular Structure

The material's code, foam density, relative density and respective gas (V_{gas}), polymer (V_{pol}) and filler ($V_{Mg(OH)2}$) volume fractions are presented in table 1 alongside the most characteristic cellular structure characterization results.

Table 1

The volume fractions of gas varied between the 0.35 of PP-70Mg and the 0.80 of some of the low density PP and PP-50Mg compression-moulded foams, the low relative density PP-50Mg even showing polymer volume fractions lower than 0.20. Typical SEM pictures are presented in figs. 2 and 3 respectively for the 50 and 70 wt.% $Mg(OH)_2$-PP foams.

Comparative cellular characterization indicates that the highest filled $Mg(OH)_2$-PP foams not only show considerably smaller cell sizes (≈ 180 μm) than the 50 wt.%

(from 670 to almost 1000 μm), but also a typical isometric-like cell structure (*AR* ≈ 1, fig. 3). Contrarily, the 50 wt.% $Mg(OH)_2$ foams present an increasingly higher cell anisotropy with foaming, as it is clearly seen from the several micrographs shown in fig. 2, *AR* gradually increasing from the 1.3 of the 0.29 relative density foam (fig. 2(a)) to a value higher than 3 for the 0.17 (fig. 2(d)), the foam showing a honeycomb-like cellular structure.

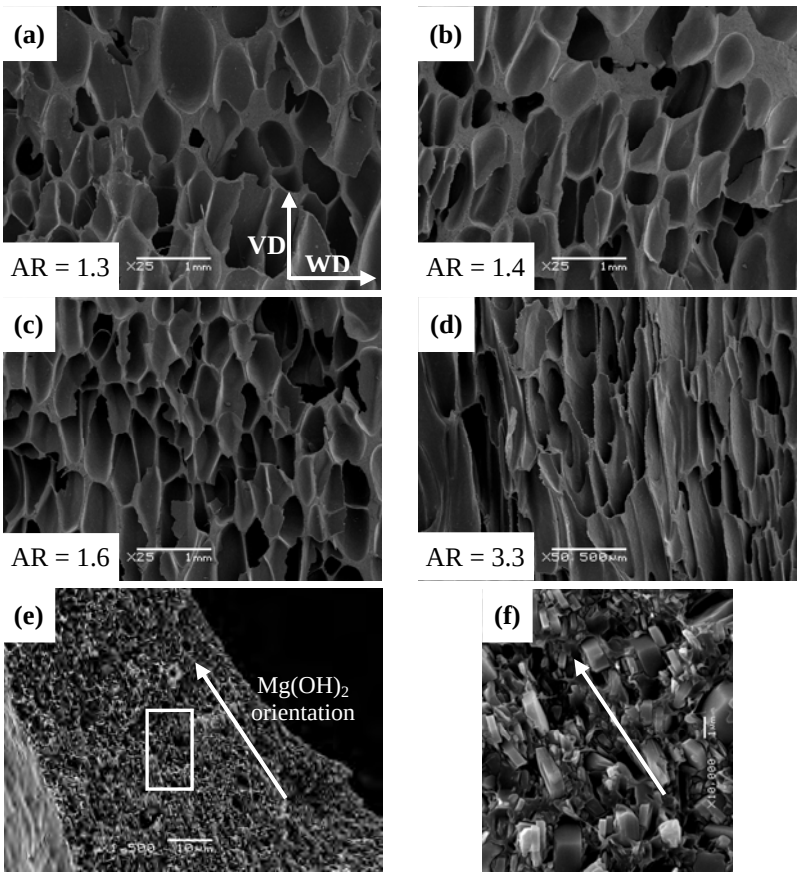

Figure 2. SEM pictures of the 50 wt.% $Mg(OH)_2$-PP foams, showing increasingly higher cellular anisotropy due to foaming: (a) 0.29, (b) 0.23, (c) 0.20 and (d) 0.17 of relative density; and (e) and (f) high magnification micrographs showing preferential $Mg(OH)_2$ particle orientation along the cell walls.

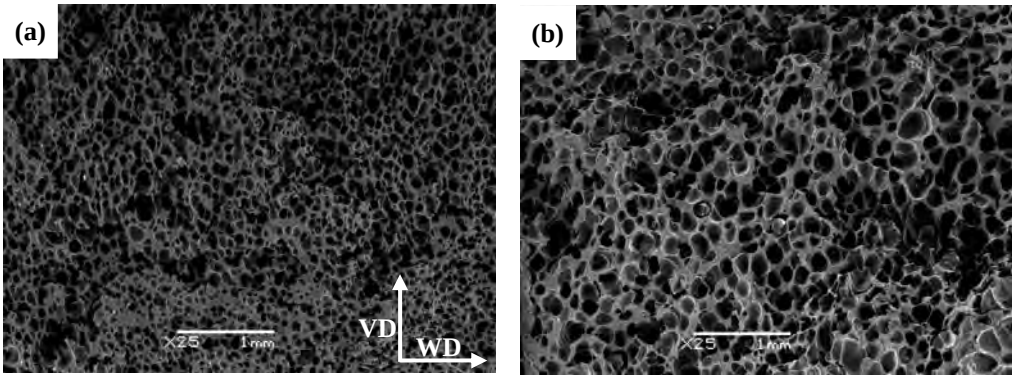

Figure 3. Characteristic SEM pictures of the 70 wt.% $Mg(OH)_2$-PP foams: (a) 0.55 and (b) 0.47 of relative density.

Particle and Crystal Orientations

Due to the high cellular anisotropy induced during foaming for the 50 wt.% $Mg(OH)_2$ foams, alongside the high particle content for all the $Mg(OH)_2$ composite foams, previous to their mechanical, thermal and flame behaviour characterizations, both particle and polymer crystalline orientations and anisotropies were measured by WAXS. Interesting results were found for the several foamed composites, as one would expect from the preliminary high magnification micrographs, showing a preferential particle orientation along the cell walls (fig. 2(e) and (f)). It is also known that magnesium hydroxide is keen to orientate and induce preferential polypropylene crystallinity under certain conditions due to its platelet-like morphology [11-12].

From the measurements carried out by WAXS, it was possible to obtain information about the orientation of both filler particles and polymer's crystal phase. Typical WAXS spectra of the 50 and 70 wt.% $Mg(OH)_2$-PP foams are respectively presented in figs. 4 and 5 for the two configurations and two different relative density specimens.

First of all, the intensity ratio between the (001) and (101) diffraction planes of $Mg(OH)_2$ (peaks found respectively at around 2θ = 18.6 and 38.0º) are presented in table 2 for the different composites in the parallel and perpendicular configurations. As seen from the hexagonal crystallographic unit schematic shown in fig. 6(a), the (001) diffraction plane is oriented parallel to the particles surface, meaning that an increase in

the intensity of this peak regarding that of the perpendicularly oriented (101) is indicating a particle orientation that is perpendicular to that of the X-Ray beam. The analysis of the relative intensity of these two crystal planes is commonly used and has been proven to be useful in quantitative characterizing possible induced $Mg(OH)_2$ particle orientations due to processing [13].

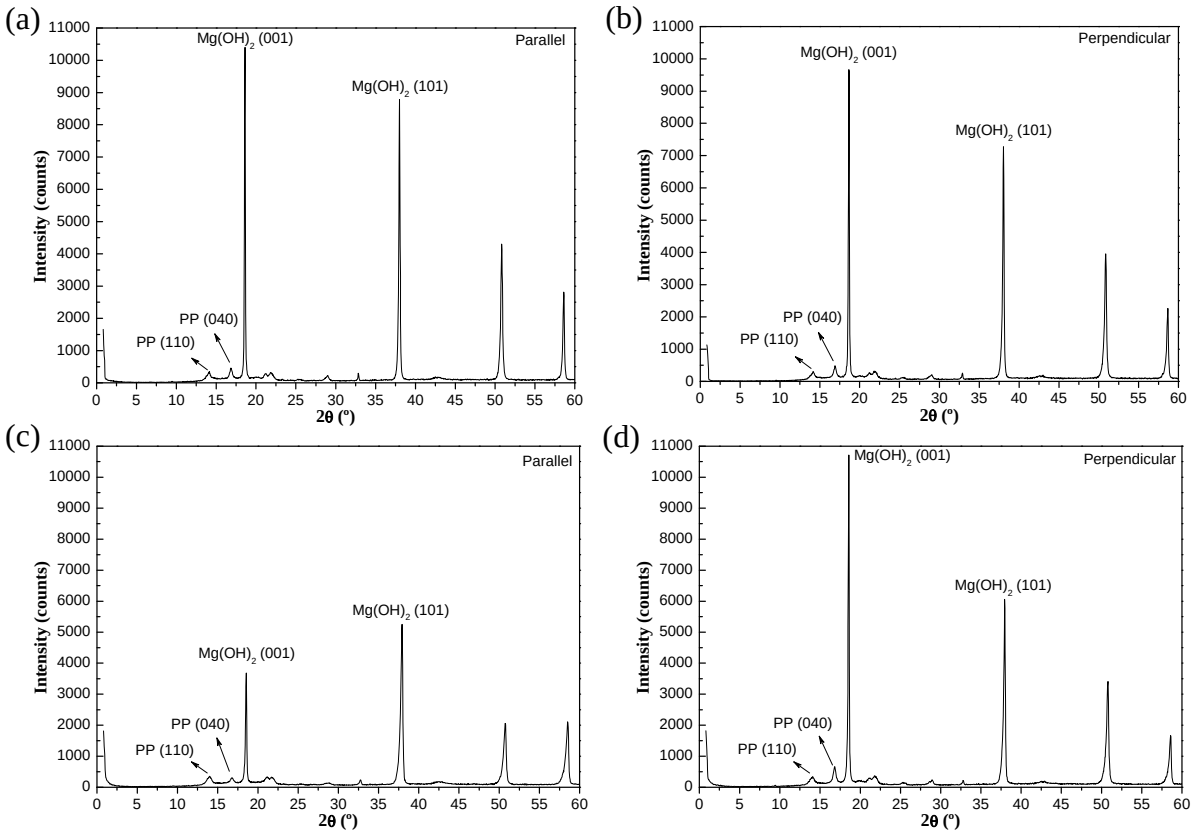

Figure 4. Typical WAXS spectra of the 50 wt.% $Mg(OH)_2$-PP foams: (a) parallel and (b) perpendicular 0.31 of relative density and (c) parallel and (d) perpendicular 0.17 of relative density.

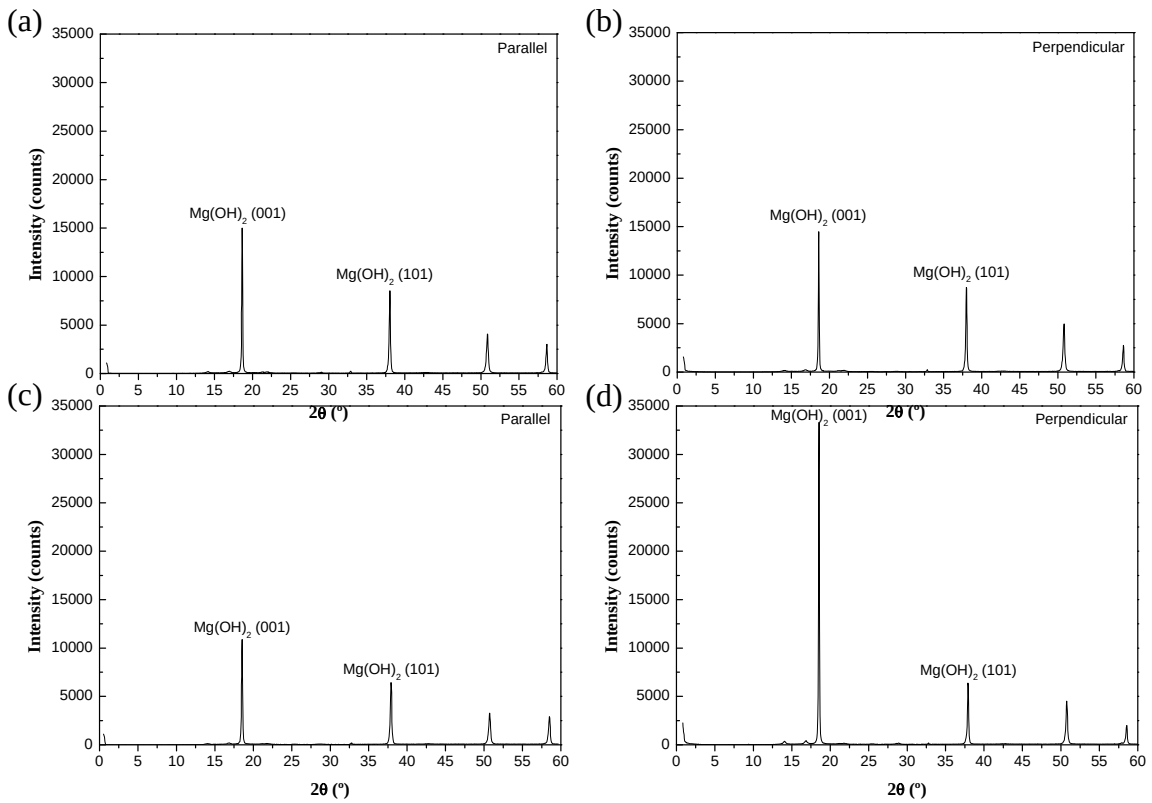

Figure 5. Typical WAXS spectra of the 70 wt.% $Mg(OH)_2$-PP foams: (a) parallel and (b) perpendicular 0.55 of relative density and (c) parallel and (d) perpendicular 0.47 of relative density.

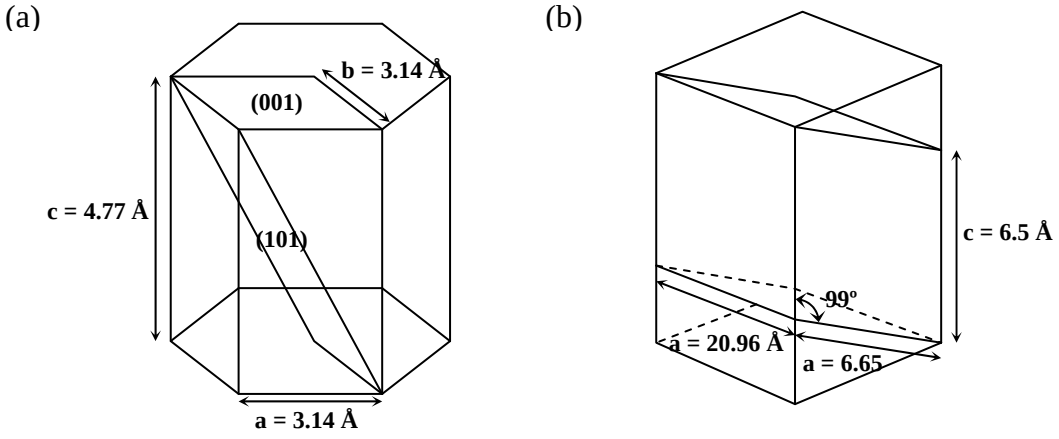

Figure 6. (a) $Mg(OH)_2$ hexagonal and (b) α PP monoclinic crystallographic units.

Table 2

There is a clear increase of the intensity ratio of the (001) and (101) diffraction planes of the magnesium hydroxide particles from the parallel towards the perpendicular configuration with foaming, i.e., with decreasing the relative density. As previously said, an increase in this ratio, related to an intensity shift from the (101) to the (001) plane, indicates an increasingly higher particle orientation perpendicular to the foam's surface.

Table 3

A similar increase, in this case of the intensity ratio of the (040) and (110) crystal basal planes, directly related to the orientation of *a* and *b* axes, is observed for PP's crystal phase in 50 wt.% $Mg(OH)_2$ with foaming. Although apparently being mainly induced by the orientation of the filler particles, as one would conclude from the analysis of the 50 wt.% $Mg(OH)_2$ WAXS intensity ratios, the orientation of PP's crystalline phase seems to be mainly related to the anisotropic cellular structure developed during foaming, thus its almost unaltered value for the isotropic-like highly-filled 70 wt.% $Mg(OH)_2$ foams.

Two parameters were defined in order to quantify both the particle's (PAD - Particle Anisotropy Degree) as well as crystal polymer's (CAD - Crystal Anisotropy Degree) orientations:

$$PAD = \frac{\left(I(001)/I(101)\right)_N - \left(I(001)/I(101)\right)_P}{\left(I(001)/I(101)\right)_N} \times 100, \quad (1)$$

$$CAD = \frac{\left(I(040)/I(110)\right)_N - \left(I(040)/I(110)\right)_P}{\left(I(040)/I(110)\right)_N} \times 100, \quad (2)$$

where P and N respectively stand for parallel and perpendicular configurations.

Typical particle and crystal anisotropy degrees evolution with the relative density are shown in fig. 7 for the 50 wt.% $Mg(OH)_2$-PP foams. As expected from the induced cellular structure anisotropies, the 50 wt.% foams showed an increasingly higher particle and polymer orientations with decreasing the relative density. For instance, a relative density reduction from 0.31 to 0.17 resulted in both a PAD and CAD parameters increase respectively from 11 and 19 % to 60 and 56 %.

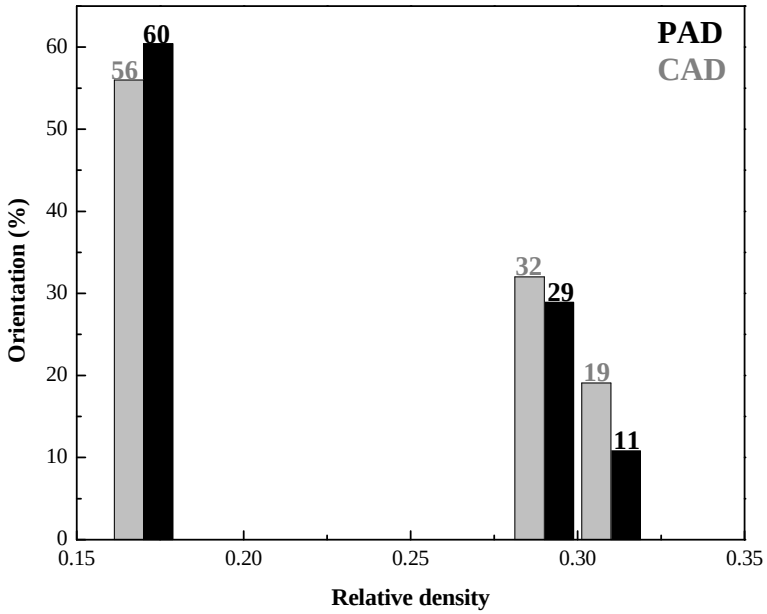

Figure 7. Typical particle (PAD) and crystal (CAD) anisotropy degrees of the 50 wt.% $Mg(OH)_2$-PP foams.

So, the increasingly more anisotropic cellular structure observed with foaming for the 50 wt.% $Mg(OH)_2$ composites, with cells being increasingly more elongated, ultimately even reaching honeycomb-like aspect ratio values (higher than 3), is the cause behind both the particle as well as polymer crystal's increasingly higher anisotropies. In the case of the 70 wt.% $Mg(OH)_2$ ones, and although displaying a globally isotropic-like cell structure, with aspect ratios close to 1, it seems that very slight variations are enough to induce considerable particle anisotropies, attained to the very high filler content, at the same time maintaining polypropylene's crystal orientation.

Dynamic-mechanical Analysis

Typical DMA curves are shown in fig. 8 respectively for the 50 and 70 wt.% parallel and perpendicular foamed specimens. As expected, the storage modulus (*E'*) increased with Mg(OH)$_2$'s content, from the almost 4000 MPa of the solid 50 wt.% composite at 20 ºC and the 550-700 MPa of the respective foamed composites to the 6000 MPa of the solid and 1300-1400 MPa of the 70 wt.% foams. If one compares the specific modulus values, i.e., the storage modulus divided by the density of the specimen, even the lowest relative density 50 wt.% foams show a specific modulus value that is comparable to that of the unfoamed solid PP.

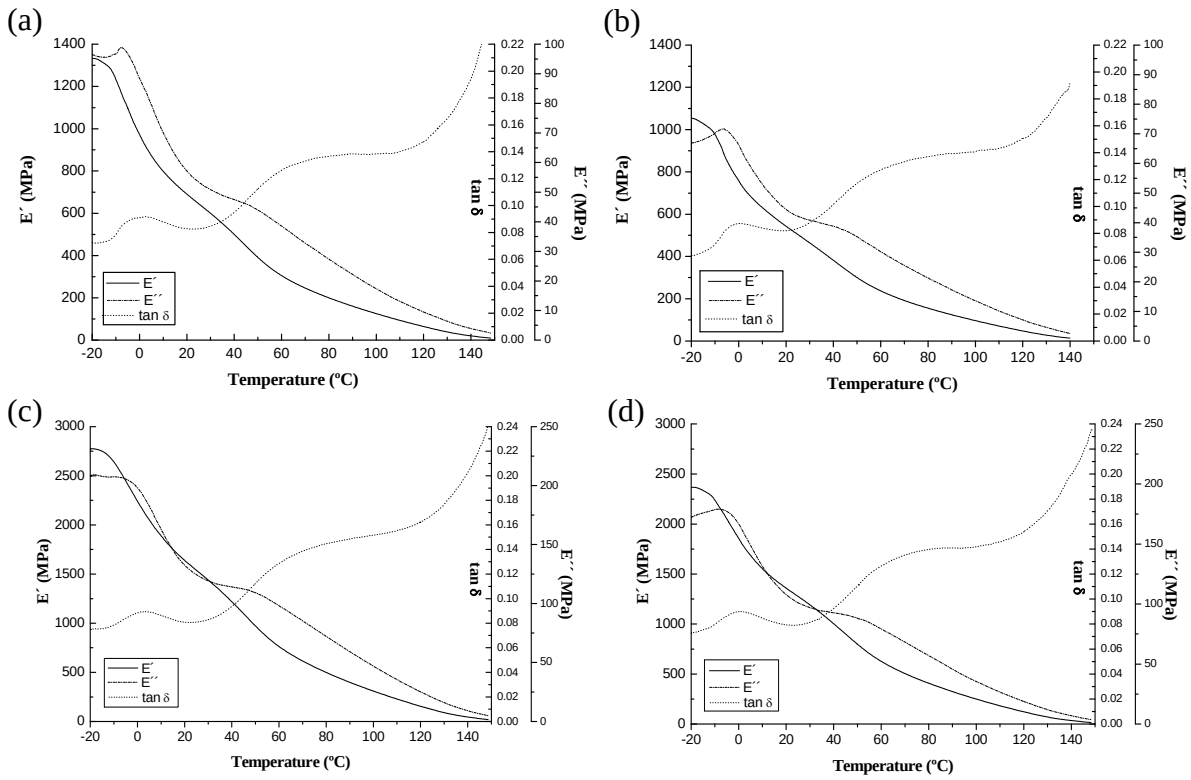

Figure 8. Typical DMA curves of (a) parallel and (b) perpendicular 50 wt.% Mg(OH)$_2$ and (c) parallel and (d) perpendicular 70 wt.% Mg(OH)$_2$ polypropylene foams.

Comparing the parallel and perpendicular configurations curves, one can clearly ascertain the highly direction-dependent dynamic-mechanical properties for both the 50 and 70 wt.% Mg(OH)$_2$ composite foams, the parallel configuration always giving a higher storage modulus, the first of which result of the anisotropic cellular structure and

thus particle and polymer orientations developed during foaming (parallel configuration: 1452.1 MPa.cm^3/g, perpendicular: 1143.3 MPa.cm^3/g) and the second from the high particle content/preferential particle orientation (parallel configuration: 2033.2 MPa.cm^3/g, perpendicular: 1813.9 MPa.cm^3/g).

Flame Retardancy Behaviour

The main dripping test and LOI results are shown in table 4 for the solid and foamed 50 and 70 wt.% $Mg(OH)_2$ composites.

Table 4

As expected, both the LOI values as well as the flame ignition times increased with adding higher amounts of $Mg(OH)_2$, while the average times of combustion extent decreased from the 62 s observed for the solid 50 wt.% $Mg(OH)_2$ composite to approximately a third of it for the 70 wt.% one (19 s).

Interesting effects due to foaming were observed, especially for the 70 wt.% $Mg(OH)_2$ foams. Despite the ignition time decrease, a significant reduction was observed regarding the combustion extent values, indicating a higher extinguishability of the foamed composites compared to the respective solid materials.

Although the higher LOI values regarding that typically observed for unfilled polypropylene (17.8 %), a 50 wt.% of $Mg(OH)_2$ was clearly insufficient to considerably increase the LOI, solids and foams showing similar results (between 23.1 and 24.0 %). Interestingly, the 70 wt.% $Mg(OH)_2$ solid and foamed composites displayed a much higher LOI, especially the foamed ones, 36.0 %, a more than 100 % increase regarding the unfilled PP and more than 50 % compared to that of the 50 wt.% $Mg(OH)_2$ composites and even an almost 10 % improvement regarding the respective 70 wt.% solid. This increase was attained to both the high extinguishability alongside charring residue consistency, result of the combined effects of the high filler content and cellular structure, which works out as a protective foamed intumescent layer. These values were even higher than typical LOI values observed for similar highly-filled $Mg(OH)_2$-

modified solid PP composites (30.2 % [14]), indicating the possibilities of using these materials as flame retardant-improved lightweight components.

None the less, no considerable differences were found in LOI values regarding the orientation of the foamed specimens. With that in mind, an adapted thermogravimetric analyzer (*macro-TGA*) was used to acquire a first notion of possible differences. Preliminary results are shown in fig. 9.

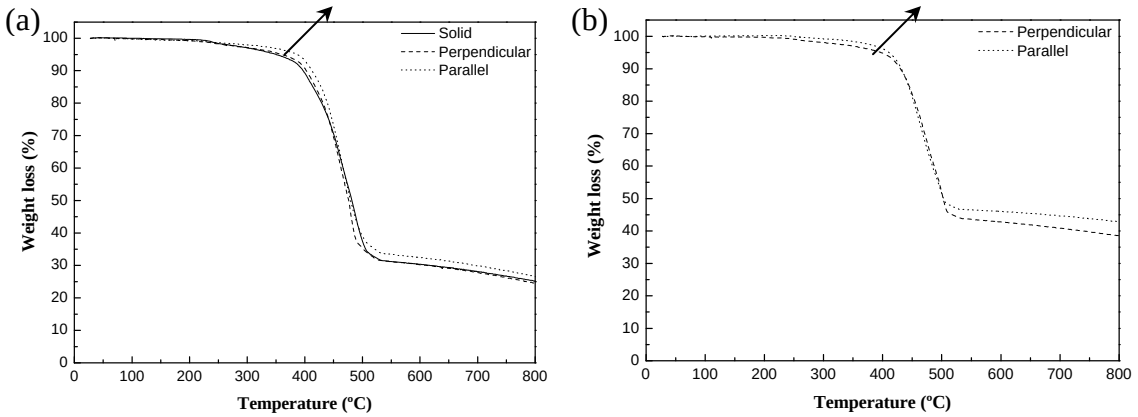

Figure 9. TGA curves obtained in air at 3 ºC/min for the solid and respective parallel and perpendicular-configuration foamed (a) PP + 50 wt.% Mg(OH)$_2$ and (b) PP + 70 wt.% Mg(OH)$_2$ composites.

As can be seen, the cellular materials show a higher thermal stabilization than the respective solid composites, slight differences being also found between the two configurations, with the foamed samples showing a slightly higher stabilization in the parallel-configuration, indicating that the microstructure developed during foaming (particle and crystal preferential orientations perpendicular to the foams' surface) is affecting the thermal behaviour of the composites.

Also, the 70 wt.% foam charring residue showed almost the foam's original cellular structure, contrarily to the 50 wt.% one, that totally loosed its form, adding to the explanation given previously regarding the higher LOI values of the 70 wt.% Mg(OH)$_2$ foams, i.e., a higher extinguishability and charring consistency due to the combined effects of a higher filler content and cellular structure.

CONCLUSIONS

This work focuses in studying the combined effects of foaming and particles presence on the microstructure and respective dynamic-mechanical and flame behaviour of highly filled magnesium hydroxide-polypropylene foams.

In view of the combined effects of the cellular structure generated during foaming, especially for the 50 wt.% $Mg(OH)_2$ foams, showing increasingly higher cellular anisotropies with foaming, even reaching aspect ratios higher than 3, compared to the typical isometric-like cell structures of the 70 wt.%, and high filler content, both particle and polymer orientation anisotropies were found to be increasingly higher with foaming. The combination of both cellular structure and particle and crystal anisotropies resulted in direction-dependent dynamic-mechanical behaviours, the parallel configuration comparatively giving higher elastic moduli than the perpendicular one, differences between both increasing with the anisotropy degree.

Preliminary characterization of the flame retardancy behaviour of the several solid and foamed composites showed interesting results due to foaming, foams globally exhibiting a higher extinguishability than the respective solid composites.

Although further experiments are required to elucidate the inner relations between the microstructure and the mechanical and flame retardancy properties of these highly filled magnesium hydroxide-polypropylene composite foams, interesting results were observed, confirming the possibilities of using these materials as flame retardant-improved lightweight components.

ACKNOWLEDGEMENTS

Financial assistance from the Spanish Ministry of Science and Education for the projects MAT2007-62956 and FIS2006-11452-C03 are gratefully acknowledged.

REFERENCES

1. Rodríguez-Pérez, M.A. (2005). Crosslinked Polyolefin Foams: Production, Structure, Properties, and Applications, Advances in Polymer Science, 184: 97-126.

2. Klempner, D. and Sendijarevic, V. (2004). Polymeric Foams and Foam Technology, Munich: Hanser.

3. Birnbaum, L.S. and Staskal, D.F. (2004). Brominated Flame Retardants: Cause for Concern?, Environmental Health Perspectives, 112(1): 9–17.

4. Wang, J.Q. and Chow, W.K. (2005). A Brief Review on Fire Retardants for Polymeric Foams, Journal of Applied Polymer Science, 97: 366-376.

5. Troitzsch, J. (1990). In: International Plastics Flammability Handbook, Hanser Publishers, Munich, p. 22.

6. Sain, M., Park, S.H., Suhara, F. and Law, S. (2004). Flame retardant and mechanical properties of natural fibre-PP composites containing magnesium hydroxide, Polymer Degradation and Stability, 83: 363-367.

7. Lomakin, S.M., Zaikov, G.E. and Koverzanova, E.V. (2005). Thermal degradation and combustibility of polypropylene filled with magnesium hydroxide micro-filler and polypropylene nanofilled aluminosilicate composite, Oxidation Communications, 28: 451-464.

8. Antunes, M., Velasco, J.I., Realinho, V. and Solórzano, E. (2009). Study of the cellular structure heterogeneity and anisotropy of polypropylene and polypropylene nanocomposite foams, Polymer Engineering and Science, 49: 2400-2413.

9. Antunes, M., Realinho, V., Martínez, A.B., Solórzano, E., Rodríguez-Pérez, M.A. and Velasco, J.I. (2010). Heat transfer of mineral-filled polypropylene foams, Defect and Diffusion Forum, 297-301: 990-995.

10. Sims, G.L.A. and Khunniteekool, C. (1994). Cell size measurement of polymeric foams, Cellular Polymers, 13(2): 137-146.

11. Chernev, B., Olbrich, M. and Zipper, P. (2005). Site-resolved X-ray investigations on injection-molded polypropylene filled with magnesium hydroxide, Composite Interfaces, 12: 221-230.

12. Velasco, J.I., Morhain, C., Martínez, A.B., Rodríguez-Pérez, M.A. and de Saja J.A. (2001). Anisotropy and Microstructure Heterogeneity of Injection-Moulded Discs of Poly(propylene) Filled with Platy Magnesium Hydroxide, Macromolecular Materials and Engineering, 286(11): 719-730.

13. Velasco, J.I., Morhain, C., Martínez, A.B., Rodríguez-Pérez, M.A. and de Saja J.A. (2002). The effect of filler type, morphology and coating on the anisotropy and

microstructure heterogeneity of injection-moulded discs of polypropylene filled with aluminium and magnesium hydroxides. Part 1. A wide-angle X-ray diffraction study, Polymer, 43: 6805-6811.

14. Chiu, S-H. and Wang, W-K. (1998). The Dynamic Flammability and Toxicity of Magnesium Hydroxide Filled Intumescent Fire Retardant Polypropylene, Journal of Applied Polymer Science, 67: 989-995.

Table 1. Cellular structure characterization results of the studied foams

Material code	Foam density (g/cm^3)	Relative density	V_{gas}	V_{pol}	$V_{Mg(OH)2}$	ϕ_{VD} (μm)	ϕ_{WD} (μm)	*AR*	Cell density (cells/cm^3)
PP	0.446	0.49	0.52	0.48	-	170	180	0.9	3.91×10^4
	0.444	0.48	0.52	0.48	-	174	175	1.0	4.52×10^4
	0.422	0.46	0.54	0.46	-	187	194	1.0	4.70×10^4
	0.346	0.38	0.62	0.38	-	194	175	1.1	4.71×10^4
	0.311	0.34	0.66	0.34	-	177	196	0.9	4.63×10^4
	0.268	0.29	0.71	0.29	-	241	266	0.9	3.52×10^4
	0.261	0.29	0.72	0.29	-	243	239	1.0	3.42×10^4
	0.236	0.25	0.75	0.25	-	456	479	1.0	1.30×10^4
	0.189	0.20	0.80	0.20	-	564	523	1.1	9.13×10^3
PP-50Mg	0.377	0.31	0.64	0.28	0.08	792	954	0.8	2.43×10^4
	0.359	0.29	0.66	0.27	0.08	984	765	1.3	3.24×10^3
	0.279	0.23	0.73	0.21	0.06	809	579	1.4	5.20×10^3
	0.251	0.20	0.75	0.19	0.05	889	544	1.6	4.83×10^3
	0.211	0.17	0.79	0.16	0.04	671	203	3.3	2.90×10^3
PP-70Mg	0.794	0.55	0.34	0.42	0.23	169	182	0.9	6.77×10^4
	0.673	0.47	0.43	0.38	0.20	206	195	1.1	3.62×10^4

Table 2. Characteristic (001) and (101) magnesium hydroxide WAXS intensity ratios

Material code	Relative density	Specimen configuration	*I* (001)/*I* (101)	$[I\ (001)/I\ (101)]_N$ - $[I\ (001)/I\ (101)]_P$
PP-50Mg	0.31	Parallel	1.184	0.144
		Perpendicular	1.328	
	0.29	Parallel	1.127	0.458
		Perpendicular	1.585	
	0.17	Parallel	0.701	1.067
		Perpendicular	1.767	
PP-70Mg	0.55	Parallel	1.756	-0.097
		Perpendicular	1.659	
	0.47	Parallel	1.688	3.532
		Perpendicular	5.220	

Table 3. Characteristic (040) and (110) polypropylene WAXS intensity ratios

Material code	**Relative density**	**Specimen configuration**	***I* (040)/*I* (110)**	**$[I\ (040)/I\ (110)]_N$ - $[I\ (040)/I\ (110)]_P$**
PP-50Mg	0.31	Parallel	1.282	0.303
		Perpendicular	1.586	
	0.29	Parallel	1.183	0.557
		Perpendicular	1.740	
	0.17	Parallel	0.874	1.113
		Perpendicular	1.987	
PP-70Mg	0.55	Parallel	1.184	0.218
		Perpendicular	1.402	
	0.47	Parallel	1.583	-0.469
		Perpendicular	1.114	

Table 4. Dripping test and limiting oxygen index (LOI) results for the solid and foamed $Mg(OH)_2$-PP composites

$Mg(OH)_2$ content (wt.%)	**Relative density**	**V_{gas}**	**Flame ignition time (s)**	**Average combustion time (s)**	**LOI (%)**
50	1	0	39	61.6	23.1
	0.29	0.66	21	50.0	23.1
	0.23	0.73	19	38.0	24.0
70	1	0	62	18.8	33.1
	0.47	0.43	48	13.8	36.0

4.5. Espumas de polipropileno reforzado con nanofibras de carbono.

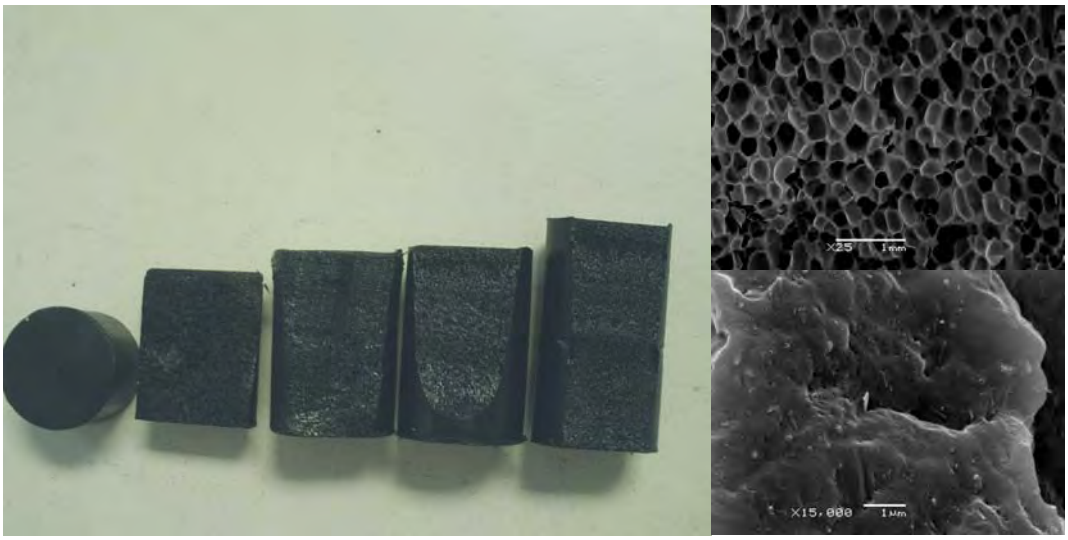

4.5.1. Justificación y objetivos.

En esta sección se recopilan las publicaciones y principales conclusiones de la preparación y caracterización de las espumas de PP reforzado con nanofibras de carbono. Estas espumas fueron ideadas no sólo pensando en el estudio de la posible sinergia entre la espumación y la incorporación de un tipo de refuerzo nanométrico de geometría fibrilar, distinta por tanto a la geometría laminar de la montmorillonita, pero sobre todo en la preparación de materiales ligeros con propiedades mejoradas, en particular con mejores propiedades de transporte (conductividad térmica y conductividad eléctrica). A las dimensiones nanométricas de las nanofibras e interés en encontrar estrategias sencillas de dispersión de las mismas, hay que añadir sus elevadas propiedades de transporte, que las hacen atractivas como posible vía de incremento de las conductividades térmica y eléctrica de materiales de matriz polimérica incluso para reducidos porcentajes de refuerzo incorporado. De esta manera se podría lograr una extensión de las propiedades del material base que no se pueden ni cubrir con los respectivos compuestos sólidos, debido a su elevada densidad y a una reducida dispersión de las nanofibras por formación de agregados y por tanto reducida funcionalidad de las mismas, ni con las espumas sin nanofibras (reducidas conductividades térmica y eléctrica).

En esta sección de resultados se ha optado por presentar las principales conclusiones derivadas de las tres publicaciones consideradas empezando por la preparación de las espumas y caracterización básica de las mismas (estructura celular y características cristalinas), siguiendo con la caracterización de las propiedades térmico-mecánico-dinámicas y por último el estudio de las propiedades de transporte (conductividades térmica y eléctrica, en ambos casos estudiadas por separado, la primera en la publicación *Thermal conductivity of carbon nanofibre-polypropylene composite foams* y la segunda en dos: *Characterization of carbon nanofibre-reinforced polypropylene foams* y más en detalle en el artículo *Broad-band electrical conductivity of carbon nanofibre-reinforced polypropylene foams*).

4.5.2. Resumen de los trabajos y conclusiones.

Antes de presentar las principales conclusiones derivadas de cada una de las publicaciones incluidas en esta sección caben resumir algunas de las características relacionadas con la preparación y espumación de los nanocompuestos de PP con nanofibras de carbono, las cuales, aunque se presenten de forma resumida en la primera parte del artículo *Characterization of carbon nanofibre-reinforced polypropylene foams*, son tratadas más en detalle en la segunda publicación incluida en la sección 4.3, *Foaming behaviour, structure and properties of polypropylene nanocomposite foams*. Así, en base a los resultados presentados en este artículo, la preparación de los diversos nanocompuestos de PP reforzado con nanofibras de carbono y azodicarbonamida por un proceso de mezclado en fundido y posterior espumación química por compresión resultó en espumas con estructuras celulares más isotrópicas y de menor tamaño de celda que las respectivas espumas sin nanofibras para grados de expansión similares. Este efecto de nucleación de celdas por parte de las nanofibras se manifiesta aún más al incrementar el porcentaje de nanofibras, obteniéndose para las espumas con un 20% en peso de nanofibras un tamaño de celda de aproximadamente la mitad que para las del 5%.

Al análisis de la estructura celular hay que añadir el estudio de las características cristalinas de la matriz polimérica e influencia de las nanofibras y del proceso de espumación en las mismas. La presencia de las nanofibras eliminó la orientación preferencial del cristal α-monoclínico del PP, observada tanto en los sólidos como en las espumas sin partículas. Además, y contrariamente a la menor perfección cristalina de las espumas sin refuerzos frente a los sólidos respectivos (superior valor de la anchura a media altura asociada al plano cristalino (110) del PP), en el caso de las espumas con nanofibras se observó el efecto opuesto, esto es, la espumación resultó en valores menores del *FWHM* y por ende en superiores perfecciones cristalinas.

La publicación titulada ***Characterization of carbon nanofibre-reinforced polypropylene foams*, Journal of Nanoscience and Nanotechnology, Vol. 10, 1241-1250, 2010**, se centra en la preparación de espumas de PP reforzadas con porcentajes variables de nanofibras de carbono (5, 10 y 20% en peso de nanofibras), caracterización de la estructura celular y de la influencia de las nanofibras en la misma y en las

características cristalinas de la matriz polimérica. Además, se presentan pinceladas sobre el comportamiento de conducción eléctrica de las espumas.

En lo que toca a la estructura celular de las espumas, y complementando los resultados de preparación y caracterización preliminar de estos materiales ya presentados en la publicación *Foaming behaviour, structure and properties of polypropylene nanocomposite foams*, y considerando que todas las espumas presentaban grados de expansión similares ($ER \approx 3$), se observó que la incorporación de porcentajes crecientes de nanofibras de carbono resulta en estructuras celulares crecientemente isotrópicas con tamaños de celda cada vez más reducidos, asociado al efecto nucleante de generación de celdas inducido por las nanofibras. Asimismo, se demostró la superior T_g y T_α (temperatura de la relajación α, una relajación cristalina observada a aproximadamente 100-130 ºC y que depende de la morfología de los cristales), ambas determinadas por análisis térmico-mecánico-dinámico, de los precursores sólidos al incrementar el porcentaje de nanofibras, indicando una superior cristalinidad inducida por las nanofibras, comprobada por los valores más elevados de las temperaturas correspondientes tanto al inicio como al máximo de cristalización y a los superiores valores de cristalinidad, determinados por calorimetría diferencial de barrido (DSC).

Desde un punto de vista térmico-mecánico-dinámico, y para grados de expansión similares, las espumas presentaron módulos elásticos de almacenamiento absolutos crecientes al incrementar el porcentaje de nanofibras, comparables a los del PP en lo que toca a valores específicos, esto es, relativos a la densidad del material, demostrando el efecto de refuerzo de las nanofibras.

Además, en esta publicación se presenta un estudio preliminar de la conductividad eléctrica de estas espumas, posteriormente ampliado en la publicación *Broad-band electrical conductivity of carbon nanofibre-reinforced polypropylene foams.* Cabe decir que se detectó la presencia de una concentración crítica para la conducción eléctrica, conocida como límite de percolación, ϕ_c (*percolation threshold*), a partir de la cual la conducción eléctrica sube de golpe en el material al dejar de ser controlada por el polímero (aislante) y pasar a ser controlada por un mecanismo de conducción eléctrica por efecto de túnel entre las nanofibras (conductoras), entre un 7.5 y 12.5% en peso de nanofibras para los precursores sólidos y entre 7.5 y 10% en las espumas, indicando que la espumación parece promover la formación de una red eléctrica conductora entre las

nanofibras presentes en el material. Las conductividades eléctricas en continuo (σ_{dc}) registradas para las espumas con porcentajes de nanofibras > 10% en peso, ≈ 10^{-6} S.cm^{-1}, abren buenas perspectivas para su uso como materiales ligeros en aplicaciones de disipación y pintado electrostático en sectores como el de la automoción. Sin embargo, y como se verá en la última publicación incluida en esta sección (*Broad-band electrical conductivity of carbon nanofibre-reinforced polypropylene foams*), en la que no sólo se hace un estudio más exhaustivo del comportamiento eléctrico de estos materiales, extendiéndolo a un rango más amplio de frecuencias (tanto en corriente continua como alterna) y porcentajes de nanofibras de carbono (añadiendo porcentajes intermedios de 12.5, 15 y 17.5% a los ya indicados 5, 10 y 20%), estos valores, al haber sido realizados sobre muestras sin metalizar, resultaron ser ligeramente inferiores a los valores reales de conducción eléctrica del material, determinados sobre muestras previamente metalizadas.

El segundo artículo, publicado en la revista **Defect and Diffusion Forum, Vols. 297-301, 996-1001, 2010**, se centra en el estudio de la conductividad térmica de las espumas y respectivos precursores sólidos de PP reforzado con las nanofibras de carbono.

Aún siendo un tipo de refuerzo que se caracteriza, además de su elevada conductividad eléctrica, ya demostrada en la anterior publicación y más en detalle en la siguiente al haber resultado en un incremento de la conductividad eléctrica final de las espumas, por una igualmente elevada conductividad térmica, la incorporación de las nanofibras no resultó en un incremento significativo de la conductividad térmica de los materiales. En particular, el valor de conductividad final resultó prácticamente constante e independiente de la cantidad de nanofibras (≈ 0.3 W.m^{-1}.K^{-1}, prácticamente idéntico al valor obtenido para el PP, 0.26 W.m^{-1}.K^{-1}). Entre las posibles causas de este reducido valor de conductividad térmica podrían estar la rotura parcial de las nanofibras durante la etapa de composición en la extrusora de doble husillo debido a los elevados esfuerzos de cizalla generados y elevada grafitización y por tanto cierta fragilidad de las nanofibras (véase sección 3.1.4), además de una insuficiente dispersión para el mecanismo de transporte térmico. Contrariamente al mecanismo de conducción eléctrica, donde existe una concentración crítica de refuerzo a partir de la cual la

conductividad sube de forma abrupta debido a la formación de una estructura tridimensional de conducción eléctrica entre las nanofibras independientemente del tipo de mecanismo de conducción predominante (percolación, efecto de túnel, entre otros), se ha demostrado que el transporte térmico es más sensible a otras características como la interfase entre refuerzo y matriz. En otras publicaciones se ha observado cómo la incorporación en matrices poliméricas de refuerzos conductores en base carbono (nanotubos o nanofibras de carbono) resultó en incrementos marginales de la conductividad térmica de los nanocompuestos [23-24].

Aunque muy alejados de los valores esperados en base a la conductividad térmica teórica de las nanofibras, la conductividad de las espumas se vio incrementada al incorporar porcentajes crecientes de nanofibras de acuerdo con la regla de las mezclas, demostrando que la espumación puede ser usada como estrategia para incrementar la eficacia de la transferencia de calor a través de la matriz. El cálculo del valor teórico de conductividad del nanocompuesto sólido de PP con CNF a partir de los valores experimentales de conductividad de los distintos nanocompuestos sólidos y espumados en base a la regla de las mezclas (ξ = 1) y un modelo asumiendo un sistema de dos componentes (gas y material compuesto de PP con nanofibras) resultó en un valor de conductividad de 0.3 $W.m^{-1}.K^{-1}$, idéntico al valor determinado experimentalmente para los sólidos independientemente del porcentaje de nanofibras. Sin embargo, el comportamiento global de conducción térmica sigue siendo regulado por la fracción de gas presente en el material, al presentar las espumas un comportamiento de conducción térmica semejante al de las espumas de PP sin refuerzos (véase fig. 4.5.1).

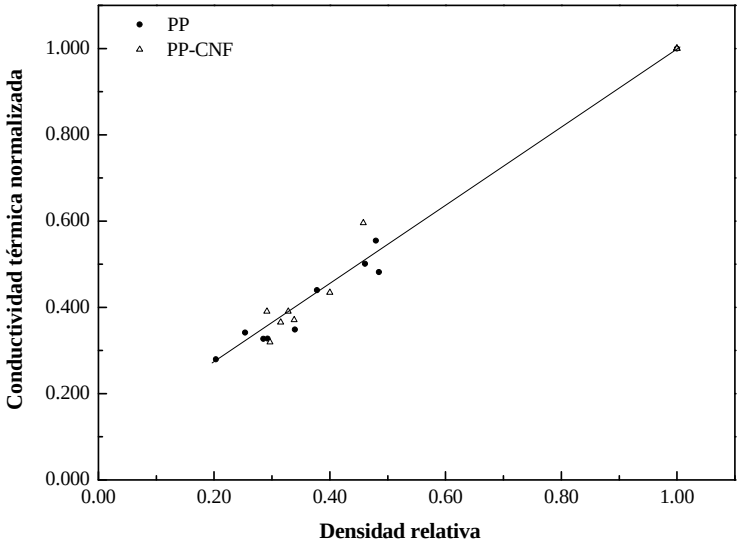

Figura 4.5.1. Conductividad térmica normalizada frente a la densidad relativa para las espumas de PP y PP con nanofibras de carbono (PP-CNF) y respectivos sólidos de referencia.

La última publicación incluida en esta sección dedicada a las espumas de PP con nanofibras de carbono, ***Broad-band electrical conductivity of carbon nanofibre-reinforced polypropylene foams***, aceptado para publicación en la revista **Carbon**, trata de extender el estudio preliminar de la conductividad eléctrica de estos materiales iniciado con el artículo *Characterization of carbon nanofibre-reinforced polypropylene foams* a frecuencias más elevadas, en que la conductividad eléctrica pasa a depender de la frecuencia (corriente alterna, ac). En base a los primeros resultados de conductividad eléctrica presentados en la ya referida primera publicación, se prepararon y estudiaron materiales con porcentajes intermedios entre los 10 y los 20%, en particular 12.5, 15 y 17.5%, con el objetivo de analizar más en detalle el mecanismo de conducción eléctrica en función del porcentaje de nanofibras y elucidar posibles efectos relacionados con la espumación de los nanocompuestos. En particular, y en lo que toca al análisis de la influencia de la estructura celular en el comportamiento de conducción eléctrica, se prepararon espumas de PP con 20% en peso de nanofibras de carbono por un proceso de disolución de CO_2 a elevada presión en autoclave, tratando de inducir una particular estructura celular con celdas altamente orientadas en una dirección específica (dirección de liberación de la presión), realizándose medidas de la conductividad eléctrica en dos direcciones diferentes, *through-plane*, esto es, en espesor, e *in-plane* (véase fig. 4.5.2),

comparándose estos valores con los obtenidos tanto para los precursores sólidos como para las respectivas espumas preparadas por compresión.

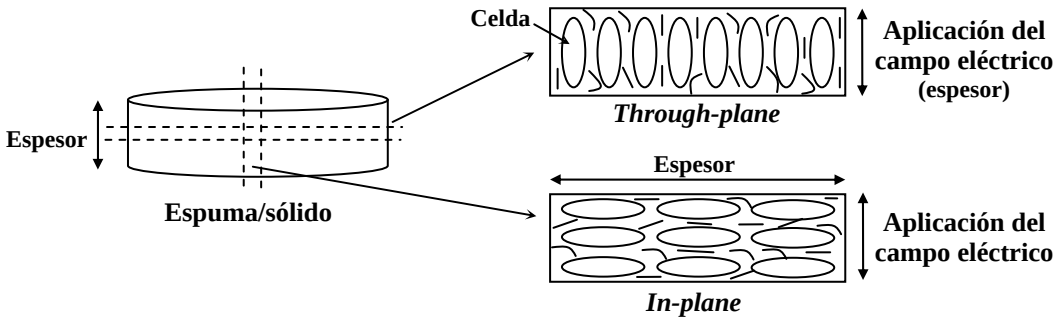

Figura 4.5.2. Esquema de las configuraciones *through-plane* e *in-plane* de medida de la conductividad eléctrica y orientación de las nanofibras de carbono en las espumas preparadas por disolución de CO_2.

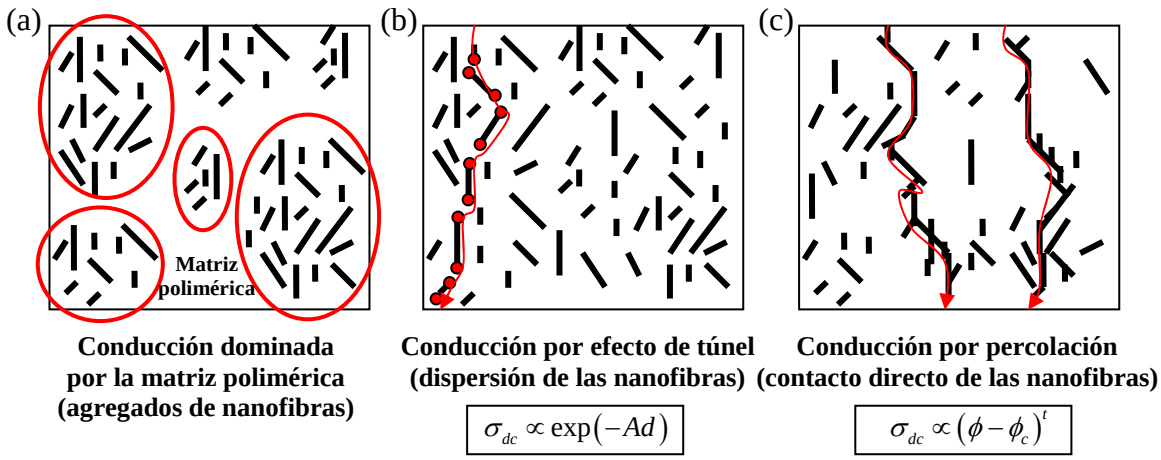

Figura 4.5.3. Esquema representando tres posibles situaciones de comportamiento eléctrico para los nanocompuestos de PP con CNF: (a) conducción dominada por la matriz polimérica, (b) conducción por efecto de túnel y (c) conducción por contacto físico entre las nanofibras (percolación). Nota: los puntos rojos representan los puntos de conducción eléctrica por efecto de túnel entre las nanofibras y las flechas el camino de conducción eléctrica.

En primer lugar, y aunque claramente las propiedades eléctricas tanto del compuesto sólido como de las espumas con un 5% en peso de nanofibras resultaron controladas por la matriz polimérica, con valores de conductividad cercanos a los de un

aislante como el PP, indicando que la gran distancia entre los agregados de nanofibras, asociada a una insuficiente dispersión durante la etapa de composición, impidió la formación de un camino conductor entre las mismas (véase fig. 4.5.3(a)), a porcentajes superiores sí que se constató un comportamiento de conducción eléctrica, tanto para los sólidos como para las espumas (véase fig. 4.5.4).

Comparando los materiales sólidos con las espumas, en estas se alcanzó antes, esto es, a menores concentraciones de nanofibras, un comportamiento considerado de conducción eléctrica, indicando la eficacia de la espumación en la formación de una red conductora a menores porcentajes de nanofibras, asociada a su superior dispersión promovida por el proceso de espumación. Aún presentando un comportamiento conductor eléctrico, este no es tan pronunciado en valores absolutos como sería expectable en base a la conductividad eléctrica teórica de las nanofibras (resistividad eléctrica de 10^{-3} Ω.m, esto es, conductividad de 10^{5} $S.cm^{-1}$ – véase tabla 3.9 del capítulo 3). Los inferiores valores de la conductividad eléctrica fueron asociados a un mecanismo de transporte eléctrico no por contacto directo entre las nanofibras (véase fig. 4.5.3(c)) sino más bien por un mecanismo de tipo efecto de túnel, asociado al transporte de los electrones por una nanofibra y salto a la siguiente a través de la matriz polimérica a partir de una determinada distancia crítica (distancia para la conducción por efecto de túnel, *d* – véase fig. 4.5.3(b)) [25-26].

Para valores superiores a la concentración crítica, la conductividad eléctrica apenas sube, ya que al estar las nanofibras demasiado rotas como para permitir la formación de una red conductora por contacto directo entre las mismas, predomina el mecanismo de transporte por efecto de túnel, y por ello superiores concentraciones de nanofibras resultan en subidas poco significativas de la conductividad. A esta situación habría que añadir la superior cristalinidad de la matriz polimérica al incrementar la cantidad de nanofibras y por ende superior dificultad en lograr una óptima conducción eléctrica a través de una matriz cada vez más cristalina (menor movilidad iónica) [27-30].

Realizando un análisis basado en una conducción eléctrica por efecto de túnel fue posible constatar cómo las espumas presentan un comportamiento más parecido al que sería expectable para un sistema formado por partículas conductoras con una geometría fibrilar distribuidas al azar, frente a un comportamiento más parecido al de un

sistema formado por partículas esféricas para los materiales sólidos. Esta diferencia, presentada en la fig. 4.5.4 (líneas continuas y punteadas), demuestra que la espumación promovió una superior dispersión de las nanofibras comparada con los materiales sólidos, con las nanofibras resultando considerablemente más aglomeradas en estos últimos (aglomerados de forma esférica, como los presentados esquemáticamente en la fig. 4.5.3(a)).

Aunque se observaron diferencias en la pendiente de comportamiento de la conductividad con la frecuencia para altos valores de esta última (valores superiores a la frecuencia crítica, ν_c, esto es, la frecuencia por debajo de la cual el valor de la conductividad pasa a ser constante), indicando la importancia que las nanofibras tienen en este rango, a diferencia de los nanocompuestos sólidos fue posible construir una curva maestra de comportamiento de la conductividad eléctrica para las espumas, que permite, dentro de ciertos límites, predecir su conductividad eléctrica en función del porcentaje de nanofibras.

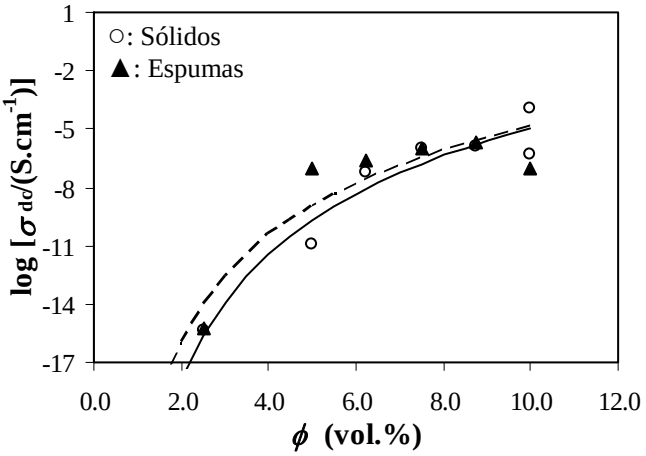

Figura 4.5.4. Log (σ_{dc}) vs. ϕ para las espumas de PP con CNF. Las líneas continuas y punteadas representan los valores predichos por el modelo de conducción por efecto de túnel respectivamente para partículas de geometría esférica y fibrilar distribuidas al azar.

Por último y de forma a elucidar la posible influencia que no sólo la concentración de nanofibras de carbono y su distribución/dispersión pero igualmente la estructura celular pueden tener en el comportamiento de conducción eléctrica de las

espumas, se realizaron medidas de conductividad eléctrica sobre espumas de PP con un 20% en peso de nanofibras preparadas por un proceso de disolución de CO_2, proceso por el cual se trató de establecer una estructura celular anisotrópica con celdas altamente orientadas en la dirección de descompresión. Se realizaron medidas de la conductividad eléctrica en espesor de la espuma (dirección *through-plane*), y en la dirección opuesta (*in-plane*), comparándose los valores con los obtenidos para el sólido de referencia y respectivas espumas preparadas por compresión. Se observó cómo la anisotropía celular generada induce una reorientación de las nanofibras de carbono, preferencialmente orientadas paralelas a la superficie tanto en los precursores sólidos preparados por moldeo por compresión como en menor medida en las espumas espumadas químicamente, en la dirección de crecimiento de la espuma (perpendiculares a la superficie), de esa manera resultando en valores más elevados de la conductividad en espesor. Así, las espumas preparadas por disolución de CO_2 presentan una conductividad eléctrica en continuo medida en espesor de 4.11×10^{-5} $S.cm^{-1}$, muy superior a la de las espumas con ADC, 9.35×10^{-8} $S.cm^{-1}$. Además, esta reorientación de las nanofibras resultó en espumas con un comportamiento eléctrico mucho más isotrópico, con las espumas preparadas por disolución de CO_2 presentando una conductividad *in-plane* prácticamente idéntica a la conductividad *through-plane*: 5.36×10^{-5} $S.cm^{-1}$.

4.5.3. Artículos publicados.

4.5.3.1. *Characterization of carbon nanofibre-reinforced polypropylene foams*.

Journal of Nanoscience and Nanotechnology
Vol. 10, 1–10, 2010

Characterization of Carbon Nanofibre-Reinforced Polypropylene Foams

M. Antunes*, J. I. Velasco, V. Realinho, and D. Arencón

Centre Català del Plàstic, Departament de Ciència dels Materials i Enginyeria Metal·lúrgica, Universitat Politècnica de Catalunya, C/ Colom 114, E-08222 Terrassa (Barcelona), Spain

In this paper, carbon-nanofibre-reinforced polypropylene foams were prepared and characterized regarding their foaming behaviour, cellular structure and both thermo-mechanical as well as electrical properties. Polypropylene (PP) nanocomposites containing 5, 10 and 20 wt% of carbon nanofibres (CNF) and a chemical blowing agent were prepared by melt-mixing inside a twin-screw extruder and subsequently water-cooled and pelletized. The extruded nanocomposites were later foamed using a one-step compression-moulding process. The thermo-mechanical properties of the CNF-reinforced PP foams were studied, analyzing the influence of the carbon nanofibres on the cellular structure and subsequent thermo-mechanical behaviour of the foams. Carbon nanofibres not only seemed to act as nucleating agents, reducing the average cell size of the foams and increasing their cell density for similar expansion ratios, but also helped produce mechanically-improved foams, even reaching for the 20 wt% CNF-reinforced ones a specific modulus around 1.2 GPa·cm^3/g for densities as low as 300 kg/m^3. An increasingly higher electrical conductivity was assessed for both the solids as well as the foams with increasing the amount of carbon nanofibres.

Keywords: Carbon Nanofibres, Polypropylene, Foams, Electrical Conductivity.

RESEARCH ARTICLE

1. INTRODUCTION

The use of small amounts of high-aspect ratio nanoscale reinforcements such as carbon nanotubes (CNT) and carbon nanofibres (CNF) combined with polymer's low densities makes them ideal candidates for high performance polymer composite systems.[1–4] The main difference between CNFs and CNTs is in the orientation of the graphene planes, the first of the two often showing a wide range of orientations with respect to the fibre axis. Carbon nanofibres can be seen as having a stacked-cup graphitic structure, for that being intrinsically less perfect due to surface graphitic edge terminations. Although affecting their mechanical and mostly transport properties, these imperfections allow CNFs to be far cheaper than commercially available multi-wall carbon nanotubes. If we consider that in some processes CNFs are obtained in the form of hollow tubes with an outer diameter as small as 5 nm, although typical values are around 50 to 100 nm, these come as a possible solution for the lack of availability in considerable quantities of high quality carbon nanotubes.

Several methods are nowadays used for the production of both carbon nanotubes and nanofibres, thus the different carbon nanostructures commercially available, with different diameters, aspect ratios or crystallinities. All these dramatically affect their intrinsic properties, as well as their processing and global behaviour in composite systems. The selection of such carbon nanostructures will mainly depend on the matrix, the processing technology, as well as the final goal(s) to be reached regarding the final composite mechanical and transport properties. CNTs and CNFs production methods can be divided into two categories, the first of which includes arc-discharge or laser ablation, and chemical vapour deposition (CVD) methods; the second considers all the catalytic-grown processes.[4] Among the second, the so-called floating catalyst technique, in which a metallic catalyst is directly carried in the carbon source gas stream inside a continuous flow reactor at temperatures close to 1100 °C,[5–8] allows the continuous production of high-graphitized carbon nanofibres, commonly referred to as sub-micron vapour grown carbon fibres (s-VGCF) due to their extremely small diameters (20–80 nm), with properties comparable to that of some types of carbon nanotubes.

Also challenging is the dispersion and distribution of such nano-reinforcements in polymer matrices. Conventionally, three different approaches have been considered

*Author to whom correspondence should be addressed.

when incorporating such nanofillers:[4] liquid-state mixing (*in-situ* polymerization), solution-mediated processes and direct melt-blending, the last of the three being the most commercially attractive because it allows the use of conventional plastic processing technologies such as extrusion or injection moulding. None the less, these are in some cases hard to apply not only due to the lack of high nanofiller quantities but mainly due to the formation of entanglements and aggregates between the individual nanotubes/nanofibres during processing. These are due to the out-of-plane π interactions that form between their surfaces, especially in the case of carbon nanotubes, and that can even lead to re-entanglement during the melt mixing process. Good nanofiller dispersion and distribution depends not only on the type of nanofiller's structure, for instance nanotubes being far more sensible than nanofibres due to their higher crystallinity and less graphitic surface imperfections, but also on the type of blending prior to conventional extrusion or injection mixing. This previous step is needed due to the apparent low density of the as-produced powder filler. High shear forces are necessary during this first stage for good nanofibre dispersion, the intrinsic high viscosity of thermoplastics minimising reaggregation.[9–11]

Although all these considerations, even at low filler loadings clusters are commonly observed after melt mixing. Several approaches have been considered in order to reduce these aggregates, such as surface modification of the as-received nanofiller, for instance introducing defects on their surface,[12] limiting π–π surface interactions and thus their aggregation, but also intrinsically reducing their mechanical as well as transport properties; nanofiller coating,[13–14] this way also limiting interactions between the individual nanofibres/nanotubes, among others.[15–18] None the less, all these techniques not only are cost-effective, but also tend to affect and decrease the nanofiller's efficiency. That is why a controlled melt-blending using less crystalline nanofillers such as carbon nanofibres, not as sensible to surface interactions as the nanotubes and thus to re-entanglement, may help produce mechanically/electrically/thermally-improved carbon nanofiller-reinforced composites.

Although highly difficult, several works have focused on determining the mechanical and transport properties of individual carbon nanotubes and nanofibres. All have found their efficiency in polymer matrices to be far from the theoretically expected values based on their individual properties.[2, 10, 19–20] This is mainly due to fibre breaking and buckling due to extensive shear during processing, cluster formation, etc. None the less, the addition of these nanofillers seem to improve the materials stiffness, results apparently showing this effect to be more prominent in semicrystalline rather than amorphous polymers.[3, 19, 21–23] Although interesting, the main current CNTs/CNFs application in polymer matrices is still as conductive fillers, its use starting to be somewhat widespread as an alternative to carbon black across the automotive and electronic sectors.[4] A characteristic electrical percolation threshold is commonly observed for these nanofiller-reinforced thermoplastic composites, the electrical conductivity abruptly increasing after a certain loading content, known as the percolation threshold, indicating the formation of a 3-D conductive carbon network. For carbon nanofibre-reinforced systems, this value is normally between 5 to 10 vol% of CNF.[24–26]

Alongside the incorporation of such carbon-based nanofillers in polymer matrices for improving properties such as the normally intrinsically low polymer electrical or thermal conductivities, there is an increasing interest in extending even further the specific properties range of such materials by foaming the base matrix. Our research group possesses considerable experience in producing and characterizing different types of polypropylene-based foams,[27–28] thus the interest in extending the polypropylene-foamed materials possibilities by incorporating conductive nanofillers. As in our case the final reinforced material is formed by a foamed matrix, it is important to study it both mechanically as well as thermally as a previous step for producing electrically/thermally improved foams by introducing carbon nanofibres. That is why the thermal conductivity of polypropylene foams produced using different foaming processes was assessed,[28] results indicating to be mainly affected by the bulk density of the foam, especially for relative densities higher than 0.2. For relative densities lower than this value the effect of the processing method is more significant, thermal conductivity being affected by the foam's cellular structure (cell size and cell orientation).

At the same time, scarce work has been dedicated to the preparation and applications of thermoplastic foams filled with conductive nanofillers. For instance, conductive carbon nanofibre-PS lightweight foam structures for EMI shielding applications have been considered,[29] results indicating that such foam structures are electrically conductive with a percolation threshold similar to that of the respective solids. In another work,[30] the inclusion of CNFs resulted in a decrease in the cell size of PS foams, macroscopic strength enhancement being observed with increasing CNF's content. The physical properties of silicone foams filled with carbon nanotubes have also been studied,[31] the incorporation of the nanofiller affecting the final foam density and cellular structure. Thermal stability was also drastically affected, with an increase of the degradation temperature of more than 50 °C.

The main goal of this work is to produce lightweight mechanically/electrically/thermally improved polypropylene materials for applications such as electrostatic painting by incorporating low loadings of carbon nanofibres using conventional melt-blending processing.

2. EXPERIMENTAL DETAILS

2.1. Materials and Compounding

A specifically formulated polypropylene-based matrix for foaming applications was melt-compounded using a co-rotating twin-screw extruder (Collin Kneter 25 × 36D, $L/D = 36$) at a constant temperature of 165 °C and constant rotating speed of 160 rpm. Three different carbon nanofibre weight percentages were used: 5, 10 and 20 wt%.

The carbon nanofibres used in this work were submicron vapour grown carbon fibres (s-VGCF) with a stacked-cup type of structure produced using a floating catalyst technique by Grupo Antolín Ingeniería, S. A. (Burgos, Spain), with a typical diameter of 20 to 80 nm, a fibre length >30 μm, a bulk density of 1.97 g/cm^3, a specific surface area BET (N_2) between 150 and 200 m^2/g, an inherently high graphitization degree of 70% with a low metallic particles content (6–8%) and an electrical resistivity of 10^{-3} $\Omega \cdot$m and theoretical Young's modulus of 230 GPa.

2.2. Foaming Process

Discs with a nominal diameter of 74 mm and thickness of 3.5 mm were compression-moulded in a hot-plate press (IQAP-LAP PL-15). The previously extrusion-compounded composite pellets were initially placed into a steel mold in order to slightly overfill it and subjected to heating at 170 °C for 4 min until melting, followed by a final step at the same temperature and applying a constant pressure of 20 bar for 2 min. The resulting discs were cooled under pressure (20 bar) using recirculating water. A single-step compression-moulding foaming process was used, the previously prepared solid discs being placed in the circular mould and heated at a temperature of 195 °C for 15 min applying a constant pressure of 40 bar.

2.3. Testing Procedure

Density of the solid discs and respective foams was measured according to standard procedures (ASTM D1622). A TGDTA92 Setaram device was used to evaluate the thermal decomposition of the several PP-CNF composites by performing thermogravimetric analysis (TGA) in air flow at a heating rate of 20 °C/min from 25 to 1000 °C.

In order to obtain the open-cell content of each specimen expressed as the percentage of the calculated volume, the geometric volume (V) and the displacement volume (V_p) of each foamed sample were determined. The geometric volume was determined by measuring the weight of the samples using a balance and a foam density based on the water displacement method described in ASTM D792. The displacement volume was determined using an air pycnometer. Since every analyzed sample could only be obtained by cutting, a fraction of the closed cells were opened due to specimen preparation. A correction procedure based on the use of the cell dimensions of the specimen was used, and corrected open-cell content values (O_v) were determined as follows:

$$O_v(\%) = \frac{V - V_p - V_s}{V} \times 100 \quad (1)$$

where V_s takes into account the volume occupied by the surface cells. All open-cell content and correction calculation procedures are described in ASTM D6226.

The cellular structure of the foams was observed using a JEOL JSM-5610 scanning electron microscope (SEM). Samples were fractured at low temperature and made conductive by sputtering deposition of a thin layer of gold-palladium. Low-magnification micrographs were analyzed using the intercept counting method,[32] measuring the distance between pairs of cell walls along 10 reference lines, in order to obtain the average cell size (ϕ) and cell density. The average cell size, being the most used cell structure parameter,[33–34] was determined using the procedure presented in Ref. [35]. Considering the type of foaming process used in this study, two different cell sizes were determined from cellular structure analysis: ϕ_{VD}, with VD stating for Vertical Direction, in this case being the cell size in the direction of pressure release, and ϕ_{WD}, being the cell size measured perpendicularly (Width Direction). The anisotropy ratio (AR), defined as the ratio between the highest (ϕ_{VD}) and smallest (ϕ_{WD}) characteristic cell sizes, was assessed for the different foams using a representative cell population. Cell density was determined for each foamed sample from the different low-magnification micrographs using the counting method.

Nanocomposite morphology was studied using a HITACHI H-800 transmission electron microscope (TEM) on ultramicrotomed sheets (Ultracut E from Reichert-Jung) with a typical thickness of 60 nm.

Differential scanning calorimetry (DSC) was used to study eventual changes in the thermal characteristics of the polypropylene matrix due to the foaming process and the presence of the carbon nanofibres. A Perkin Elmer Pyris 1 model with a glycol-based Perkin Elmer Intracooler IIP calorimeter was employed with samples weighting around 8.0 mg. The following program was used applying a constant rate of nitrogen: heating from 30 to 200 °C at 10 °C/min and holding for 1 min to erase the thermal history before cooling at 10 °C/min from 200 °C to 30 °C. After a second isothermal step (1 min) at 30 °C, the samples were heated a second time at 10 °C/min from 30 °C to 200 °C to analyze the PP melting signal.

The crystallinity percentage (X_c) was determined according to the following equation:

$$X_c^m(\%) = \frac{\Delta H_m}{\Delta H_m^0 w_p} \times 100 \quad (2)$$

where w_p is the weight fraction of PP, ΔH_m is the melting enthalpy of the sample and ΔH_m^0 the theoretical, 100% crystalline, polypropylene enthalpy (207.1 J/g[36]). A minimum of five experiments were done for each material.

In order to study the viscoelastic behaviour of the polymer matrix and how the foaming process as well as the presence of different amounts of carbon nanofibres may affect it, dynamic mechanical analysis (DMA) experiments were carried out at low strain and frequency values. The DMA equipment (TA Instruments Q800 Dynamic Mechanical Analyzer, DMA) was calibrated according to the standard procedure. The storage modulus (E'), loss modulus (E'') and loss tangent (tan δ) were obtained in a three-point bending configuration using a span length of 50.00 mm. Two configurations, P (parallel to the foam's surface) and N (perpendicular) were considered. In order to obtain the dynamic mechanical properties as a function of the temperature, experiments were performed under nitrogen atmosphere at a frequency of 1 Hz from −20 to 150 °C at a heating rate of 2 °C/min using liquid nitrogen as cryogenic fluid. A static strain of 2% and a dynamic of 0.02% with a preload force of 0.01 N and force track of 120% were chosen. Test specimens were prepared in prismatic shape with a nominal length of 55.00 ± 0.10 mm, width of 13.00 ± 0.10 mm and thickness of 3.00 ± 0.05 mm in the case of the solids and 3.50 ± 0.10 mm for the foamed samples.

The electrical conductivity of the several solid and respective foamed composites was measured as a function of the frequency between 10^{-2} and 10^6 Hz using an impedance analyzer (HP 4192 A LF). A typical thickness of 130 μm and 1.8 mm was respectively used for the solid and foamed materials, with the measurements being made directly over their surface without metallic conductive coating.

3. RESULTS AND DISCUSSION

3.1. Foaming Behaviour and Cellular Structure

The main foaming behaviour and cellular structure results are presented in Table I and Figure 1. As can be seen, PP-CNF nanocomposite foams were prepared with a typical expansion ratio (ER) of around 3 (3.2 for both PP + 5 wt% CNF and PP + 10 wt% CNF and slightly lower, 3.0, for PP + 20 wt% CNF), that is, a bulk density of ≈300 kg/m^3, and in all cases showed a closed-cell type of cell structure, with an open-cell content of less than 10%. The analysis

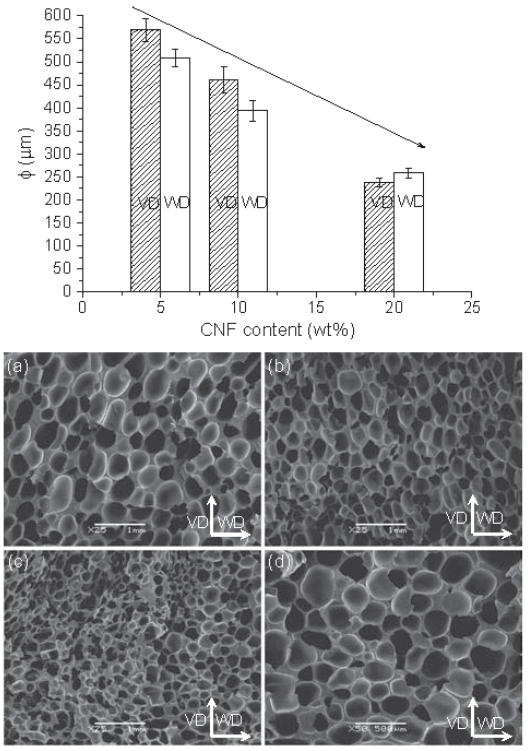

Fig. 1. Average cell size as a function of the CNF content for the PP-CNF nanocomposite foams; characteristic SEM pictures (×25) of (a) PP + 5 wt% CNF, (b) PP + 10 wt% CNF, (c) PP + 20 wt% CNF; (d) SEM picture at a higher magnification (×50) of the PP + 20 wt% CNF foam. VD: Vertical direction of foaming; WD: Width direction.

of the cellular structure for the different foamed samples was done using low and high-magnification SEM pictures, the most characteristic ones being shown in Figure 1. The characteristic cell parameters are compiled alongside the expansion ratio and the open-cell content in Table I.

As it is clearly seen, not only CNFs contribute to obtain an isotropic-type of cell structure (anisotropy ratios, AR, close to 1 in all cases), they also act as nucleating sites promoting cell bubble nucleation and thus finer cell structures. For similar expansion ratios, smaller cell sizes are obtained with increasing the amount of carbon nanofibres. The 5 wt% CNF foams exhibited an average cell size a bit higher than 500 μm (≈570 μm in VD direction and ≈510 μm in WD); increasing the CNF content

Table I. Cellular structure characterization results of the studied foams.

CNF content (wt%)	ER	O_v (%)	ϕ_{VD} (μm)	ϕ_{WD} (μm)	AR	Cell density (cells/cm^3)
5	3.2	569.2 ± 25.0	508.2 ± 18.8	1.1	8.126×10^3	
10	3.2	<10.0	461.5 ± 28.4	393.6 ± 22.0	1.2	1.347×10^4
20	3.0		238.8 ± 10.0	258.3 ± 11.0	0.9	3.049×10^4

to 10 wt% resulted in the decrease of the average cell size to ≈460 μm in VD direction and ≈400 μm in WD; finally, the 20 wt% CNF foams showed an average cell size around half of that of the 5 wt% ones ($\phi_{VD} \approx 240$ μm and $\phi_{VD} \approx 260$ μm), as seen when comparing Fig. 1(a)) with Fig. 1(d)).

High magnification SEM pictures (Fig. 2) allowed to visualize the dispersion and orientation of the carbon nanofibres alongside the cell walls of the foams. Although some bundle-like aggregates were observed after melt blending the materials and even after foaming them (Fig. 2(e)), these were a lot more disperse than in similar thermoplastic CNTs composites.[37] Normally the challenge of these types of carbon nanofiller-reinforced materials is in breaking the aggregates that tend to form between the carbon nanotubes/nanofibres due to out-of-plane $\pi-\pi$ surface interactions, that is, being able to separate them, but at the same time maintaining a 3D type of continuous conductive carbon network, allowing the material to be electrically conductive. Due to the fact that this network is favoured with the formation of local CNF clusters, the presence of some of these together with individual nanofibres should help to obtain a both mechanically as well as thermally and electrically-conductive improved material. This means that if it is possible to control and limit the formation of these aggregates, conductive PP-CNF foams

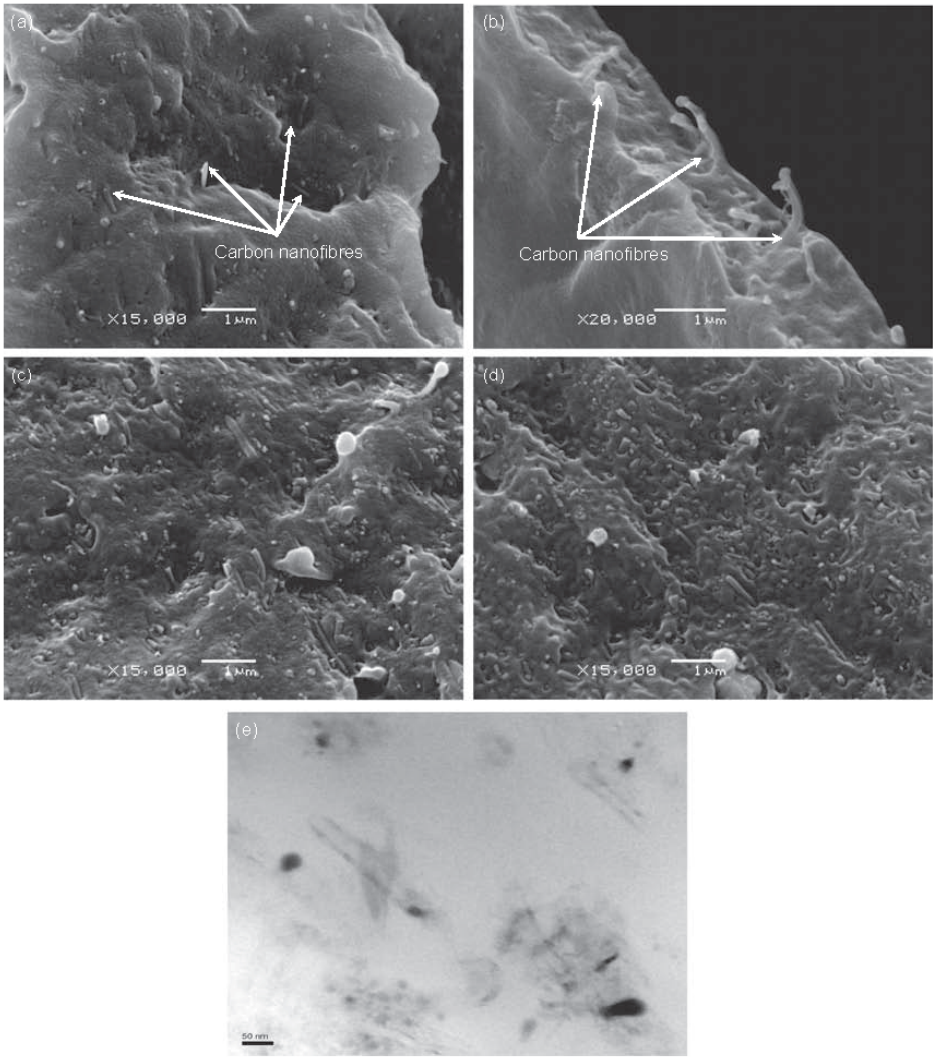

Fig. 2. High magnification SEM pictures of: (a) (×15000) and (b) (×20000) PP + 5 wt% CNF, (c) PP + 10 wt% CNF (×15000) and (d) PP + 20 wt% CNF (×15000) foams; (e) TEM picture showing a typical CNF distribution.

could be obtained using conventional processing/foaming technologies even for low nanofiller contents.

3.2. Thermal Analysis

The thermogravimetric analysis (TGA) of the several PP-CNF composites in air atmosphere is shown in Figure 3. The weight loss starting at around 450 °C and ending at approximately 500 °C corresponds to the decomposition of polypropylene, the final residues corresponding to the amount of carbon nanofibres present in the material. The final weight loss step at around 650–675 °C is related to the graphitization of the carbon nanofibres, resulting in an amorphous-type of carbon residue.

The viscoelastic behaviour of the polymer matrix previous and after foaming and how the presence of different amounts of carbon nanofibres may affect it was analyzed using dynamic-mechanical analysis (DMA) at low frequency and strain values. At low strain values, the main mechanisms governing the materials response are bending and stretching of the cell walls, and thus the viscoelastic behaviour of the matrix is predominant and can be assessed. First of all, and prior to analyze the DMA results of the several solid and foamed materials, it has to be stated that PP commonly shows at least two DMA relaxations, conventionally known as α and β (or T_g). The first

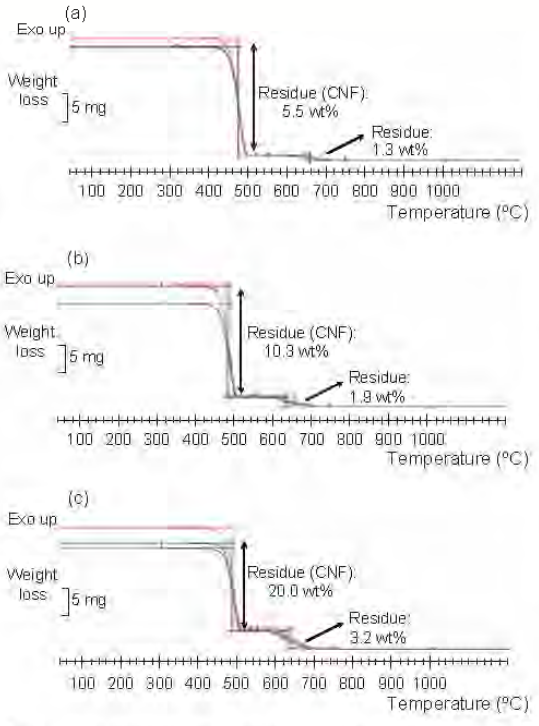

Fig. 3. TGA curves obtained in air at 20 °C/min for the (a) PP + 5 wt% CNF, (b) PP + 10 wt% CNF and (c) PP + 20 wt% CNF nanocomposites.

of the two is commonly observed between 100 and 130 °C for solid PP, and it is a crystal relaxation that depends on crystal morphology, being related to crystalline lamellae movements and crystalline phase rotations. The β transition, also known as T_g or glass transition temperature, is commonly observed between −10 and 10 °C and is the glass-rubber relaxation of the amorphous portions of the solid.

DMA curves of the several materials (solids and foams) are presented in Figure 4. As can be seen, the loss factor (tan δ) is presented as a function of the temperature separately for each CNF content, and a characteristic tan δ curve is presented for both the unfoamed as well as the foam measured in a direction parallel (P) and perpendicular (N) to its surface. The glass transition is detected as a very intense peak at around 2 to 7 °C; meanwhile, the α transition is seen as a very broad transition starting at around 50–60 °C and ending at approximately 80–100 °C.

If we start by analyzing the influence of CNF's presence in the glass transition, we can see that the T_g increases with increasing the CNF content, from 5.2 °C in the case of the solid 5 wt% CNF to 7.3 and 7.5 °C respectively in the case of the 10 and 20 wt% CNF. This means that the matrix mobility is being influenced by the presence and increasing amount of carbon nanofibres. None the less, its value decreases with foaming for all the materials: in the PP + 5 wt% CNF from the 5.2 °C of the solid material to 4.5 and 2.5 °C of the P and N configuration foam; in PP + 10 wt% CNF from 7.3 °C of the solid to 6.9 and 5.2 °C of the P and N configuration foam; and in PP + 20 wt% CNF from 7.5 °C of the solid to 4.5 and 4.3 °C of the P and N configuration foam.

As expected, Table II shows how the storage modulus (E') increases with increasing the amount of carbon nanofibres. In the case of the foams, the storage modulus depends mainly on the relative density, only slightly increasing with CNF's content. None the less, if the specific modulus, i.e., the storage modulus relative to the foam's density, is to be compared, we reach the conclusion that it is increasing with adding more nanofibres (around 800 MPa·cm^3/g for the 5 wt% CNF foams, 1000 MPa·cm^3/g for the 10 wt% CNF foams and around 1200 MPa·cm^3/g for the 20 wt% CNF foams), indicating the carbon nanofibres efficiency as mechanical reinforcements.

If we introduce a parameter (S_1) that takes into account the amount of amorphous phase present and/or its mobility, we can quantify the possible differences due not only to the presence of different CNF contents but also due to foaming:

$$S_1 = \frac{E'_b - E'_a}{E'_a} \quad (3)$$

where E'_a and E'_b are respectively the storage modulus values before (measured at −20 °C) and after the transition (measured at the temperature of the inflexion point after the T_g maximum in the tan δ curve).

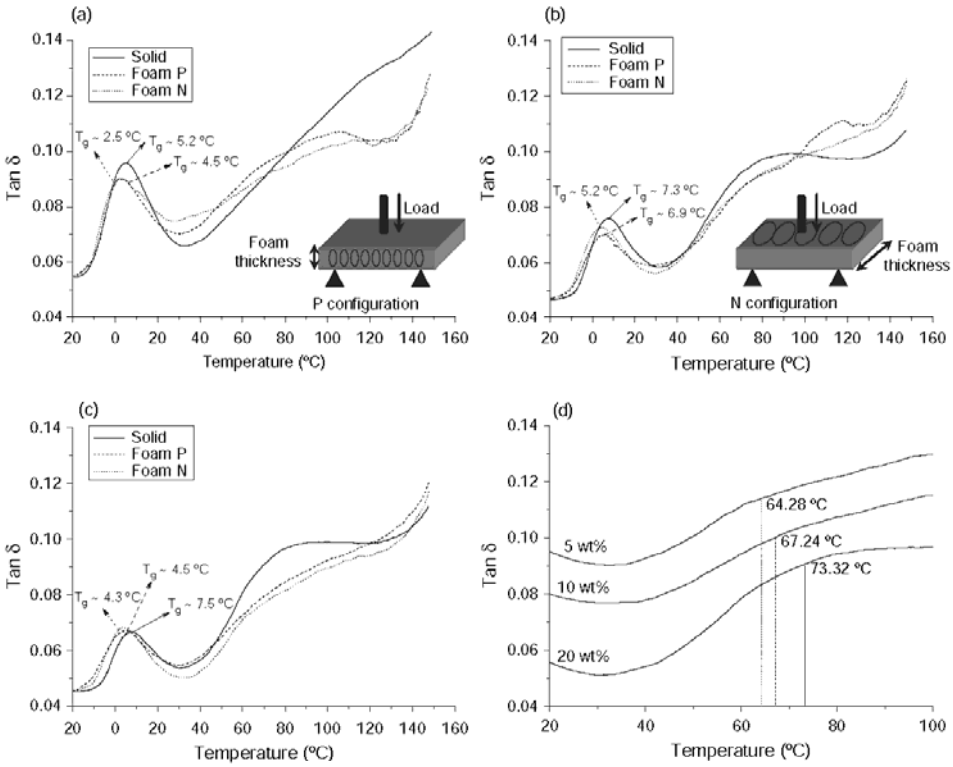

Fig. 4. Loss factor (tan δ) curves for (a) PP+5 wt% CNF, (b) PP+10 wt% CNF and (c) PP+20 wt% CNF solid and foamed nanocomposites; (d) tan δ curve showing a typical α transition behaviour for the 5, 10 and 20 wt% CNF nanocomposites. P: Parallel to the foam's surface; N: Perpendicular to the foam's surface.

As can be seen in Table II, with increasing the amount of CNF the value of S_I decreases for the solid materials, from 0.485 for the 10 wt% CNF to 0.412 for the 20 wt%, indicating a higher crystallinity of the 20 wt% CNF nanocomposites induced by the nucleating effect of the nanofibres or less mobility of its amorphous phase. Foams, independently of the amount of nanofibres, show a higher S_I value, in conformity with the lower T_g values presented previously.

Analyzing the α transition (Fig. 4(d)), its characteristic temperature (T_α), obtained as the intersection of the tangent to the steepest slope of the tan δ curve and the tangent to the final transition plateau, increases with increasing the amount of nanofibres (from approximately 64 °C for the 5 wt% CNF to a value higher than 73 °C for the 20 wt% CNF) but decreases with foaming, thus supporting the higher crystallinity previously stated when comparing S_I parameter values.

Table II. DMA results of the solid PP-CNF nanocomposites and respective foams.

CNF content (wt%)	Solid/foam	ER	Direction	T_g^* °C	E' at 20 °C (MPa)	Specific modulus (MPa·cm³/g)	S_I
5	Solid	1	—	5.2	1827.5	1827.5	0.868
	Foam	3.2	P	4.5	235.4	801.5	0.768
			N	2.5	209.6	713.6	0.824
10	Solid	1	—	7.3	2300.3	2300.3	0.485
	Foam	3.2	P	6.9	231.4	806.6	0.500
			N	5.2	328.6	1100.9	0.562
20	Solid	—	—	7.5	2732.7	2732.7	0.412
	Foam	3.0	P	4.5	543.5	1230.0	0.510
			N	4.3	473.6	1185.5	0.521

*T_g—Glass transition temperature measured in tan δ.

Differential scanning calorimetry (DSC) results support the higher nucleation rate induced by the nanofibres. Higher crystallization temperatures were observed with increasing the amount of nanofibres: from 130.2 and 126.7 °C corresponding respectively to the beginning and maximum of the crystallization peak observed during the cooling step for the polypropylene matrix without nanofibres, to 135.6 and 131.8 °C for the 20 wt% CNF material. A steady increase of around 2 °C was observed for both crystallization temperatures with adding increasingly amounts of CNFs (comparing the peak's maximum, from the already mentioned 126.7 °C for the material without nanofibres, to 128.8 °C for the 5 wt%, 129.6 °C for the 10 wt% and 131.8 °C for the 20 wt%). Crystallinity values, determined using Eq. (2) taking into account the weight fraction of PP in each material, also support the results observed using DMA in both T_g and β relaxations, with a steady increase from the 46.2% of the material without nanofibres, to 46.5, 48.9 and 49.6%, respectively for the 5, 10 and 20 wt% CNF materials.

3.3. Electrical Conductivity Measurements

The incorporation of carbon fillers to polymers leads to an electrical behaviour that tends to show an electrical percolation value, below which the electrical properties of the composite are controlled by the matrix because the conductive particles are too far appart; at a certain filler concentration value (known as the critical concentration, ϕ_c, or percolation threshold), local clusters of particles form a conductive 3D network, resulting in an exponential jump in the electrical conductivity; higher concentrations only slightly increase the electrical conductivity, and thus its specific value stays almost unaltered. The main consideration is in reducing this critical concentration value in order for these less conventional carbon fillers to be competitive with the already well-known carbon black.

In Figure 5 the electrical conductivity (σ) of the several solid and foamed CNF nanocomposites is shown as a function of CNF's content. Clearly, both the solid as well as the foamed 5 wt% CNF composites show an electrical conductivity typical of that of insulating materials such as polypropylene, indicating that under these conditions, a 5 wt% CNF content is not enough to create a conductive network throughout the matrix. So, the electrical conductivity is being controlled by the matrix, thus a final σ of approximately the value of solid isotactic PP (around 10^{-16} S/cm). A totally opposite behaviour was found for the solid 20 wt% CNF composites, showing a typical semiconducting electrical behaviour. The 10 wt% CNF composites show a behaviour that is somewhat between the non-conductive 5 wt% CNF and the highly conductive 20 wt%. In both cases (10 and 20 wt% CNF unfoamed and foamed composites), a typical conductive material behaviour as a function of the frequency is observed, with a critical frequency value (ν_c) below which conductivity gets frequency independent. This frequency-independent electrical conductivity value is known as the dc conductivity. As shown in Figure 5, representing this dc conductivity versus the CNF content we observe an increasingly higher electrical conductivity with increasing the amount of carbon nanofibres: 1.04×10^{-15} S/cm and 1.84×10^{-14} S/cm, respectively for the 5 wt% CNF solid and foamed material, 1.81×10^{-9} S/cm and 2.09×10^{-10} S/cm for the 10 wt% CNF solid and foamed material and 3.91×10^{-2} S/cm and 5.11×10^{-6} S/cm for the 20 wt% solid and foam. If we take into account that the electrostatic paintability limit is around 10^{-6} S/cm, we can see that the foamed 20 wt% CNF materials, even for expansion ratios higher than 3 (≈300 kg/m^3), show promising electrical properties (5.11×10^{-6} S/cm) in this field. Although it is clearly seen that a 5 wt% amount of carbon nanofibres was just not enough to produce an electrically conductive composite material, the differences found between the 10 and 20 wt% solid and foamed materials do not allow to conclude if the percolation threshold is between 5 and 10 wt% CNF or between 10 and 20 wt%, mainly due to the fact that measurements were done directly over the surface of the samples without metallic conductive deposition. Complementary electrical conductivity measurements should be done on samples coated with a thin conductive layer in order to elucidate the percolation threshold concentration.

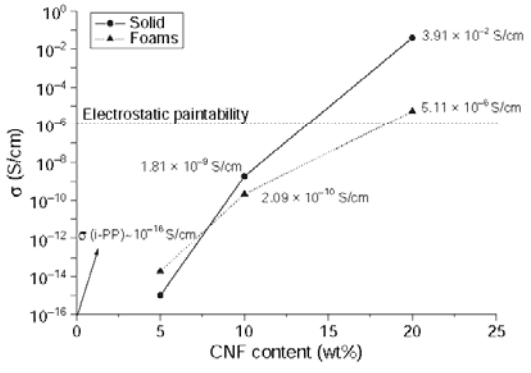

Fig. 5. Electrical conductivity (σ) as a function of CNF's content for the several solid and foamed PP-CNF nanocomposites.

4. CONCLUSIONS

This paper presents the characterization of chemically-foamed compression-moulded carbon nanofibre-reinforced polypropylene foams, regarding their foaming behaviour and final cellular structure, as well as their thermo-mechanical and electrical conductivity properties, with the main objective of producing lightweight rigid mechanically/electrically-improved PP materials for electrical applications.

Regarding the cellular structure of the as-produced foams, the incorporation of different carbon nanofibres

contents (5, 10 and 20 wt%) to a PP matrix and later foaming resulted in the formation of an increasingly finer isotropic cell structure with increasing the amount of carbon nanofibres, with anisotropy ratios close to 1 in all cases and an average cell size decrease from the approximately 500 μm of the 5 wt% CNF foams to almost half of it ($\approx$250 μm) in the case of the 20 wt% ones, indicating a bubble nucleation effect promoted by the presence of the nanofibres.

Different glass transition (β or T_g) and α relaxations values, determined by dynamic-mechanical analysis (DMA), were attained to the different local crystallinities induced by the presence of different CNF contents, mainly if we consider that similar expansion ratios (around 3) and cellular structures were obtained for the three foamed composites. With increasing the amount of carbon nanofibres, the unfoamed materials showed both a higher glass transition as well as α relaxation temperatures, indicating a higher crystallinity induced by the nanofiller. Higher crystallization temperatures and crystallinities with increasing the carbon nanofibres content, determined using differential scanning calorimetry (DSC), support these conclusions. When comparing specific storage modulus values, the mechanical efficiency of the nanofibres is observed, its value increasing from around 800 MPa $\cdot$ cm^3/g for the 5 wt% CNF foams to around 1200 MPa $\cdot$ cm^3/g for the 20 wt% ones.

Although the electrical properties of the 5 wt% CNF composite were controlled by the polypropylene matrix, indicating that the nanofibres were too far apart, a typical electrical conduction behaviour was observed for both the solid as well as the foamed 10 and 20 wt% CNF composites. None the less, an electrical percolation threshold concentration (ϕ_c) could not be assessed. In the particular case of the 20 wt% CNF composites, both the solid as well as the foamed materials, even for expansion ratios higher than 3 ($\approx$300 kg/m^3), showed promising electrical conductivities (>10^{-6} S/cm) for electrostatic painting.

Future experiments should consider the influence of coating a thin conductive layer to improve the electrical contact between the impedance analizer electrodes and the sample's surface on the conductivity values, and thus clarify the possible presence of a critical percolation concentration.

Acknowledgments: Financial assistance from the Spanish Ministry of Science and Education for the project MAT2007-62956 is gratefully acknowledged.

References and Notes

1. J.-P. Salvetat, A. J. Kulik, J.-M. Bonard, G. A. D. Briggs, T. Stökli, K. Metenier, S. Bonnamy, F. Beguin, N. A. Burnham, and L. Forro, *Adv. Mater.* 11, 161 **(1999)**.
2. J. Sandler, P. Werner, M. S. P. Shaffer, V. Demchuk, V. Altstädt, and A. H. Windle, *Comp. Part A* 33, 1033 **(2002)**.
3. G. G. Tibbetts and J. J. M. Hugh, *J. Mater. Res.* 14, 2871 **(1999)**.
4. M. Shaffer and J. Sandler, Processing and Properties of Nanocomposites, edited by S. Advani, World Scientific **(2006)**, p. 1.
5. G. G. Tibbetts, D. W. Gorkiewicz, and R. L. Alig, *Carbon* 31, 809 **(1993)**.
6. C. Merino and P. Soto, Furnace for the manufacture of carbon fibers, procedure for obtaining using said furnace and the fiber thus obtained. Grupo Antolín Ingeniería, S. A., European Patent Application EP04381014 **(2005)**.
7. European Patent Application EP04381015: Gas reusing system for carbon fiber manufacturing processes. Grupo Antolín Ingeniería, S. A.
8. European Patent Application EP2007009540: Carbon nanofibers and procedure for obtaining said nanofibers. Grupo Antolín Ingeniería, S. A.
9. C. A. Cooper, D. Ravich, D. Lips, J. Mayer, and H. D. Wagner, *Comp. Sci. Tech.* 62, 1105 **(2002)**.
10. W. Tang, M. H. Santare, and S. G. Advani, *Carbon* 41, 2779 **(2003)**.
11. E. T. Thostenson and T.-W. Chou, *J. Phys. D: Appl. Phys.* 35, 77 **(2002)**.
12. Y.-P. Sun, *Acc. Chem. Res.* 35, 1096 **(2002)**.
13. S. Bredeau, L. Boggioni, F. Bertini, I. Tritto, F. Monteverde, M. Alexandre, and P. Dubois, *Macromol. Rapid Commun.* 28, 822 **(2007)**.
14. A. Toti, G. Giambastiani, C. Bianchini, A. Meli, S. Bredeau, P. Dubois, D. Bonduel, and M. Claes, *Chem. Mater.* 20, 3092 **(2008)**.
15. X. Zhang, T. Liu, T. V. Sreekumar, S. Kumar, V. C. Moore, R. H. Hauge, and R. E. Smalley, *Nano Lett.* 3, 1285 **(2003)**.
16. K. L. Lu, R. M. Lago, Y. K. Chen, M. L. H. Green, P. F. Harris, and S. C. Tsang, *Carbon* 34, 814 **(1996)**.
17. A. Koshio, M. Yudasaka, M. Zhang, and S. Iijima, *Nano Lett.* 1, 361 **(2001)**.
18. A. Dufresne, M. Paillet, J. L. Putaux, R. Canet, F. Carmona, P. Delhaes, and S. Cui, *J. Mater. Sci.* 37, 3915 **(2002)**.
19. R. J. Kuriger, M. K. Alam, D. P. Anderson, and R. L. Jacobsen, *Comp. Part A* 33, 53 **(2002)**.
20. B. Safadi, R. Andrews, and E. A. Grulke, *J. Appl. Polym. Sci.* 84, 2660 **(2002)**.
21. O. S. Carneiro, J. A. Covas, C. A. Bernardo, G. Caldeira, F. W. J. Van Hattum, J.-M. Ting, R. L. Alig, and M. L. Lake, *Comp. Sci. Tech.* 58, 401 **(1998)**.
22. F. W. J. Van Hattum, C. A. Bernardo, J. C. Finegan, G. G. Tibbetts, R. L. Alig, and M. L. Lake, *Polym. Comp.* 20, 683 **(1999)**.
23. J. K. W. Sandler, Ph.D. Thesis, University of Cambridge, UK **(2005)**.
24. K. Lozano, J. Bonilla-Rios, and E. V. Barrera, *J. Appl. Polym. Sci.* 80, 1162 **(2001)**.
25. S. A. Gordeyev, F. J. Macedo, J. A. Ferreira, F. W. J. Van Hattum, and C. A. Bernardo, *Physica B* 279, 33 **(2000)**.
26. I. C. Finegan and G. G. Tibbetts, *J. Mater. Res.* 16, 1668 **(2001)**.
27. M. Antunes, J. I. Velasco, V. Realinho, and E. Solórzano, *Polym. Eng. Sci.*, under Review.
28. M. Antunes, J. I. Velasco, V. Realinho, A. B. Martínez, M. A. Rodríguez-Pérez, and J. A. de Saja, *Adv. Eng. Mater.*, accepted for Publication.
29. Y. Yang, M. C. Gupta, K. L. Dudley, and R. W. Lawrence, *Adv. Mater.* 17, 1999 **(2005)**.
30. J. Shen, X. Han, and L. J. Lee, *J. Cell. Plas.* 42, 105 **(2006)**.
31. R. Verdejo, C. Saiz-Arroyo, J. Carretero-González, F. Barroso-Bujans, M. A. Rodríguez-Pérez, and M. A. López-Manchado, *Eur. Polym. J.* 44, 2790 **(2008)**.
32. G. L. A. Sims and C. Khunniteekool, *Cell. Polym.* 13, 137 **(1994)**.
33. M. A. Rodríguez-Pérez, O. Alonso, A. Duijsens, and J. A. de Saja, *J. Polym. Sci. Part B Polym. Phys.* 36, 2587 **(1998)**.

34. J. Kuhn and H. P. Ebert, *Int. J. Heat Mass Transfer* 35, 1795 **(1992)**.
35. J. I. Velasco, M. Antunes, O. Ayyad, J. M. López-Cuesta, P. Gaudon, C. Saiz-Arroyo, M. A. Rodríguez-Pérez, and J. A. de Saja, *Polymer* 48, 2098 **(2007)**.
36. B. Wunderlich, Thermal Analysis, Academic Press, New York **(1990)**.
37. J. Sandler, G. Broza, M. Nolte, K. Schulte, Y.-M. Lam, and M. S. P. Shaffer, *J. Macrom. Sci. Part B: Phys.* 42, 479 **(2003)**.

Received: 14 November 2008. Accepted: 25 January 2009.

4.5.3.2. *Thermal conductivity of carbon nanofibre-polypropylene composite foams.*

Defect and Diffusion Forum Vols. 297-301 (2010) pp 996-1001
Online available since 2010/Apr/13 at www.scientific.net

doi:10.4028/www.scientific.net/DDF.297-301.996

Thermal Conductivity of Carbon Nanofibre-Polypropylene Composite Foams

M. Antunes[1], V. Realinho[1], E. Solórzano[2,3], M.A. Rodríguez-Pérez[2], J.A. de Saja[2] and J.I. Velasco[1]

[1] Centre Català del Plàstic. Universitat Politècnica de Catalunya. C/ Colom 114, E-08222 Terrassa (Barcelona), Spain
[2] Cellular Materials Laboratory (CellMat). Condensed Matter Physics Department, University of Valladolid, E-47011 Valladolid, Spain
[3] SF-3 Dept., Helmholtz-Zentrum Berlin, Glienicker Strasse 100, D-14190, Berlin, Germany

marcelo.antunes@upc.edu; vera.realinho@upc.edu; esolo@fmc.uva.es; marrod@fmc.uva.es; sajasaez@fmc.uva.es; jose.ignacio.velasco@upc.edu

Keywords: Thermal conductivity, carbon nanofibres, polypropylene, foams

Abstract. Carbon nanofibre-reinforced polypropylene nanocomposites containing from 5 to 20 wt.% of carbon nanofibres and a chemical blowing agent were melt-compounded and later foamed using compression-moulding. Alongside their foaming behaviour analysis and cellular characterization, foams showing an increasingly finer isometric cellular structure with increasing the amount of nanofibres, their thermal conductivity was determined using the Transient Plane Source Method (TPS). Contrarily to the electrical conductivity, which has previously been shown to rise with increasing the amount of carbon nanofibres [1], the addition of the nanofibres did not significantly alter the thermal conductivity of the PP foams, their value being mainly affected by the relative density, only slight differences being assessed for the higher expansion ratio PP-CNF foams.

Introduction

The multifunctionality of some high-aspect ratio nanoscale reinforcements such as carbon nanofibres (CNF) makes them ideal candidates for high performance polymer composites [2]. Nowadays their main application in polymeric systems is as conductive fillers, their use starting to be widespread as a low filler content alternative to carbon black across the automotive and electronic sectors [3]. Carbon nanofibres often show a stacked-cup graphitic structure with surface edge imperfections, making them far cheaper than commercial multi-wall carbon nanotubes. Altogether, carbon nanofibres produced using the floating catalyst technique, commonly known as sub-micron vapour grown carbon fibres, can display fibre diameters as small as 20 nm, allowing them to have properties comparable to that of some types of carbon nanotubes.

Although previous stages are commonly used to improve the dispersion and distribution of these nanofillers in polymer matrices, in the end clusters are commonly observed even at low filler loadings. Different approaches have been considered to minimize reaggregation, with the problems of being costly and tending to decrease the nanofiller's efficiency [4-5].

Beside their incorporation in polymers for increasing properties such as the thermal and electrical conductivities, there is an interest in extending the specific properties range of the composite by foaming it. With that in mind, the preparation, cellular characterization and thermal conduction behaviour of different polypropylene-based foams has been previously investigated, results indicating the thermal conductivity to be mainly a function of the foam's bulk density [6,7]. Also, we have previously observed the existence of a characteristic electrical percolation threshold to both solid as well as foamed PP-CNF composites, foams even exhibiting an apparently lower percolation threshold due to the higher CNF dispersion induced during the foaming process [1].

Considering the scarce work dedicated to the preparation and study of thermoplastic foams filled with conductive nanofillers [8,9], PP nanocomposites containing 5, 10 and 20 wt.% of CNF and a chemical blowing agent were melt-mixed and foamed, the foams being characterized regarding their foaming behaviour and cellular structure as well as their thermal characteristics and thermal

conduction behaviour, three-phase (air, polymer and conductive filler) theoretical models being used to predict the thermal conductivity of the foamed composite materials.

Experimental

Materials and compounding. A PP-based matrix specifically formulated for foaming applications was prepared by melt-compounding using a co-rotating twin-screw extruder 50 phr of a high melt strength polypropylene (PP-HMS) and 50 phr of an extrusion grade-type.

Three different carbon nanofibre-polypropylene composites, with CNF contents of 5, 10 and 20 wt.%, were prepared. The carbon nanofibres used in this work were sub-micron vapour grown stacked-cup carbon fibres, with a typical diameter of 20-80 nm, a fibre length higher than 30 μm, a bulk density of 1.97 g/cm^3, a specific surface area BET (N_2) of 150-200 m^2/g, a graphitization degree of 70 % and an electrical resistivity of 10^{-3} Ω.m.

Azodicarbonamide, with an average particle size of 3.9 ± 0.6 μm, was added as blowing agent. All the melt-compounded extrudates were water-cooled and pelletized.

Foaming process. Compression-moulded 8.5 mm-thick discs with a diameter of 74 mm were prepared in a hot-plate press from the previously extruded composite pellets. A one-step compression-moulding foaming process was used, the prepared solid discs being placed in the circular mould and heated at 195ºC for 15 min applying a pressure of 40 bar, at the end the material being allowed to grow by sudden decompression. Cubic samples approximately 34 mm in side were directly cut from the several solid and foamed composites to measure the thermal conductivity.

Testing procedure. Density of the solid discs and respective foams was measured according to standard procedures (ISO 845). The cellular structure of the several foams was analyzed using a JEOL JSM-5610 scanning electron microscope (SEM) from samples prepared by fracturing at low temperature and made conductive by sputtering deposition of a thin layer of gold. The average cell size (ϕ) and cell density were both obtained from low-magnification micrographs using the procedure presented in [10]. Two different cell sizes were determined: ϕ_{VD}, measured in the pressure release direction, and ϕ_{WD} (Width Direction). The aspect ratio (AR = ϕ_{VD}/ϕ_{WD}), was determined using a representative cell population.

The dispersion and distribution of the carbon nanofibres was studied with a HITACHI H-800 transmission electron microscope (TEM) using 60 nm-thick ultramicrotomed samples.
A Perkin Elmer Pyris 1 model differential scanning calorimeter (DSC) was employed to study the thermal characteristics of the samples. The following program was used: heating from 30 to 200ºC at 10ºC/min and holding for 1 min to erase the thermal history before cooling at 10ºC/min from 200ºC to 30ºC. Samples were heated a second time at 10 ºC/min from 30ºC to 200ºC to analyze PP's melting signal.

A thermal constants Transient Plane Source (TPS) Hot Disk analyzer was used to measure the thermal conductivity (λ) of the several solid and foamed PP-CNF samples. Experiments were performed with a sensor radius of 3.189 mm, optimizing both the power output and measured time according to the thermal characteristics of each sample (0.005-0.015 W and 15-80 s, respectively). Five experiments were performed for each sample set-up at room temperature. The calculations of the thermal properties were performed according to the equations presented in [11,12].

Results and discussion

Foaming behaviour and cellular structure. The material's code, foam density and gas (V_{gas}), polypropylene (V_{PP}) and carbon nanofibre (V_{CNF}) volume fractions are presented in Table 1 alongside the main cellular structure characterization results.

Table 1. Cellular characterization results of the unfilled (PP) and carbon nanofibre (PP-CNF) polypropylene foams

Material code	Foam density [g/cm^3]	V_{gas}	V_{PP}	V_{CNF}	ϕ_{VD} [µm]	ϕ_{WD} [µm]	AR	Cell density [cells/cm^3]
PP	0.446	0.52	0.48	-	170	180	0.9	3.91×10^4
	0.444	0.52	0.48	-	174	175	1.0	4.52×10^4
	0.422	0.54	0.46	-	187	194	1.0	4.70×10^4
	0.346	0.62	0.38	-	194	175	1.1	4.71×10^4
	0.311	0.66	0.34	-	177	196	0.9	4.63×10^4
	0.268	0.71	0.29	-	241	266	0.9	3.52×10^4
	0.261	0.72	0.29	-	243	239	1.0	3.42×10^4
	0.236	0.75	0.25	-	456	479	1.0	1.30×10^4
	0.189	0.80	0.20	-	564	523	1.1	9.13×10^3
PP-CNF	0.265	0.70	0.29	0.01	569	508	1.1	8.13×10^3
	0.298	0.66	0.32	0.02	462	394	1.2	1.35×10^4
	0.442	0.52	0.44	0.04	239	258	0.9	3.05×10^4

The carbon nanofibre-polypropylene foams were prepared with a typical expansion ratio of 3 ($V_{gas} \approx$ 0.60-0.70) and a closed-cell type of cell structure. Typical SEM and TEM pictures of the cell-characterized foams are presented in Fig. 1. Clearly, all the PP-CNF foams showed an isometric-like cellular structure (AR ≈ 1), smaller cell sizes being obtained with increasing the amount of CNF. Particularly, the addition of 5, 10 and 20 wt.% of nanofibres respectively resulted in foams with average cell sizes slightly higher than 500, 400 and around 250 µm for the 20 wt.% CNF foam. The high magnification SEM micrograph displayed in Fig. 1(d) shows the typical dispersion and distribution of the carbon nanofibres along the cell walls of the foams. Some of the carbon nanofibres were clearly polymer-coated, indicating a good interaction between the PP matrix and the surface of the nanofibres. Although this apparently good compatibility between matrix and nanofibres, some bundle-like CNF aggregates were still visible after melt blending and foaming the materials, as seen in the TEM pictures of Fig. 1. The tendency to form these aggregates was higher with increasing the amount of nanofibres, the 5 wt.% CNF foamed composite showing a well-dispersed CNF morphology (Fig. 1(e)), while the 20 wt.% displayed some of these characteristic clusters (Fig. 1(f)).

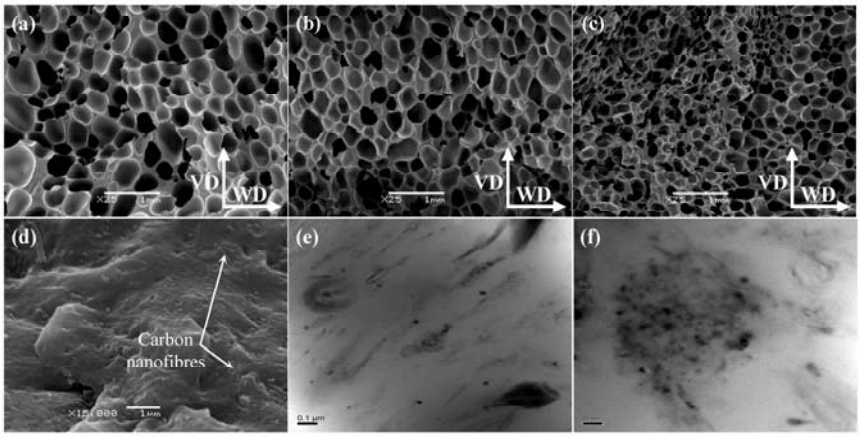

Fig. 1: Typical low-magnification (×25) SEM micrographs of (a) PP + 5 wt.% CNF, (b) PP + 10 wt.% CNF and (c) PP + 20 wt.% CNF foams; (d) high-magnification (×15000) SEM micrograph showing typical CNF distribution; and TEM pictures of (e) PP + 5 wt.% CNF and (f) PP + 20 wt.% CNF.

Thermal analysis. Differential scanning calorimetry (DSC) results support the increasingly smaller cell sizes of the foams with increasing the amount of nanofibres, a higher nucleation rate being assessed due to the presence of the nanofillers. A steady increase of around 2ºC was observed for both the onset and maximum crystallization temperatures with adding the nanofibres, from the

130.2 and 126.7, respectively the onset and maximum temperatures of the crystallization peak, of the unfilled PP to the 135.6 and 131.8ºC of the 20 wt.% CNF composite. The crystallinity also increased, from the 46.2 % of the material without nanofibres, to the 49.6 % of the 20 wt.% CNF.

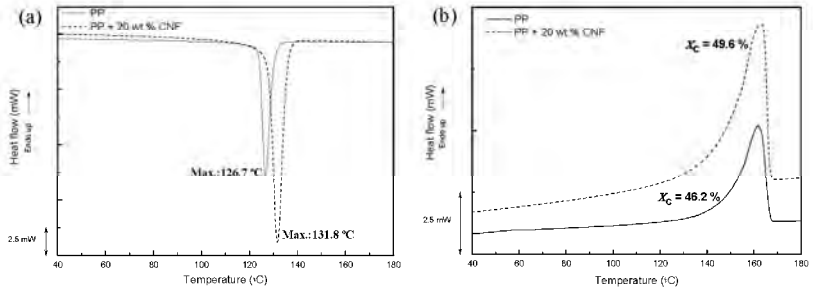

Fig. 2: Differential scanning calorimetry results for the unfilled and 20 wt.% CNF polypropylene foams showing (a) the peak's maximum crystallization temperatures and (b) crystallinity determination.

Thermal conductivity. The experimental thermal conductivities (λ_{exp}) as well as the theoretical (λ_{theo}) and normalized (λ_{norm}) ones are presented in Table 2 for all the unfilled and carbon nanofibre-polypropylene composite foams.

Table 2. Experimental (λ_{exp}), theoretical (λ_{theo}) and normalized (λ_{norm}) thermal conductivity values for the unfilled (PP) and carbon nanofibre-reinforced (PP-CNF) solid and foamed polypropylene composites

Material code	Relative density	λ_{exp} [W/m·K]	λ_{theo} [W/m·K]		λ_{norm} [W/m·K]
			Model 1	Model 2	
PP	1	0.276	0.276		1
	0.49	0.133	0.147		0.482
	0.48	0.153	0.146		0.555
	0.46	0.138	0.141		0.501
	0.38	0.121	0.120		0.440
	0.34	0.096	0.111		0.348
	0.29	0.090	0.099		0.327
	0.29	0.090	0.097		0.327
	0.25	0.094	0.089		0.342
	0.20	0.077	0.077		0.280
PP-CNF	1	0.284	0.284	0.284	1
	0.29	0.111	0.101	0.102	0.391
	1.00	0.302	0.302	0.292	1
	0.33	0.118	0.117	0.116	0.391
	1	0.316	0.316	0.296	1
	0.30	0.101	0.112	0.109	0.319
	1	0.319	0.319	0.301	1
	0.32	0.116	0.118	0.117	0.365
	0.34	0.118	0.125	0.123	0.371
	1	0.315	0.315	0.305	1
	0.40	0.137	0.142	0.143	0.434
	1	0.299	0.299	0.310	1
	0.46	0.178	0.151	0.162	0.595

The theoretical thermal conductivity (λ_{theo}) was determined using two different models, the first of which considering the thermal conductivity of each of the solid PP-CNF composites (model 1) and the second one considering a three-phase system, where each of its components (gas, polymer and conductive filler) contributes to the global foamed composite thermal conductivity (model 2):

$$\lambda_{theo}\ (\text{model 1}) = \lambda_{gas} V_{gas} + \xi \lambda_{PP-CNF} V_{PP-CNF}\ , \tag{2}$$

$$\lambda_{theo}\ (\text{model 2}) = \lambda_{gas} V_{gas} + \xi \left(\lambda_{PP} V_{PP} + \lambda_{CNF} V_{CNF} \right), \tag{3}$$

where λ_{gas} is the conductivity of air (0.026 W/m.K [13]), $\lambda_{PP\text{-}CNF}$, λ_{PP} and λ_{CNF} are respectively the conductivity of the composite, PP matrix and CNF, V_{gas}, $V_{PP\text{-}CNF}$, V_{PP} and V_{CNF} are their respective volume fractions, and ξ is a parameter related to the tortuosity of the cellular structure [14].

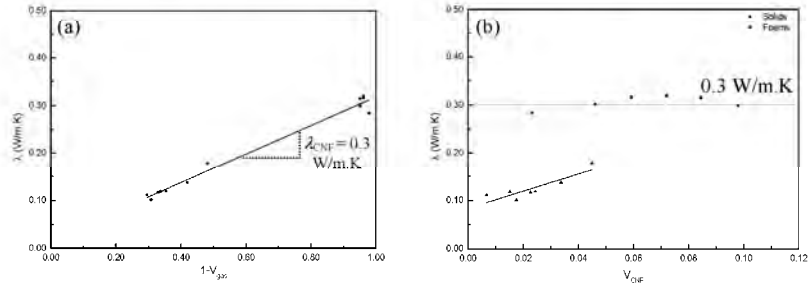

Fig. 3: Thermal conductivity as a function of the (a) volume fraction of PP-CNF and (b) carbon nanofibres.

The representation (Fig. 3(a)) of the experimental thermal conductivities of the several unfoamed and foamed PP-CNF composites as a function of the volume fractions of composite ($1\text{-}V_{gas}$) allowed the determination of the thermal conductivity of the solid PP-CNF using model 1 and assuming ξ = 1 (mixtures rule). A value of 0.3 W/m.K was obtained, in accordance with the value determined experimentally for the solid PP-CNF composites, independently of the amount of nanofibres (Fig. 3(b)). Contrarily to the solid's composite thermal behaviour, the thermal conductivity of the PP-CNF foams increased with CNF's volume fraction in a sort of way one would expect when comparing similar-expanded materials with increasing the amount of conductive filler. Although the low thermal conductivity values compared to the expected ones considering the theoretical CNF thermal conductivity (≈ 2000 W/m.K [15]), the foaming process seemed to induce a better CNF dispersion, improving the thermal conduction through the matrix.

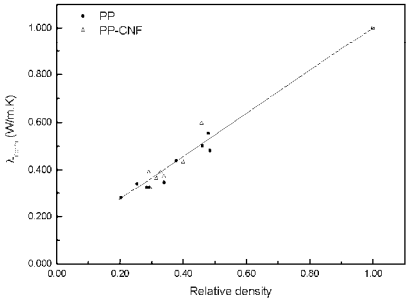

Fig. 4: Normalized thermal conductivity versus relative density for the solid and foamed PP and PP-CNF.

Both the density and thermal conductivity have been normalized to those of the reference solid materials (respectively relative density and normalized thermal conductivity, λ_{norm}), the plotted results being shown in Fig. 4. As can be seen, PP-CNF foams followed the global behaviour with the relative density as the unfilled PP foams, with only slight differences being observed when comparing foams with similar relative densities, PP-CNF foams showing a slightly higher value than the unfilled ones. None the less, it is possible to conclude that PP-CNF foams followed the same type of thermal conduction behaviour than the PP foams, their value increasing steadily with the relative density, indicating that the global thermal conductivity is being controlled by the foamed matrix and not by the presence of the conductive fillers.

Conclusions

This work focuses in comparing the cellular structure and thermal conductivity of compression-moulded unfilled and carbon nanofibre-reinforced PP foams. All the CNF-reinforced foams showed increasingly finer isotropic cell structures with increasing the amount of nanofibres, the average cell size decreasing from the 500 μm of the 5 wt.% CNF foams to half of it in the case of the 20 wt.% ones. Carbon nanofibres were not efficient in increasing the thermal conductivity of PP composites, its value resulting constant and independent of CNF's volume fraction. Possible CNF mechanical damage produced during melt-compounding, alongside bad dispersion, may explain the low efficiency of the filler. Although far from the expected results based on CNF's theoretical conductivity, the thermal conductivity of the PP-CNF foams increased with CNF's content according to the mixtures rule ($\xi = 1$), the foaming process seeming to increase the efficiency of the heat transfer through the matrix. Also, PP-CNF foams globally followed the same type of thermal conduction behaviour as the unfilled PP foams, indicating that the thermal conductivity is being controlled by the foamed matrix and not by the conductive carbon nanofibres.

Acknowledgements

Financial assistance from the Spanish Ministry of Science and Innovation (MICINN) for the project MAT2007-62956 is gratefully acknowledged.

References

[1] M. Antunes, J.I. Velasco, V. Realinho and D. Arencón: *Characterization of carbon nanofibre-reinforced polypropylene foams*, J. Nanosci. Nanotechnol. (in press, DOI: 10.1166/jnn.2010.1831).

[2] M. Shaffer and J. Sandler: in *Processing and Properties of Nanocomposites*, S. Advani, Ed., World Scientific (2006), p. 1.

[3] M.H. Al-Saleh and U. Sundararaj: Carbon Vol. 47 (2009), p. 2.

[4] Y.-P. Sun, K. Fu, Y. Lin and W. Huang: Acc. Chem. Res. Vol. 35 (2002), p. 1096.

[5] A. Koshio, M. Yudasaka, M. Zhang and S. Iijima: Nano Lett. Vol. 1 (2001), p. 361.

[6] M. Antunes, J. I. Velasco, V. Realinho and E. Solórzano: Polym. Eng. Sci. (2009), p. 1.

[7] M. Antunes, J. I. Velasco, V. Realinho, A. B. Martínez, M. A. Rodríguez-Pérez and J. A. de Saja: Adv. Eng. Mater. Vol. 21 (2009), p. 1.

[8] Y. Yang, M. C. Gupta, K. L. Dudley and R. W. Lawrence: Adv. Mater. Vol. 17 (2005), p. 1999.

[9] J. Shen, X. Han and L. J. Lee: J. Cell. Plas. Vol. 42 (2006), p. 105.

[10] J. I. Velasco, M. Antunes, O. Ayyad, J. M. López-Cuesta, P. Gaudon, C. Saiz-Arroyo, M. A. Rodríguez-Pérez and J. A. de Saja: Polymer Vol. 48 (2007), p. 2098.

[11] S.E. Gustafsson: Rev. Sci. Inst. Vol. 62 (1991), p. 797.

[12] M. Gustavsson, E. Karawacki, S.E. Gustafsson: Rev. Sci. Inst. Vol. 65 (1994), p. 3856.

[13] R.C. Weast: *Handbook of Chemistry and Physics*, 53rd ed, The Chemical Rubber Co. (1973).

[14] L.J. Gibson and M.F. Ashby: *Cellular Solids*, 2nd ed, Cambridge University Press, Cambridge (1997), p. 285.

[15] P. Kim, L. Shi, A. Majumdar and P.L. McEuen: Phys. Rev. Lett. Vol. 87 (2001), p. 215502.

4.5.3.3. *Broad-band electrical conductivity of carbon nanofibre-reinforced polypropylene foams*.

Broad-band electrical conductivity of carbon nanofibre-reinforced polypropylene foams

Marcelo Antunes[1], Miguel Mudarra[2], José Ignacio Velasco[1]*

[1] Centre Català del Plàstic, Departament de Ciència dels Materials i Enginyeria Metal.lúrgica, Universitat Politècnica de Catalunya, C/ Colom 114, E-08222 Terrassa (Barcelona), Spain.
[2] Departament de Física i Enginyeria Nuclear, Universitat Politècnica de Catalunya, ETSEIAT, C/Colom 11, E-08222 Terrassa (Barcelona), Spain.

Abstract

The influence of foaming a semi-crystalline polymer reinforced with different concentrations of carbon nanofibres (0-20 wt.%) in the formation of an electrically conductive network was studied at room temperature using an impedance analyzer over a wide interval of frequencies (from 10^{-2} to 10^{6} Hz). The composites were prepared by melt-compounding in a twin-screw extruder and later chemically foamed. Although composite materials displayed lower conductivities than expected assuming a percolative behaviour, foaming promoted a tunnel-like conduction at lower CNF concentrations than in the solids. At higher CNF concentrations no considerable improvements were achieved, as tunnelling conduction decreased with increasing local crystallinity. Foams showed conduction characteristics of a random-distributed fibre-like system while in the solids the behaviour was closer to that of nanofibres in the form of spherical particles, related to CNF aggregation. The anisotropic cellular structure of 20 wt.% CNF composite foamed by a physical foaming process disrupted the preferential in-plane CNF orientation attained during solid preparation, with foams showing a higher through-plane conductivity and more isotropic electrical properties than the chemically-foamed ones. It has been demonstrated that foaming a PP-CNF composite resulted in the formation of a conductive network at lower CNF concentrations than in the solids, foams showing possibilities as conductive high performance lightweight composite systems.

1. Introduction

It is well-known that an optimal nanoparticle distribution and dispersion is essential in the overall properties, and especially in the transport properties, of polymer-based composites. Amidst some of the most used synthesis and preparation techniques of polymer matrix composites are the in-situ polymerization, melt-compounding, ultrasonication, etc. [1]. Particularly, melt-blending comes as the most attractive because it allows the use of conventional processing technologies such as twin-screw extrusion or injection moulding. Nonetheless, these are hard to use due to the out-of-plane $\pi-\pi$ surface interactions between the individual nanofillers, leading to the formation of entanglements and reaggregation during processing [1]. That is why high shear forces are often required during melt mixing processing for good nanofiller dispersion, the intrinsic high viscosity of thermoplastics minimising reaggregation [2-3]. In spite of that, even at low filler contents clusters are commonly observed. Several approaches have been considered in order to minimize this problem, such as nanofiller surface modification, coating, among others [4-8]. These not only increase the cost but also tend to decrease the nanofiller's efficiency, as they reduce the inherent transport properties of the filler by affecting its surface and improve the interaction with the polymer, promoting the formation of local electrical contact resistances [1,9].

Electrically conductive polymer composites have been developed and studied over the last years by incorporating carbon-based conductive fillers. Among them, carbon nanotubes (single-wall, SWCNT, or multi-wall, MWCNT), carbon nanofibres (CNF), carbon black (CB), graphene nanosheets, etc., have been used. Although their extremely high theoretical electrical conductivities, in some cases even reaching for some types of SWCNTs the in-plane conductivity of graphite, 2.5×10^6 S m^{-1} [10], it has been proven that their efficiency in polymers is extremely affected by the composite's microstructure. Particularly, the potential of these conductive fillers is influenced by their dispersion and distribution, as well as to fibre breaking and buckling due to extensive shear during processing, cluster formation, etc. [2,11-12].

Only under very controlled conditions it is possible to reach electrical conductivity values for composites close to the expected ones based on the intrinsic electrical properties of both matrix and conductive filler. An abrupt increase of the electrical

conductivity is commonly reached after a certain loading content, known as the percolation threshold, indicating the formation of a 3-D conductive network by physical contact between the conductive filler particles [13-14]. In the case of carbon-based polymer composites, this has mainly been achieved using thermosets such as PU, epoxy, phenolic, etc. [15-18], with composites displaying a percolative behaviour with electrical conductivities as high as 2 S m^{-1} for a 1 wt.% CNT content [18]. Although rather effortless to achieve in thermosets due to the ease of dispersion of the filler in an initially liquid resin, this conductive network is quite hard to obtain in thermoplastics, and especially in semi-crystalline polymers. Electrical efficiency of the filler has been shown to directly depend upon the presence of polymer chains between filler particles and particularly on local crystal formation, as electrical conductivity considerably decreases in crystalline regions compared to the amorphous ones, where ion conductivity is the dominating conduction mechanism [19-22]. Polymer chains create a relatively high electrical resistance between conductive particles, thus limiting electrical conduction. For instance, in the case of untreated carbon nanofibres, the critical volume fraction is usually between 5 and 10 vol.%, although this is highly dependant on the processing technique, as it affects the degree of filler dispersion and alignment [9,23-24].

The direct (dc) and alternating (ac) currents of polymer-CNT composites have been recently studied in a frequency range up to 10^6 Hz [16,18,25-26]. Different conduction models, including anomalous diffusion in percolating clusters [26] and hopping [16,25], have been proposed to explain the frequency dependence of conductivity. However, a clear picture of the electrical conduction mechanism in carbon-based reinforced composites is still lacking.

Alongside the incorporation of such conductive nanofillers, there is an increasing interest in extending even further the materials range of properties by foaming the base matrix. Foams are vastly used in sectors such as insulation, cushioning or packaging [27]. Nonetheless, foam applications are limited by their poor mechanical properties. Different strategies have been used to generate better foams with improved mechanical behaviour and/or added functionalities. One of them considers a careful control of the cellular structure, enabling the development of lightweight structures with improved specific mechanical properties, in some cases even higher than that of respective solids. Improving the melt strength and cell nucleation efficiency by using polymer branching,

blending of linear and branched polymers [28] or more recently incorporating nano-sized fillers [29-30], it is possible to obtain finer closed-cell foams, in some cases with cell sizes < 10 μm (microcellular foams [31]). Altogether, the incorporation of these high aspect ratio nanofillers may lead not only to mechanical reinforcement of the foams due to a combined cell wall confinement of the particles and improved cellular structure related to limited gas diffusion in the polymer matrix, but also, depending on the nature of said nanofillers, add other characteristics, such as thermal or electrical conduction.

Our research group possesses considerable experience in preparing and characterizing different PP-based foams [32-34], thus the interest in extending the materials possibilities by incorporating conductive nanofillers. Limited work has been dedicated to the preparation and applications of thermoplastic foams filled with conductive fillers, mainly regarding their electrical conduction behaviour. A couple of works have considered the development of CNF-filled amorphous polymer foams for electromagnetic interference (EMI) shielding, as it is known that weight reduction is a key requirement for the development of practical EMI shielding systems for applications such as electronics or telecommunications [35-36]. Results indicate the presence of a critical concentration for electrical conduction by physical contact between the nanofibres (percolation threshold), similar to that of the respective solids (5 wt.% CNF). Altogether, the incorporation of nanofibres to PS and PMMA and later foaming resulted in foams with finer and more isotropic cellular structures [37-38], macroscopic strength enhancement being observed with increasing CNFs content [39-40]. As much as we are aware of, there are no previous works dedicated to the study of the electrical conduction behaviour of semi-crystalline polymer foams filled with carbon-based conductive fillers.

In this work, different CNF-reinforced PP-based materials (5, 10, 12.5, 15, 17.5 and 20 wt.% of CNF) were prepared using a twin-screw extruder and later chemically foamed by compression-moulding, with the main objective of producing lightweight materials for applications such as electrostatic painting by incorporating low loadings of carbon nanofibres. In order to assess possible electrical conduction differences due to the foaming process and developed cellular structure, the 20 wt.% CNF composite was also foamed using a high pressure CO_2 dissolution process. Particularly, in the last part

of the results section, we comparatively analyze the differences observed between the in-plane and through-plane electrical conductivities of 20 wt.% CNF composites foamed by these two foaming processes.

2. Experimental

2.1. *Preparation of the PP-CNF composites*

A PP matrix specifically prepared for foaming applications and comprising 50 phr of a high melt strength PP (PP-HMS) and 50 phr of an extrusion grade-type was melt-compounded using a co-rotating twin-screw extruder (Collin Kneter 25×36D, *L/D* = 36) at 165 ºC and 160 rpm with different amounts of carbon nanofibres: 5, 10, 12.5, 15, 17.5 and 20 wt.%. In the case of the chemically foamed PP-CNF composites, 1.5 phr of a chemical blowing agent, azodicarbonamide (ADC), was also added to the formulation.

The PP-HMS used was an especially modified long-chain branched PP with a density of 0.902 g cm^{-3} and melt flow index (MFI) of 2.1 dg min^{-1} at 230 ºC and 2.16 kg. The linear extrusion-grade type of PP had a density of 0.905 g cm^{-3} and MFI of 5.8 dg min^{-1} (230 ºC and 2.16 kg). The azodicarbonamide (Porofor® ADC/M-C1), with an ADC content of 99.1%, a density of 1.65 g cm^{-3} and an average particle size of 3.9 ± 0.6 μm, was added in-situ to the polymer blend in the extruder. The carbon nanofibres used in this work were submicron vapour grown carbon fibres (s-VGCF) with a stacked-cup structure produced by Grupo Antolín Ingeniería, S.A. (Burgos, Spain), with a diameter of 20-80 nm, a fibre length > 30 μm, a bulk density of 1.97 g cm^{-3} and a graphitization index of 70%.

2.2. *Foaming of the PP-CNF composites*

The extrusion-compounded pellets were initially placed into a 3.5 mm-thick steel mould (Ø=74 mm) and compression-moulded to solid discs at 170 ºC and 20 bar using a hot-plate press IQAP-LAP PL-15.

From these solid discs, PP-CNF foams were prepared using two different foaming processes: first of all by compression-moulding, by placing the solid discs of the ADC-compounded composites in the same mould and heating at 195 ºC applying a constant pressure of 40 bar. After 15 min, the pressure was suddenly released, allowing the material to expand. The 20 wt.% CNF composite was also foamed by a high pressure

CO_2 dissolution foaming process. In this process, foams were obtained by initially saturating the solid discs with CO_2 in a high-pressure vessel and later applying a sudden pressure drop. Pressurized at 200 bar and 165 ºC for 30 min, the CO_2 saturated discs were cooled to 140 ºC and foamed by sudden decompression from 170 to 0 bar.

2.3. *Testing Procedure*

Cellular structure of the foams was attained using a JEOL JSM-5610 scanning electron microscope. Average cell size (ϕ) and cell density were obtained from low-magnification micrographs using the intercept counting method. Two different cell sizes were determined: ϕ_{VD} (VD: Vertical Direction), and ϕ_{WD} (Width Direction). Anisotropy ratio ($AR=\phi_{VD}/\phi_{WD}$) was assessed using a representative cell population. Morphology of the composites was studied using a HITACHI H-800 transmission electron microscope on 60 nm-thick ultramicrotomed sheets. A Perkin Elmer Pyris 1 model calorimeter was employed for DSC measurements. The following program was used: heating from 30 to 200 ºC (10 ºC min^{-1}) and holding for 1 min to erase the thermal history before cooling at 10 ºC min^{-1} from 200 ºC to 30 ºC. After a second isothermal step at 30 ºC, samples were heated a second time at 10 ºC min^{-1} from 30 ºC to 200 ºC. Crystallinity percentages were determined considering a theoretical, 100% crystalline, PP enthalpy of 207.1 J g^{-1} [41].

2.3.1. *Broad-band electrical conductivity*

The electrical conductivity of solid and respective foamed composites was measured between 10^{-2} and 10^{6} Hz using a Novocontrol impedance analyzer (HP 4192 A LF). A typical thickness of 130 μm and 1.5 mm was respectively used for solid and compression-moulded foamed materials. Circular gold electrodes with a diameter slightly over that of the upper measuring electrode (9 mm) were deposited onto the surfaces of the samples in order to guarantee perfect electrical contact. In the case of the 20 wt.% CNF batch-foamed samples, two different specimen configurations were considered for the electrical conductivity measurements: horizontal, i.e., specimens being cut parallel to the foams surface (through-plane direction), and vertical (in-plane direction).

3. Results and discussion

PP-CNF foams were prepared with a typical expansion ratio, *ER* ($ER=\rho_s/\rho$, where ρ_s and ρ are respectively the density of solid and foam) of 3 (bulk density ≈ 300 kg m^{-3}) in all cases showing a closed-cell cellular structure. The analysis of the cellular structure was done using low and high-magnification SEM pictures, the most characteristic ones being shown in fig. 1.

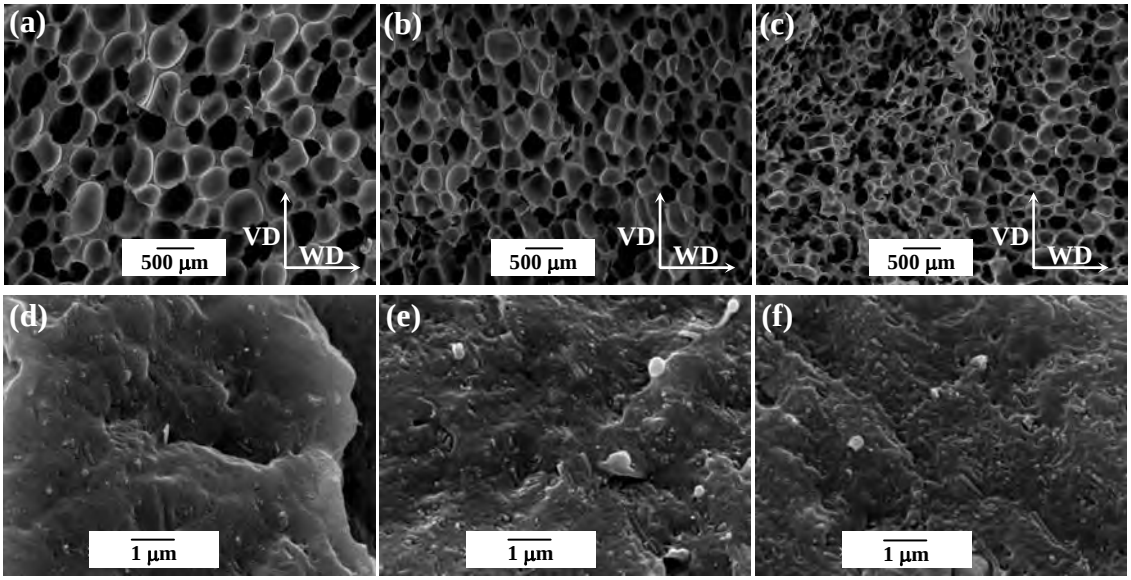

Fig. 1 - Low-magnification (a) PP + 5 wt.% CNF, (b) PP + 10 wt.% CNF and (c) PP + 20 wt.% CNF and high-magnification (d) PP + 5 wt.% CNF, (e) PP + 10 wt.% CNF and (f) PP + 20 wt.% CNF compression-moulded foams SEM pictures.

Not only CNFs contribute to obtain an isotropic-type of cellular structure (*AR* ≈ 1), they also promote the formation of finer cell structures. For similar expansion ratios, smaller cell sizes are obtained with increasing the amount of carbon nanofibres. The 5 wt.% CNF foams exhibited an average cell size a bit higher than 500 μm (≈ 570 μm in VD direction and ≈ 510 μm in WD); increasing the CNF content to 10 wt.% resulted in the decrease of the average cell size to ≈ 460 μm in VD direction and ≈ 400 μm in WD; finally, the 20 wt.% CNF foams showed an average cell size around half that of the 5 wt.% ones (ϕ_{VD} ≈ 240 μm and ϕ_{VD} ≈ 260 μm). Cell densities increased accordingly, from the 8.126×10^3 of the 5 wt.% CNF to the 1.347×10^4 and 3.049×10^4 cells cm^{-3} of the 10 and 20 wt.%. High magnification SEM pictures (figs. 1d, e and f) allowed to visualize the dispersion and orientation of the carbon nanofibres along the cell walls of

the foams. Although some bundle-like aggregates were observed after melt blending the materials (fig. 3e) and even after foaming (fig. 3f), these were a lot more disperse than in similar composites prepared by melt mixing, where nanotube or nanofibre clusters are observed even at low filler concentrations [19, 42-44].

Higher crystallization temperatures were observed by DSC with increasing the amount of nanofibres: from 130.2 and 126.7 ºC corresponding respectively to the beginning and maximum of the crystallization peak observed during the cooling step for the PP matrix without nanofibres, to 135.6 and 131.8 ºC for the 20 wt.% CNF composite. A steady increase of around 2 ºC was observed for both crystallization temperatures with adding increasingly higher amounts of CNFs (comparing the peak's maximum, from the already mentioned 126.7 ºC for the material without nanofibres, to 128.8 ºC for the 5 wt.%, 129.6 ºC for the 10 wt.% and 131.8 ºC for the 20 wt.%). Crystallinity values showed a steady increase from 46.2% of the material without nanofibres, to 46.5, 48.9 and 49.6%, respectively for 5, 10 and 20 wt.% CNF composites.

3.1. *Broad-band electrical conductivity measurements*

As can be seen in fig. 2a, for CNF concentrations below 10 wt.%, i.e., 5 vol.%, the electrical conductivity of both solids and foams follows a linear-like dependence with frequency in the whole frequency range, a behaviour that is characteristic of insulating materials such as PP, indicating that the electrical properties of the composite are being controlled by the matrix ($\sigma_{PP} \approx 10^{-16}$ S cm^{-1}). Below this concentration, the conductive particles are too far apart to allow electrical conduction. Nonetheless, for CNF amounts higher than 5 vol.%, the materials start to show a characteristic electrical conduction behaviour that can be depicted by $\sigma(\nu) = \sigma_{dc} + \sigma_{ac} = \sigma_{dc} + A\nu^{S}$. This law considers a critical frequency (ν_c) below which conductivity gets frequency-independent (known as the direct current conductivity, σ_{dc} – see fig. 2b). For comparative purposes, the dc conductivity, i.e. σ_{dc}, was always taken at a frequency of 10^{-1} Hz.

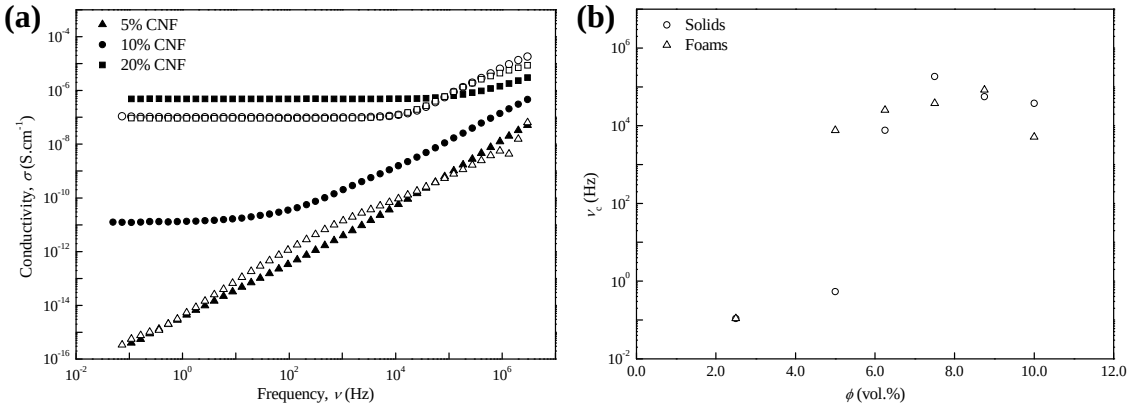

Fig. 2 – (a) Conductivity vs. frequency and (b) critical frequency, ν_c vs. ϕ for PP-CNF solid and foamed composites.

Filled and unfilled symbols presented in (a) correspond respectively to solids and foams.

Figure 3 depicts the σ_{dc} data as a function of CNF concentration for both solids and foams. The foamed composites reach a high conductivity value earlier than the solids (5 vol.% of CNF compared to around 6 vol.%), indicating that the foaming process is adding to a better dispersion/distribution of the nanofibres, thus promoting electrical conduction by tunnelling effect. That is why, for contents higher than the aforementioned values, conductivity only slightly increases.

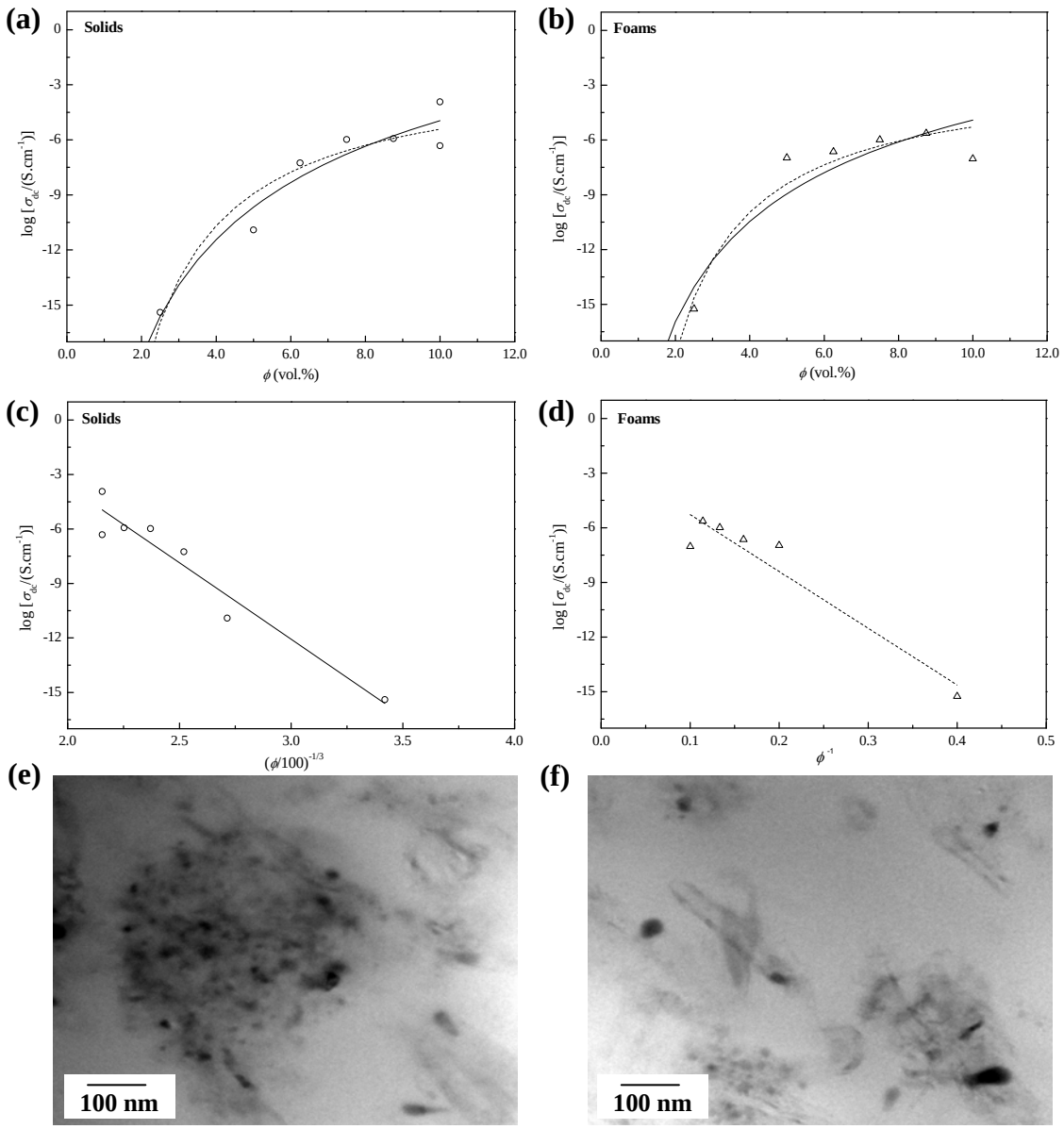

Fig. 3 - (a), (b) Log (σ_{dc}) vs. ϕ, (c) log (σ_{dc}) vs. $(\phi/100)^{-1/3}$ and (d) log (σ_{dc}) vs. ϕ^{-1} respectively for the solid and compression-moulded foamed PP-CNF composites. TEM micrographs showing typical CNF distribution in (e) solid and (f) foam.

Continuous and dashed lines correspond to the predictions given by tunnelling conduction respectively for random-distributed spherical and fibre-like particles.

The dc conductivity above the critical concentration can be analyzed in terms of the percolation theory by means of the standard scaling law given by $\sigma_{dc} \propto (\phi - \phi_c)^t$, where *t* is a critical exponent that depends on the dimensionality of the system [13-14].

If tunnel conductivity is considered, the dc electrical conductivity can be described by $\sigma_{dc} \propto \exp(-Ad)$ [45-46], where *A* is a tunnel parameter and *d* is the so-called tunnel distance. In the particular case of random spherical particle distribution, the mean average distance between particles can be initially assumed to be proportional to $\phi^{-1/3}$ [47]. Nonetheless, if one considers the mean average distance in a three-dimensional random fibre network such as the one expected here, *d* is proportional to ϕ^{-1} ($d = (\pi D)/(8\phi)$, where *D* is the fibre diameter) [48].

Although slight deviations from the linear expected tendency are observed, especially for the foamed composites, a good agreement was found between experimental data and tunnel conductivity, suggesting that the higher electrical conductivity of solid and foamed materials starting at around 5 vol.% of CNF can be attributed to tunnel conduction. This predominant tunnelling conduction behaviour has previously been shown in other research works to be typical of CNF-filled polyolefin composites, due to fibre breaking during processing, the dispersed short carbon nanofibres making less likely to reach a direct contact between the fibres at low contents [49].

Quantitatively comparing the electrical behaviour from a tunnel-like approach, the best fitting for the electrical conduction of the solids corresponds to the random-distributed spherical particles system, indicating that carbon nanofibres are aggregated in a spherical-like shape. Contrarily, the electrical behaviour of the foams fits best that of a random-distributed fibre-like system, demonstrating that the foaming process is helping in reducing and breaking the aggregates seen in the solids and thus in obtaining a dispersed carbon nanofibre-polymer system (compare TEM micrographs displayed in figs. 3e and f showing typical CNF distribution, respectively in solid and foam).

The broad-band electrical conductivity measurements provide information about the ac conductivity as described by the frequency-dependent part. Electrical conductivity remains constant until a certain critical frequency (ν_c) is reached. For frequencies higher than this critical value, conductivity exhibits a frequency dependence which, in a first approximation, can be described by $\sigma_{ac} \sim \nu^S$. The experimental data also indicates that the higher the dc conductivity the higher is the critical frequency. This effect has been observed in several disordered materials and depicted by $\nu_c \propto \sigma_{dc}^{\ b}$, where *b* is an

exponent that usually takes values close to 1 [50]. Critical frequency has been calculated for each composite as the frequency at which a 5% increase in conductivity with respect to the σ_{dc} value is observed. Although the power law previously portrayed is quite well fulfilled, *b* values lower than 1 were observed for solids (*b* = 0.69) and foams (*b* = 0.60).

Figures 4a and b respectively show the different values for ν_c and *S* as a function of the vol.% of CNF. While the logarithm of ν_c increases in a linear fashion with volume concentration, only a slight decrease being observed for both solid and foamed PP-10 vol.% CNF composites, the *S*-exponent starts from a value close to 1 for the composites where the electrical conduction is being controlled by the insulating matrix (solid and foamed PP-2.5 vol.% CNF composites), with a continuous decrease being observed with increasing the amount of CNF. The existence of *S*-exponents in the range of 0.4-0.7 and 0.6-0.9 respectively for solids and foams over a wide interval of frequencies and concentrations above 10 vol.% of CNF is well supported by the broad-band electrical conductivity measurements.

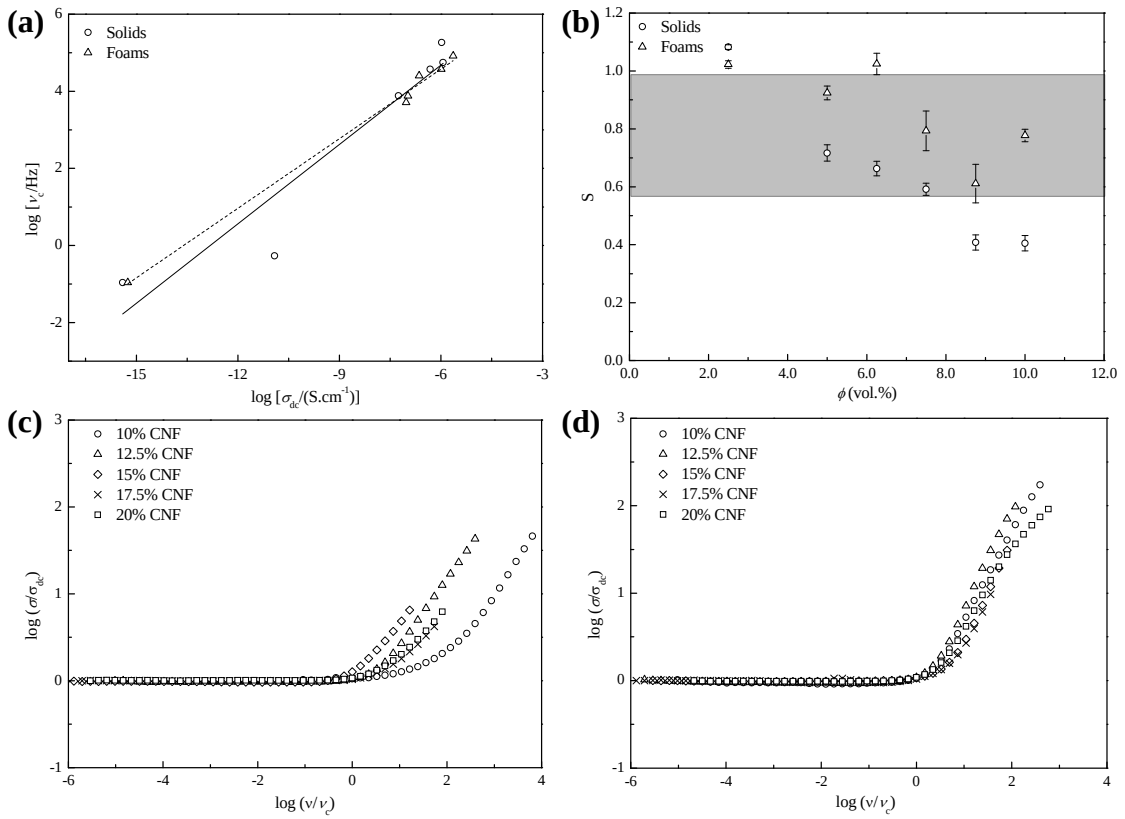

Fig. 4 - (a) Log (ν_c) vs. log (σ_{dc}) and (b) exponent *S* as a function of ϕ for the several solid and compression-moulded foamed PP-CNF composites. Gray area delimits the

region commonly described by percolation theory [51-53]. Master curves for (c) solid and (d) foamed PP-CNF composites.

The dc conductivity data indicate that tunnel conductivity is dominant at low CNF concentrations. This fact implies that conduction takes place much before a continuous network of physically connected nanofibres sets on. In this situation the frequency dependence of the electrical conductivity is expected to be caused by the influence of large polymeric gaps between conductive clusters. Therefore the *S*-exponent values close to 1, which is the characteristic value of the polymer matrix. As the concentration increases and although tunnelling continues to be the predominant charge conduction mechanism, the size of the finite-size cluster tends to increase. In this situation, as clusters get bigger [54-55], the frequency dependence of the conductivity reflects in the *S*-exponent, resulting in values between 0.58 and 0.9. As nanofiller concentration further increases, a continuous network of physically connected nanofibres appears through the sample. In this case, the frequency-dependent part of conductivity is controlled by the nature of the conductive filler and a weaker frequency dependence of the conductivity is expected since electrical conductivity of carbon fibres has been shown to weakly depend on frequency [56].

Altogether, the law describing the frequency dependence of conductivity has been proposed to be universal for a great amount of disordered materials [50], manifested by the possibility to plot the ac conductivity data from a range of experiments on the same plot normalizing both conductivity and frequency (master curve). However, as seen previously, the values of the *S*-exponent may vary with the amount of nanofiller. It seems pertinent to check under which conditions the proposed universality is valid for the studied solid and foamed composites. In order to construct a master curve, conductivity values were normalized by the corresponding σ_{dc} data and the frequencies by ν_c (figs. 4c and d). Although a master plot could not be found for solid composites, within certain limits a reasonable master curve could be constructed for the foamed ones, indicating that the electrical behaviour of the foams is more predictable than that of the respective solids, mainly due to improved nanofibre distribution. However, due to the different slopes measured for different nanofiller concentrations, the occurrence of this

master plot should be considered more as a working rule rather than a universal behaviour.

3.1.1. *In-plane vs. through-plane electrical conductivity*

It is well known that the compression-moulding process, in this case used to prepare the solid precursor discs, induces a preferential orientation of fibre-like conductive fillers like the carbon nanofibres used in this work, parallel to the sample's surface (in-plane direction). This orientation results in a bulk anisotropy of the electrical conductivity, with the material showing a considerably higher in-plane value [57].

One of the main objectives of foaming the solid discs by dissolving CO_2 in a high-pressure chamber and applying a sudden pressure drop was to induce an anisotropic cellular structure with cells highly elongated in the thickness direction. The outcome is an out-of-plane fibre reorientation parallel to the thickness of the foamed material (through-plane direction), as seen in fig. 5. Concerning the electrical conductivity, this partially induced through-plane nanofibre reorientation results in a higher electrical conductivity in the through-plane direction regarding the conventionally higher in-plane one. Although previously mentioned [58], the possibility that the cellular structure affects the electrical conductivity via its influence on the conductive filler's distribution and concentration has not been studied.

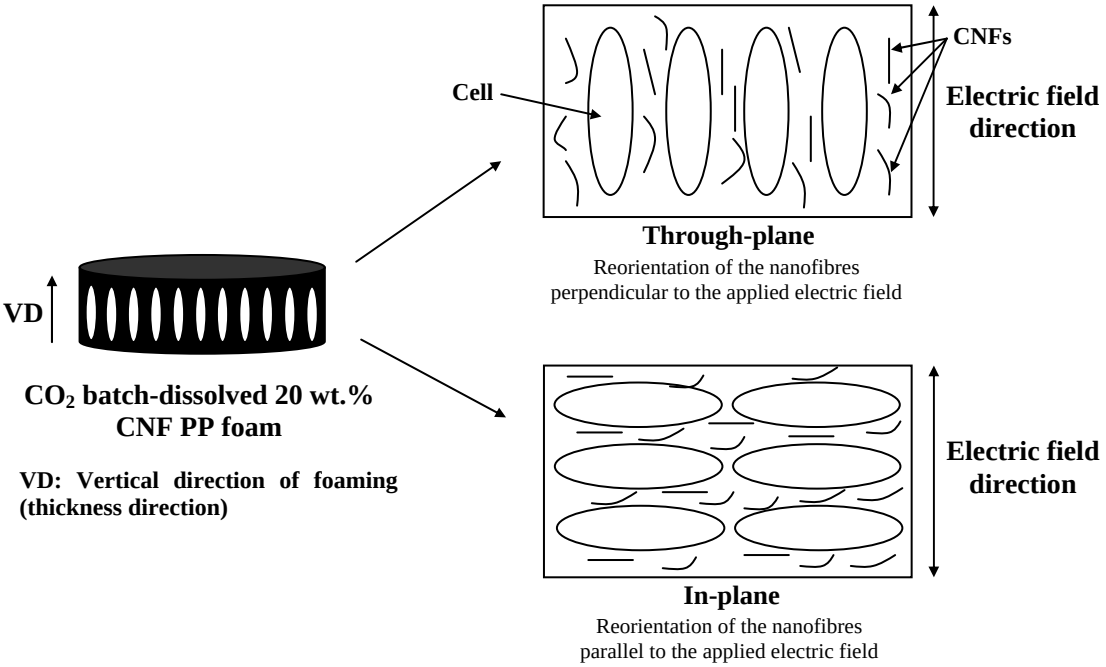

Fig. 5 - Schematic showing carbon nanofibre through-plane reorientation due to foaming for the CO_2 batch-dissolved 20 wt.% CNF PP foams.

Table 1 - Through and in-plane electrical conductivities for the compression-moulded (chemical foaming) and CO_2 dissolved (physical foaming) 20 wt.% CNF PP foams.

Type of foaming	Electric field direction	σ_{dc} (S cm^{-1})	ν_c (Hz)
Chemical foaming	Through-plane	9.346×10^{-8}	5.12×10^{3}
Physical foaming	Through-plane	4.107×10^{-5}	1.24×10^{5}
	In-plane	5.358×10^{-5}	1.85×10^{5}

As seen by the values presented in Table 1, there is a clear increase in the through-plane electrical conductivity from both solid and foamed compression-moulded 20 wt.% CNF composites (9.346×10^{-8} S cm^{-1} for the foam) compared to the CO_2 dissolution one (4.107×10^{-5} S cm^{-1}). Albeit the increase towards the through-plane direction, in-plane electrical conductivity is still a little bit higher than the one measured in through-plane direction (5.358×10^{-5} compared to 4.107×10^{-5} S cm^{-1}).

4. Conclusions

In summary, this paper presents the characterization of compression-moulded CNF-reinforced polypropylene foams regarding their broad-band electrical conduction behaviour, with the main objective of producing lightweight rigid PP materials for electrical applications. A second foaming process was also considered (CO_2 dissolution) in order to assess the influence of cellular structure on the in-plane and through-plane electrical conductivities of the composites.

Regarding the cellular structure of the as-produced foams, incorporation of different carbon nanofibre contents to a PP matrix and later foaming resulted in the formation of increasingly finer isotropic cell structures with increasing the amount of nanofibres, with anisotropy ratios close to 1 and an average cell size decrease from approximately 500 μm for 5 wt.% CNF foams to almost half of it for the 20 wt.% ones, indicating a cell nucleation effect promoted by the presence of the nanofibres. Higher crystallization temperatures and crystallinities with increasing the amount of carbon nanofibres are indicative of a higher crystallinity induced by the nanofiller.

Although electrical properties of the 5 wt.% CNF composite were controlled by the matrix, indicating that nanofibres were too far apart, a typical electrical conduction behaviour was observed at higher CNF percentages for solids and foams. Foamed composites reached a high conductivity value earlier than solid materials, indicating that

foaming is adding to a better dispersion/distribution of the nanofibres, thus promoting electrical conduction by tunnelling effect. For contents higher than the aforementioned values, conductivity only slightly increases, with the nanofibres being too broken to allow direct physical contact. Besides, as the electrical conduction by tunnelling is directly related to the network formed by the carbon nanofibres and the polymer gaps between them, as the amount of CNF increases and so does polymer crystallinity, a local reduction in the conduction through the polymer is observed, limiting the efficiency of nanofibres.

Comparing the electrical response from a tunnel conduction point of view, foams showed a behaviour closer to a random-distributed fibre-like system while solids presented a behaviour closer to that of random-distributed spherical particles, related to nanofibre agglomeration, indicating that the foaming process globally reduces CNF aggregation.

Within certain limits a master curve could be constructed for the foamed composites. However, and due that slightly different slopes were observed for each nanofiller concentration, this master plot should be considered as an empirical model.

Preferential cell orientation induced with foaming by CO_2 dissolution increased the through-plane electrical conductivity with regard to the in-plane one, thus confirming that the foaming process may reorientate the nanofibres, disrupting the induced in-plane fibre orientation of the solid discs and helping to produce an electrically conductive foam with a more isotropic electrical conduction behaviour.

Acknowledgements

Financial assistance from the Spanish Ministry of Science and Education for the project MAT2007-62956 is gratefully acknowledged.

References

[1] Shaffer M, Sandler J. Carbon Nanotube/Nanofibre Polymer Composites. In: Advani S, editor. Processing and Properties of Nanocomposites, World Scientific; 2006 p. 1-59.

[2] Tang W, Santare MH, Advani SG. Melt processing and mechanical property characterization of multi-walled carbon nanotube/ high density polyethylene (MWNT/HDPE) composite films. Carbon 2003;41:2779-85.

[3] Thostenson ET, Chou T-W. Aligned multi-walled carbon nanotube-reinforced composites: processing and mechanical characterization. J. Phys. D : Appl. Phys. 2002;35:77-80.

[4] Sun Y-P, Fu K, Lin Y, Huang W. Functionalized carbon nanotubes: properties and applications. Acc. Chem. Res. 2002;35:1096-104.

[5] Bredeau S, Boggioni L, Bertini F, Tritto I, Monteverde F, Alexandre M, et al. Ethylene-Norbornene Copolymerization by Carbon Nanotube-Supported Metallocene Catalysis: Generation of High-Performance Polyolefinic Nanocomposites. Macromol. Rapid Commun. 2007;28:822-7.

[6] Toti A, Giambastiani G, Bianchini C, Meli A, Bredeau S, Dubois P, et al. Tandem Action of Early-Late Transition Metal Catalysts for the Surface Coating of Multi-Walled Carbon Nanotubes with Linear Low Density Polyethylene. Chem. Mater. 2008;20:3092-8.

[7] Zhang X, Liu T, Sreekumar TV, Kumar S, Moore VC, Hauge RH, et al. Poly(vinyl alcohol)/SWNT Composite Film. Nano Lett. 2003;3:1285-8.

[8] Dufresne A, Paillet M, Putaux JL, Canet R, Carmona F, Delhaes P, et al. Processing and characterization of carbon nanotube/poly(styrene-co-butyl acrylate) nanocomposites. J. Mater. Sci. 2002;37:3915-23.

[9] Finegan IC, Tibbetts GG. Electrical conductivity of vapour-grown carbon fiber/thermoplastic composites. J. Mater. Res. 2001;16:1668-74.

[10] Charlier JR, Issi J-P. Electrical conductivity of novel forms of carbon. J. Phys. Chem. Solids 1996;57:957-65.

[11] Safadi B, Andrews R, Grulke EA. Multiwalled carbon nanotube polymer composites: Synthesis and characterization of thin Films. J. Appl. Polym. Sci. 2002;84:2660-9.

[12] Sandler J, Werner P, Shaffer MSP, Demchuk V, Altstädt V, Windle AH. Carbon-nanofibre-reinforced poly(ether ether ketone) composites. Comp. Part A 2002;33:1033-9.

[13] Stauffer D, Aharony A. Introduction to Percolation Theory, Taylor & Francis. London; 1985.

[14] Kirkpatrick S. Percolation and Conduction. Rev. Mod. Phys. 1973;45:574-88.

[15] Sandler J, Shaffer MSP, Prasse T, Bauhofer W, Schulte K, Windle AH. Development of a dispersion process for carbon nanotubes in an epoxy matrix and the resulting electrical properties. Polymer 1999;40:5967-71.

[16] Barrau S, Demont P, Peigney A, Laurent C, Lacabanne C. DC and AC Conductivity of Carbon Nanotubes-Polyepoxy Composites. Macromolecules 2003;36(14):5187-94.

[17] Prasse T, Cavaillé J-Y, Bauhofer W. Electric anisotropy of carbon nanofibre/epoxy resin composites due to electric field induced alignment. Comp. Sci. Tech. 2003;63:1835-41.

[18] Sandler JKW, Kirk JE, Kinloch IA, Shaffer MSP, Windle AH. Ultra-low electrical percolation threshold in carbon-nanotube-epoxy Composites. Polymer 2003;44:5893-9.

[19] Pötschke P, Dudkin SM, Alig I. Dielectric spectroscopy on melt processed polycarbonate-multiwalled carbon nanotube composites. Polymer 2003;44:5023-30.

[20] Pötschke P, Abdel-Goad M, Alig I, Dudkin SM, Lellinger D. Rheological and dielectrical characterization of melt mixed polycarbonate-multiwalled carbon nanotube composites. Polymer 2004;45:8863-70.

[21] Alig I, Dudkin SM, Jenninger W, Marzantowicz M. Ac conductivity and dielectric permittivity of poly(ethylene glycol) during crystallization: Percolation picture. Polymer 2006;47:1722-31.

[22] Alig I, Lellinger D, Dudkin SM, Pötschke P. Conductivity spectroscopy on melt processed polypropylene-multiwalled carbon nanotube composites: Recovery after shear and crystallization. Polymer 2007;48:1020-9.

[23] Lozano K, Bonilla-Rios J, Barrera EV. A Study on Nanofiber-Reinforced Thermoplastic Composites II: Investigation of the Mixing Rheology and Conduction Properties. J. Appl. Polym. Sci. 2001;80:1162-72.

[24] Gordeyev SA, Macedo FJ, Ferreira JA, Van Hattum FWJ, Bernado CA. Transport properties of polymer-vapour grown carbon fibre composites. Physica B 2000;279:33-6.

[25] Kilbribe BE, Coleman JN, Fraysse J, Fournet P, Cadek M, Drury A, et al. Experimental observation of scaling laws for alternating current and direct current conductivity in polymer-carbon nanotube composite thin Films. J. Appl. Phys. 2002;92:4024-30.

[26] Nogales A, Broza G, Roslainec Z, Schulte K, Sics I, Hsiao BS, et al. Low Percolation Threshold in Nanocomposites Based on Oxidized Single Wall Carbon Nanotubes and Poly(butylene terephthalate). Macromolecules 2004;37:7669-72.

[27] Klempner D, Sendijarevic V. Polymeric foams and foam technology, 2nd edn. Hanser, Munich, 2004.

[28] Nam PH, Maiti P, Okamoto M, Kotaka T, Nakayama T, Takada M, Ohshima M, Usuki A, Hasegawa N, Okamoto H. Foam processing and cellular structure of polypropylene/clay nanocomposites, Polym. Eng. Sci. 2002;42(9): 1907-18.

[29] Bhattacharya S, Gupta RK, Jollands M, Bhattacharya SN. Foaming Behavior of High-Melt Strength Polypropylene/Clay Nanocomposites. Polym. Eng. Sci. 2009;49(10):2070-84.

[30] Lee LJ, Zeng C, Cao X, Han X, Shen J, Xu G. Polymer Nanocomposite Foams, Comp. Sci. Tech. 2005;65:2344-63.

[31] Kumar V, Nadella KV. Microcellular foams. In: Handbook of polymer foams, ed. Eaves D. Rapra Technology Limited, Shawbury, UK, 2004.

[32] Antunes M, Velasco JI, Realinho V, Solórzano E. Study of the Cellular Structure Heterogeneity and Anisotropy of Polypropylene and Polypropylene Nanocomposite Foams. Polym. Eng. and Sci. 2009;49:2400-13.

[33] Antunes M, Velasco JI, Realinho V, Martínez AB, Rodríguez-Pérez MA, de Saja JA. Heat Transfer in Polypropylene-Based Foams Produced Using Different Foaming Processes. Adv. Eng. Mater. 2009;11:811-7.

[34] Antunes M, Realinho V, Martínez AB, Solórzano E, Rodríguez-Pérez MA, Velasco JI. Heat Transfer of Mineral-Filled Polypropylene Foams, Def. Diff. Forum 2010;297-301:990-5.

[35] Yang Y, Gupta MC, Dudley KL, Lawrence RW. Novel Carbon Nanotube-Polystyrene Foam Composites for Electromagnetic Interference Shielding. Nano Lett. 2005;5(11):2131-4.

[36] Yang Y, Gupta MC, Dudley KL, Lawrence RW. Conductive Carbon Nanofiber-Polymer Foam Structures. Adv. Mater. 2005;17(16):1999-2003.

[37] Shen J, Zeng C, Lee LJ. Synthesis of Polystyrene-Carbon Nanofibers Nanocomposite Foams. Polymer 2005;46(14):5218-24.

[38] Zeng C, Hossieny N, Zhang C, Wang B. Synthesis and Processing of PMMA Carbon Nanotube Nanocomposite Foams. Polymer 2010;51(3):655-64.

[39] Shen J, Han X, Lee LJ. Nanoscaled Reinforcement of Polystyrene Foams using Carbon Nanofibers. J. Cell. Plas. 2006;42:105-26.

[40] Lee LJ, Zeng C, Cao X, Han X, Shen J, Xu G. Polymer Nanocomposite Foams. Comp. Sci. Tech. 2005;65:2344-63.

[41] Wunderlich B. Thermal Analysis. New York: Academic Press; 1990.

[42] Peeterbroeck S, Laoutid F, Taulemesse J-M, Monteverde F, López-Cuesta J-M, Nagy JB, Alexandre M, Dubois P. Mechanical Properties and Flame-Retardant Behavior of Ethylene Vinyl Acetate/High-Density Polyethylene Coated Carbon Nanotube Nanocomposites. Adv. Funct. Mater. 2007;17:2787-91.

[43] Pötschke P, Fornes TD, Paul DR. Rheological behavior of multiwalled carbon nanotube/polycarbonate composites. Polymer 2002;43(11):3247-55.

[44] Meincke O, Kaempfer D, Weickmann H, Friedrich C, Vathauer M, Warth H. Mechanical properties and electrical conductivity of carbon-nanotube filled polyamide-6 and its blends with acrylonitrile/butadiene/styrene. Polymer 2004;45(3):739-48.

[45] Sichel EK, Gittleman JI, Sheng P. In: Sichel EK, editor. Carbon Black Polymer Composites, New York; Dekker; 1982.

[46] Ryvkina N, Tchmutina I, Vilcakova J, Peliskova M, Saha P. The deformation behavior of conductivity in composites where charge carrier transport is by tunneling: theoretical modeling and experimental results. Synth. Met. 2005;148:141-6.

[47] Boettger H, Bryksin UV. In: Hopping Conduction in Solids, Berlin; Akademie Verlag; 1986 p. 108 and 148.

[48] Allaoui A, Hoa SV, Pugh MD. The electronic transport properties and microstructure of carbon nanofiber/epoxy composites. Comp. Sci. Tech. 2008;68:410-6.

[49] Linares A, Canalda JC, Cagiao ME, García-Gutiérrez MC, Nogales A, Martín-Gullón I, et al. Broad-Band Electrical Conductivity of High Density Polyethylene Nanocomposites with Carbon Nanoadditives: Multiwall Carbon Nanotubes and Carbon Nanofibers. Macromolecules 2008;41:7090-7.

[50] Dyre JC, Schroder TB. Universality of ac conduction in disordered solids. Rev. Mod. Phys. 2000;72:873-92.

[51] Gefen Y, Aharony A, Alexander S. Anomalous Diffusion on Percolating Clusters. Phys. Rev. Let. 1983;50:77-80.

[52] Laibowitz RB, Gefen Y. Dynamic scaling near the percolation threshold in thin Au films. Phys. Rev. Let. 1984;53:380-3.

[53] Song Y, Won-Noh T, Lee SI, Gaines R. Experimental study of the three-dimensional ac conductivity and dielectric constant of a conductor-insulator composite near the percolation threshold. Phys. Rev. B 1986;33:904-8.

[54] Martin JE, Hurd J. Scattering from fractals. J. Appl. Crystallogr. 1987;20:61-78.

[55] Kaye BH. A Random Walk Through Fractals. Weinheim: VCH; 1989.

[56] Ezquerra TA, Connor MT, Fernandes-Nascimento J, Kullescza M, Baltá-Calleja FJ. Alternating-current electrical properties of graphite, carbon-black and carbon-fiber polymeric composites. Compos. Sci. Technol. 2001;61:903-9.

[57] Motlagh GH, Hrymak AN, Thompson MR. Properties of a Carbon Filled Cyclic Olefin Copolymer. J. Polym. Sci.: Part B: Polym. Phys. 2007;45:1808-20.

[58] Motlagh GH, Hrymak AN, Thompson MR. Improved Through-Plane Electrical Conductivity in a Carbon-Filled Thermoplastic via Foaming. Polym. Eng. Sci. 2008;48(4):687-96.

4.6. Estudio *in-situ* de la espumabilidad de las formulaciones de base poliolefínica.

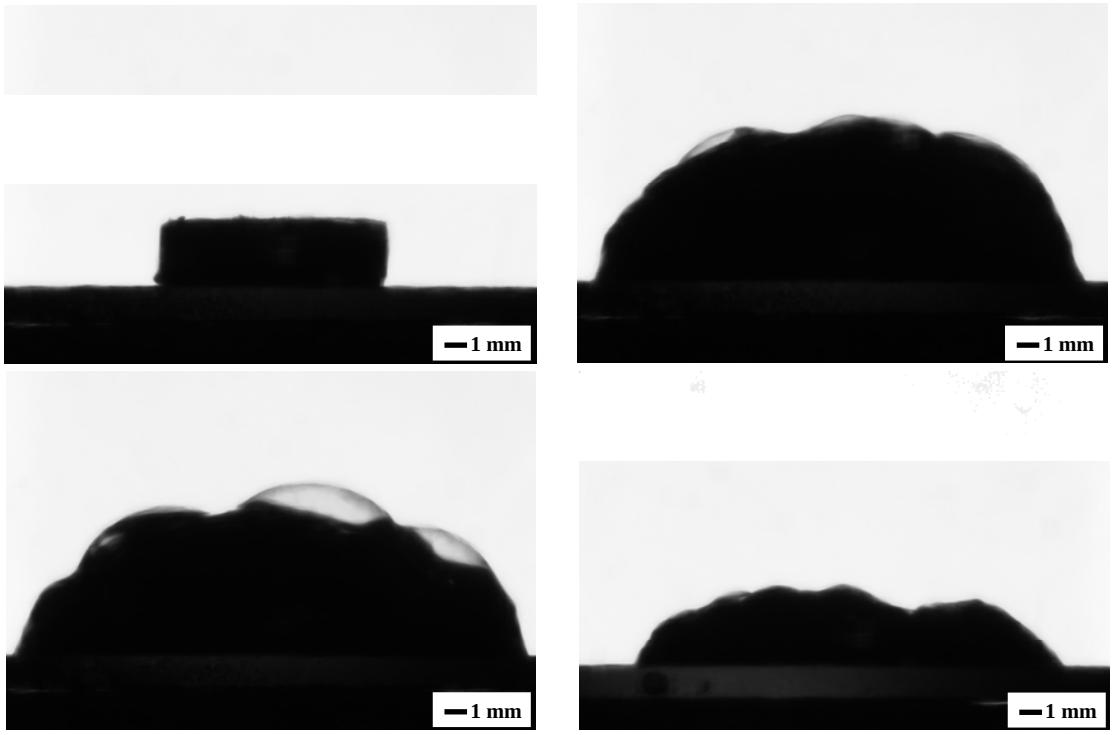

4.6.1. Justificación y objetivos.

A lo largo de los anteriores capítulos y secciones de resultados se ha podido constatar cómo las propiedades de las espumas poliméricas vienen enormemente afectadas por su estructura celular y morfología, por ello resultando esencial conocer su evolución y control. Hasta el momento la gran mayoría de trabajos dedicados a este tema se han basado en metodologías *ex-situ* empleando técnicas como la microscopía electrónica de barrido para el análisis de la estructura celular de la espuma una vez formada y estabilizada [[31]-3[3]]. Sin embargo, y de cara a poder conocer la evolución del material durante las distintas etapas de la espumación, en particular, la nucleación, expansión y estabilización, y poder controlar las mismas, ya sea regulando la formulación (reología de la matriz polimérica, cantidad y tipo de espumante, presencia de partículas, etc.) u optimizando la preparación de los precursores sólidos, se han venido desarrollando en los últimos años métodos que permiten estudiar *in-situ* el proceso de espumación. Aún así, la gran mayoría están basados en técnicas de contacto en molde cerrado, como el análisis térmico-mecánico, imposibilitando una visualización directa de la espumación del material.

De cara a establecer la puesta a punto de un nuevo método *in-situ* para el estudio de la espumabilidad de formulaciones poliméricas termoplásticas pensadas para aplicaciones de espumación y posterior metodología de análisis, en esta sección se presentan los resultados en forma de publicación a enviar titulada *A novel method to examine the foaming behaviour of thermoplastic foams*. En esta, cuyos resultados derivan del trabajo conjunto con el laboratorio *CellMat* del Departamento de Física de la Materia Condensada de la Universidad de Valladolid, se presentan las características básicas de un nuevo método basado en la visualización óptica *in-situ* de la espumación libre de precursores sólidos de poliolefinas, designado expandometría óptica, y posterior procedimiento de análisis de imagen para establecimiento de las llamadas curvas de expandometría (expansión volumétrica normalizada vs. tiempo normalizado), donde se pueden establecer las condiciones de expansión (inicio, velocidad de expansión y expansión máxima alcanzada) y posterior estabilización/colapso del material. Se demuestran con ejemplos prácticos las enormes posibilidades de esta técnica a la hora de optimizar una formulación dada de cara a su espumación, incluso dejando entrever la

posibilidad de en combinación con otras técnicas poder ser usada como técnica de caracterización *in-situ* de la evolución de la estructura celular.

4.6.2. Resumen del trabajo y conclusiones.

El nuevo método y metodología respectiva presentado en la publicación en formato para enviar titulada ***A novel method to examine the foaming behaviour of thermoplastic foams***, basado en la visualización *in-situ* por métodos ópticos del proceso de espumación, en particular de las etapas de crecimiento y estabilización/colapso, designado expandometría óptica, y posterior análisis de las imágenes obtenidas para establecimiento de las llamadas curvas de expandometría, resultó preciso a la hora de determinar la expansión volumétrica de sistemas poliolefínicos espumados por vía química.

Se compararon los resultados obtenidos y particularidades del método con otros más convencionales, en particular técnicas basadas en medidas de la expansión por análisis térmico-mecánico (TMA), demostrándose, como se puede ver en la fig. 4.6.1 después del procedimiento de normalización tanto de la expansión volumétrica como del tiempo de ensayo, ser un método fiable en lo que toca a analizar el inicio y velocidad de la etapa de crecimiento, así como expansión máxima y posterior estabilización/colapso. Asimismo, se ha concluido que presenta una serie de ventajas frente a las técnicas de contacto como el TMA, entre las que destacan: la posibilidad de medir de forma precisa la expansión volumétrica sin necesidad de molde, eliminando posibles problemas relacionados con la limitación de crecimiento en el interior de un molde, así como el contacto del plato superior del analizador de TMA usado para determinar la evolución de la expansión y posibles problemas asociados, como la adhesión del material durante la etapa de colapso, en ocasiones falseando la evolución de la expansión volumétrica post-máximo de crecimiento; eliminación de los problemas de crecimiento unidireccional relacionados con las dimensiones del molde, sobre todo en lo que toca a su expansión radial, y por tanto, posibilidad de analizar posibles anisotropías de expansión en un único experimento. Además de los resultados numéricos, al ser una técnica óptica de análisis de imagen, posibilita la visualización *in-situ* de lo que está pasando al material durante su expansión (estabilidad, coalescencia, colapso).

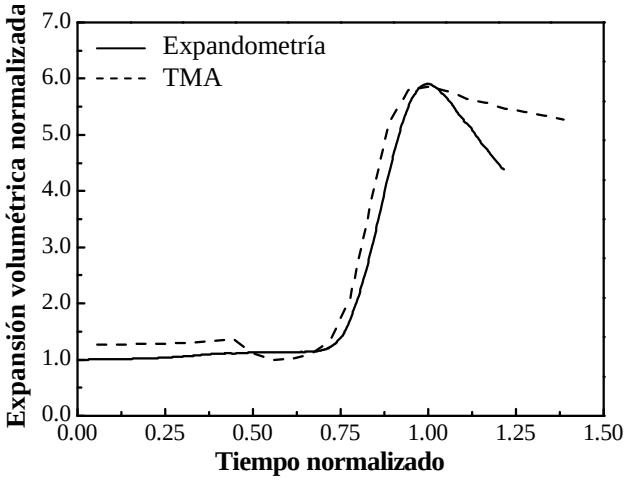

Figura 4.6.1. Comparativa entre las curvas de expansión volumétrica normalizada obtenidas por expandometría y TMA para las espumas de PP sin refuerzos.

Junto con la comparativa entre los resultados obtenidos por expandometría óptica y los de TMA, se ilustran diversos ejemplos demostrando las posibilidades de la expandometría como técnica para el estudio de la espumabilidad de diversas formulaciones de base poliolefínica. Así, esta técnica permite analizar la influencia de parámetros de espumación como la temperatura, de los componentes de la formulación (porcentaje de agente espumante y características reológicas del polímero) e incluso del procesado previo del material (como por ejemplo la etapa de mezclado de los distintos componentes de la formulación) en el comportamiento de espumación, esto es, en el inicio de la expansión, velocidad de crecimiento y máxima expansión alcanzada, y posterior estabilización/colapso celular. Por tanto, esta nueva técnica de visualización óptica del proceso de expansión y posterior estabilización/colapso aplicada a formulaciones poliolefínicas pensadas para aplicaciones de espumación y posterior metodología de tratamiento de las imágenes obtenidas, ha sido considerada muy útil como etapa preliminar al desarrollo de formulaciones poliméricas “a la carta” pensadas para las más variadas aplicaciones.

Además de las curvas de expansión recopiladas en esta publicación a enviar, demostrando con ejemplos prácticos las diversas posibilidades de esta técnica, se

presentan a continuación algunos resultados complementarios, en particular la posibilidad de empleo de esta técnica para estudiar la influencia de refuerzos nanométricos en el comportamiento de espumación de formulaciones poliméricas.

4.6.3. Resultados complementarios.

Como resultados complementarios se presentan las curvas obtenidas por expandometría para dos de los materiales espumados por compresión presentados en anteriores secciones: PP con un 5.0 phr de monmorillonita, MMT (véase sección 4.3) y PP con un 5% en peso de nanofibras de carbono, CNF (sección 4.5). Hay que tener en cuenta que estos materiales, inicialmente pensados para ser espumados químicamente por compresión, aquí fueron espumados sin aplicar presión (espumación libre), permitiendo una comparativa entre la posible influencia de añadir partículas de dimensión nanométrica de distinta geometría (laminar en el caso de la MMT y fibrilar en el caso de las nanofibras) en el comportamiento de espumación de los materiales, en particular en el inicio de la expansión (posible efecto nucleante), velocidad de expansión y expansión máxima, y etapa final de estabilización/colapso.

Así, y aunque se observen diferencias en la expansión volumétrica máxima entre los materiales sin y con MMT (véase fig. 4.6.2(a)), superior en el primer caso, las principales diferencias se aprecian en el inicio de la etapa de expansión y respectiva velocidad de crecimiento. Los nanocompuestos de PP con MMT empiezan la expansión considerablemente antes y expanden a menor velocidad (0.029 frente a una velocidad de 0.051 NVE/s para el material sin MMT, siendo NVE la expansión volumétrica normalizada), en el primer caso relacionado con el efecto de nucleación de celdas de las nanopartículas exfoliadas y en el segundo con la superior resistencia en fundido del material por efecto rigidizante local de las láminas nanométricas de arcilla (pico de expansión más ancho). Además, y de forma similar a lo que se observa en la publicación incluida referente a la importancia de las características reológicas de la matriz polimérica, por ejemplo una fracción de PP-HMS limitando el proceso de coalescencia y posterior colapso celular observado en las espumas de EPR (véase fig. 7 de la publicación), la incorporación de este refuerzo nanométrico y exfoliación parcial por espumación resultó en expansiones más suaves con menor coalescencia celular asociada, en último caso resultando en estructuras celulares más isotrópicas.

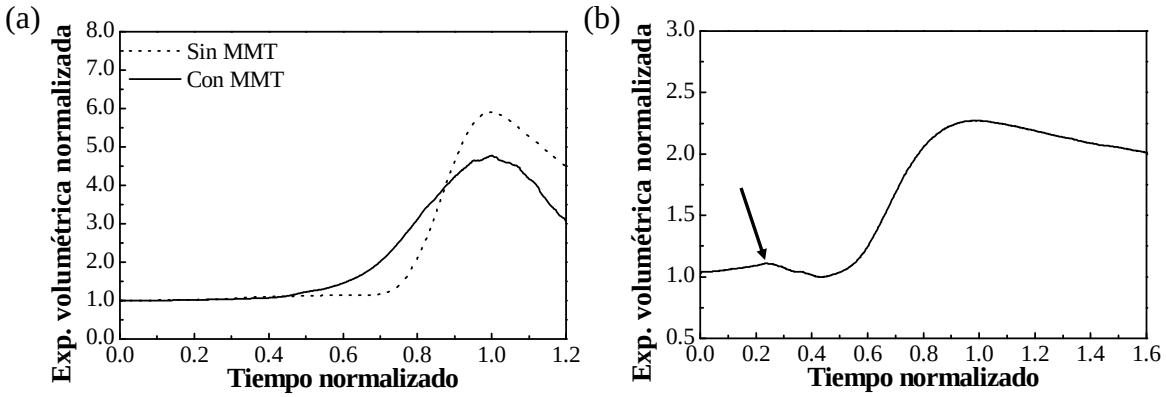

Figura 4.6.2. (a) Comparativa de la evolución de la expansión volumétrica vs. tiempo normalizado entre el PP sin y con MMT y (b) curva de expansión para el PP con un 5% en peso de nanofibras de carbono.

En el caso de la expansión libre del PP con un 5% de nanofibras de carbono se observa un comportamiento más curioso, y que radica sobre todo en la reducida expansión máxima del mismo (expansión volumétrica normalizada de aproximadamente 2.3). Además se observa una expansión ligera del material previa a su espumación, señalada con una flecha en la fig. 4.6.2(b), y que es debida a una dilatación inicial como forma de liberar las tensiones internas acumuladas durante la etapa de moldeo del precursor sólido. Por lo demás se observa un comportamiento en lo que toca tanto al inicio de la expansión como a la velocidad de crecimiento bastante parecido al de los materiales con MMT, indicando que también las nanofibras contribuyen a la nucleación de celdas y a una expansión más controlada del material. Debido a los reducidos valores de expansión volumétrica, los valores absolutos de la velocidad de expansión son considerablemente más reducidos (en torno a 0.007 NVE/s). El análisis de las imágenes obtenidas *in-situ* durante la etapa de expansión permitió constatar que tal como con la MMT, la presencia de las nanofibras limitó la coalescencia de celdas, con la particularidad de que, debido en parte a los grados de expansión más reducidos, no se observa prácticamente un colapso de la espuma una vez alcanzado el máximo de expansión.

Por tanto, y aunque se requiera un análisis más sistemático de la técnica de expandometría para el estudio de la espumación libre de diversas formulaciones pensadas para aplicaciones de espumación y optimización de la misma tanto en lo que

toca a materiales como parámetros, tanto los diversos ejemplos recopilados en la publicación indexada como las curvas presentadas en el subapartado de resultados complementarios demuestran las enormes posibilidades de esta técnica de análisis de imagen para el estudio *in-situ* de la espumación de materiales poliméricos.

4.6.4. *A novel method to examine the foaming behaviour of thermoplastic foams*.

A NOVEL METHOD TO EXAMINE THE FOAMING BEHAVIOUR OF THERMOPLASTIC FOAMS

E. Solórzano[1,*], M. Antunes[2], C. Saiz-Arroyo[1], M.A. Rodríguez-Pérez[1], J.I. Velasco[2], J.A. de Saja[1]

[1] Cellular Materials Laboratory (CellMat). Condensed Matter Physics Department, University of Valladolid, 47011 Valladolid, Spain.

[2] Centre Català del Plàstic. Universitat Politècnica de Catalunya. C/ Colom 114, E-08222 Terrassa, Barcelona, Spain.

[*] Currently at Institute of Advanced Materials., Helmholtz-Zentrum Berlin für Materialien und Energie, Glienicker Strasse 100, D-14190, Berlin, Germany.

Abstract

A novel technique to determine *in-situ* the free expansion kinetics of chemically foamed thermoplastic foams –so-called optical expandometry– is presented in this work. This technique is based on the camera monitoring of a free-foaming material placed on a furnace. Images are acquired under special illumination conditions to facilitate the later image processing. The present article explains in detail the experimental set-up and the image processing methods used to numerically determine the free volumetric expansion of different polyolefin-based materials. The results are compared with those obtained using thermo-mechanical analysis (TMA). In addition, several possible applications of this method are detailed, such as the effect of the polymer rheology, temperature and blowing agent content or even the anisotropy of the expansion due to processing on the foamability of the materials. Advantages of this method over TMA are also discussed.

Keywords: thermoplastic foams, expansion kinetics, thermo-mechanical analysis, foamability, optical expandometry.

1. Introduction

Nowadays there is an increasing demand for the development of lightweight materials with tailor-made properties. The extension of the specific properties range due to the weight reduction, alongside the less raw material requirements and thus cost reductions, as well as the easiness in adding specific characteristics through both microstructure and cellular structure control and addition of functional fillers, easily explain the great interest and promising future of cellular materials in sectors such as the automotive, aeronautical, renewable energies, construction, cushioning and packaging, biotechnology, etc. However, there is still an important lack of knowledge concerning several of the scientific and technological aspects of these materials, limiting the development of new and improved products. Particularly, the understanding of the foaming behaviour of polymeric systems is still a field in which further studies are required.

Foaming is a phenomenon in which many physical and chemical mechanisms occur simultaneously [1-3]. Cell nucleation and growth, drainage -in some particular materials- and pore coarsening mainly due to cell coalescence, play a key role during foaming. Traditionally, *ex-situ* techniques, in which the density and cellular structure of the foam are analyzed after foaming, have been considered [4-6]. In these studies, the evolution of the material during foaming is usually not measured, making it a lot harder to perform a proper analysis of the involved mechanisms and foamability of a given formulation and specific foaming parameters (temperature, time, etc.).

Due to this reason, some developments regarding the *in-situ* analysis of the foaming behaviour have appeared along the years. Different experimental challenges have to be considered if the base material is a thermoset or a thermoplastic. In the case of thermosets -usually foamed at room temperature and atmospheric pressure- the experimental set-up is commonly simpler than that needed for thermoplastic foams -usually foamed at temperatures above the melting temperature of the base polymer and in several cases under pressure-. Due to this reason and to the significant market of these materials [7], there are several research works dealing with the *in-situ* measurement of the foaming behaviour of thermoset foams. For instance, several methods have been used to the study of polyurethane foams. These include floats riding the foam’s surface [8], recording the foam height by simply using rulers [9], optical

devices [10-11] or ultrasonic sensors [12]. By far the most elegant method is based on the measurement of the buoyancy force exerted by air during the expansion [13].

In the case of thermoplastic materials, it is necessary to distinguish between foams produced at an atmospheric pressure and those produced under high pressure conditions. In the last few years some papers have been published proposing experimental set-ups for the analysis of cell nucleation in foams obtained in an autoclave reactor by a high-pressure gas dissolution process followed by pressure drop (quenching) [14-15]. On the other hand, the foamability of thermoplastics chemically foamed at atmospheric pressure has been measured using thermo-mechanical analysis methods [16-17], although foaming needed to be done inside a mould to avoid radial flow, eventually modifying the unidirectional expansion, i.e., the measured volume expansion.

Aluminium foams produced via the powder metallurgical route by incorporating a chemical blowing agent [18] are by far the materials that have been more intensively studied by these *in-situ* techniques (the term *expandometry* was actually used for the first time with these materials). Particularly, their foaming mechanisms and expansion behaviour have been deeply studied during the last 10 years by *in-situ* techniques considering the necessity that researchers had on finding potential foaming alloys and understanding the stabilization mechanisms. Initially, mechanical expandometers similar to a thermo-mechanical analyzer were used [19]. Later on these were replaced by optic contactless systems. Among others we can cite the laser beam expandometer [20] or optical expandometers based on image analysis [21]. In parallel, X-ray radioscopy was identified as a promising technique in the early 2000 considering the advantage of monitoring the internal evolution of the cellular structure, successful results being obtained using synchrotron radioscopy [22]. In the last couple of years, the resolution of X-ray synchrotron radioscopy has been greatly improved reaching ultrahigh time and spatial resolutions and providing some new data on aluminium foams [23]. Finally, we can mention that X-ray lab facilities have been built in the last years with the objective of providing a deeper knowledge on these metallic cellular materials [24].

There are several possible applications of the *in-situ* techniques to the study of the foaming behaviour of polymer-based materials. Some of them are compiled as follows:

1) Expansion kinetics: To determine the characteristic expansion rate and its onset temperature for different polymer-based foaming formulations. Considering that many polymeric foamed systems contain a thermally-activated decomposing chemical blowing agent, the expansion behaviour is expected to depend on the heating rate, maximum temperature and blowing agent content [25].
2) Maximum expansion: The material will reach a maximum that will depend on the heating rate, the blowing agent content and the polymer stability. Although these materials may be later foamed using different processes, such as compression-moulding, direct extrusion, etc., these tests may give an idea of the maximum expansion and the required heating rates to obtain the lowest possible densities for a particular formulation.
3) Collapse/stability kinetics: After reaching the maximum expansion, if the sample is maintained at a constant temperature it will eventually collapse. The inner rheological nature of the base polymer or composite, additionally influenced by crosslinking, grafting or by a secondary inorganic phase incorporation, may allow the material to reach a higher expansion and/or a slower foam decay by limiting cell coalescence and gas loss.
4) In addition, for several processing methods it is important to study the possible anisotropic expansion of precursor materials and the eventual influence of previous blending/processing conditions and/or polymer thermal treatments. As it is demonstrated in this work, under certain processing conditions it is possible to observe considerable direction-dependent expansions.

Bearing the previous ideas in mind, this investigation is focused on establishing a better and simpler technique than the existing ones (such as TMA) to follow up the free expansion of chemically foamed thermoplastics. Particularly, it introduces a testing method based on optical measurements (optical expandometry) to determine the foaming behaviour of samples at considerably high temperatures.

2. Experimental

2.1. Expandometry devices

2.1.1. Optical expandometry

An especially designed optical expandometer was built up at CellMat's Laboratory in order to measure the expansion of the several foaming samples. The system is based on an isolating plate suspended inside a 2000 W tubular infrared heating furnace. The inner furnace consists of four symmetrically-arranged curved infrared ceramic heaters and four cooling blowers (by using compressed air) symmetrically disposed at the top part. Both heating and cooling systems are designed to provide maximum temperature homogeneity. In order to allow for the visualization of the sample's expansion, two glass windows are placed at both sides of the tubular furnace. Thus the shadow image of the free-foaming sample can be acquired by setting a camera and a light source one in front of each other at both sides. A schematic drawing of the optical expandometry system is provided in fig. 1.

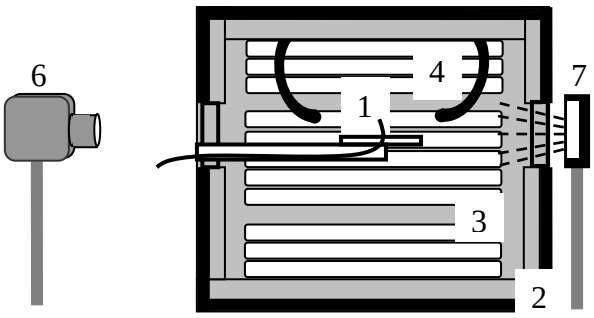

1. Suspended plate and thermocouple
2. Steel box and internal insulating layer
3. Infrared ceramic heaters
4. Cooling blowers
6. Camera
7. LED backlight

Figure 1. Schematic draw of the optical expandometer.

An IDS camera model UI-1485LE-C is employed, incorporating a high resolution lens (Kreuznach Xenoplan 2.8/50-0511). Although the theoretical spatial resolution according to the working distance and the field of view can be as low as 10 μm, the experimental value is closer to 20 μm. A LED backlight model INF-L-IBL-W 50/50 from Infaimon is used as light source, providing a homogenous bright backfield,

facilitating the subsequent image analysis. Acquisition is conventionally carried out at 8 bits pixel depth (256 grey-level) and frame rate of 1 fps.

The temperature is controlled using a PID controller with the input temperature being obtained from a thermocouple suspended inside the furnace. Temperature recording is synchronized with image capture. Heating ramps can be adjusted to a maximum rate of 40 K/min.

2.1.2. Thermal Mechanical Analysis (TMA)

Thermo-mechanical experiments were carried out in a DMA7 from Perkin Elmer in the thermal-mechanical analysis mode (TMA). The thickness (height) of the tested samples was measured as a function of temperature and time using a temperature program similar to that of the optical expandometer.

The DMA7 presents four main components: a precise linear force motor, a central core rod and measuring system assembly attached to its lower end, a high sensitivity displacement detector (LVDT) and a tubular furnace. The LVDT is the detection system of the DMA7, accurately gathering any changes in the sample's thickness. The precision of the LVDT sensor is around 2 μm. It provides high sensitivity as well as a broad dynamic range to accommodate a variety of sample sizes and geometries. The linear force motor provides precise control of all forces applied to the sample. The furnace allows the use of different temperature programs to a maximum controlled heating rate of 20 K/min. A schematic diagram of this equipment is showed in fig. 2.

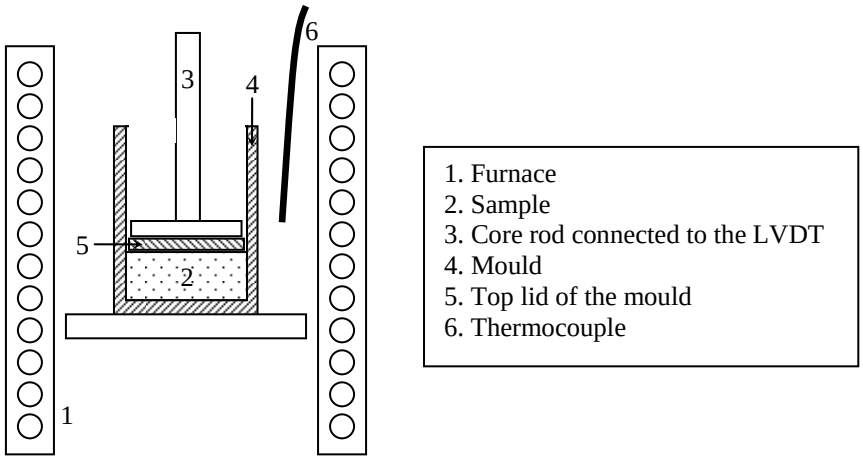

Figure 2. Schematic of the thermo-mechanical analyzer.

Foamability tests were performed in a parallel-plate (Ø=10 mm) measuring system. A cylindrical stainless-steel mould, opened in its upper part, was used, allowing the upper plate to be introduced and in permanent contact with the sample. The total height of the mould was of 14 mm, with an inner diameter of 11 mm and wall thickness of 1 mm. The mould had a metallic 1 mm-thick lid which was placed between the sample and the plate's measuring system with enough fitting tolerance to prevent any sticking during expansion.

2.2. Methodology

2.2.1. Optical Expandometry

a) Geometrical and experimental conditions

In contrast to mould-foaming (TMA), materials under free foaming do not present a well defined shape and therefore volumetric expansion calculation is not trivial. Two different approaches can be considered to accurately study the volumetric expansion of free-expanded materials by using optical techniques:

- The first one consists in measuring the expansion in two perpendicular directions by rotating the sample (or having two cameras), allowing to register both perspectives. A rotating-plate system has been previously applied with success to the study of the volumetric expansion of metal foams by some of the present authors [21]. This approach can be also carried out by doing two different tests in the two different perspectives, with the main inconvenient of requiring at least two tests for each sample and, although highly reproducible, carrying out the measurements in not exactly the same experiment.

- The second approach is based on the use of samples with a known symmetry. If a cylindrical sample is used and we assume uniform expansion in the radial direction, it is possible to extrapolate the volumetric expansion as we will explain in the subsequent section.

This second approach is the one adopted in most of the tests shown in this work, while the first one is only used for the anisotropic expansion curves (see section 3.4). Polymer disks (thickness 3 mm) were previously prepared by compression-moulding in a hot-plate press. Circular pre-forms with a typical diameter of 11 mm were directly machined from these plates and used in the foaming experiments. In addition, circular extrusion

profiles (7 mm long, 3.5 mm in diameter) were also tested to observe the influence of the geometric shape in the foaming behaviour of the materials (section 3.4).

Experiments were carried out at the maximum heating rate of the heating system in order to reduce the amount of collected images (1000 images are the equivalent to 5 Gb of collected data). Typical foaming tests were below the 1000 seconds. Therefore the temperature program used in all experiments consisted in heating, under controlled conditions, at the maximum heating rate until reaching the set-point temperature (between 190 and 215 ºC in this work) and later applying an isotherm till the foamed sample had collapsed considerably.

b) Image Analysis

After acquisition, an image analysis protocol based on the *ImageJ* software [26] was carried out in order to extract quantitative data from the image sequence. This protocol consisted in applying to each image an edge-preserving filtering to homogenize the grey level, a subsequent binarization of the region of interest and a dimensional analysis of the growing binarized foam, all by using *ImageJ* conventional tools. Among all the available numerical outputs, the ones considered in this work were the *projected area* (number of pixels) and the *minor* (*a*) and *major* (*b*) *axis of the equivalent ellipse* (ellipse with the same area). Particularly, the volume expansion was determined as:

$$V = \frac{4}{3}\pi \cdot a \cdot b^2, \tag{1}$$

under the assumptions described in section 2.2.1.a).

2.2.2. Thermal mechanical Analysis

In the case of using the commercial system DMA7 where the sample is placed inside a constant-shape cylindrical mould, data can be directly obtained without the necessity of any post-treatment, as required in optical expandometry (image analysis processing). In addition, the increase in height observed during foaming can be directly translated into volume expansion since the sample, at a first approach, can not expand in the radial

direction. Nevertheless, as it will be shown later, this last statement is not totally accurate and a minor correction is sometimes required.

Samples used in these tests were extracted from 1 mm thick plates prepared by compression-moulding in a hot-plate press. Circular pre-forms with a typical diameter of 11 mm where machined from these plates. A minimum of three experiments were carried out for each material.

The mould was previously coated with silicone oil to facilitate the later extraction of the foamed material. In addition, thanks to silicone oil, a better cap sliding is provided, limiting the chances of polymer sticking to the inner mould's surface.

Heating rate was selected as the maximum of the DMA7 under controlled conditions (20 K/min). After reaching the set-point temperature, it was held for the necessary time to study the foam's stabilization and collapse. The force applied during the foamability experiments was kept at zero [16].

2.3. Materials and compounding

Several polyolefin-based materials specifically formulated for foaming were prepared using the following base polymers: a propylene random copolymer (EPR) and a high melt strength (HMS)-based polypropylene. The melt flow index (MFI) values were of 10 dg/min and 4 dg/min, both measured at 230 ºC and 2.16 kg, respectively for the EPR and HMS-based formulations. Azodicarbonamide (ADC) was used as chemical blowing agent in amounts ranging from 1.5 to 5.0 parts per hundred of resin (phr). Stearic acid was used as lubricant.

3. Results

Results shown in this section intend to demonstrate using several examples the validity of the optical expandometry to the study of the foamability of polymeric systems. First of all, experimental results are compared with those obtained with TMA, already used for this kind of studies in previous publications [16-17]. After demonstrating the equivalency between both methods, different examples are displayed illustrating the usefulness of this technique to *in-situ* foaming characterization.

3.1. Comparison between optical and mechanical techniques

Probably the most important issue to know is whether the optical expandometry and TMA are comparable methods and/or give equivalent results. To this end, TMA experiments will be taken as reference. This task is, at first, even harder considering the different heating rates used in both techniques. On the other hand, the fact of having used different heating rates makes this comparison even more interesting.

Initially, if we compare the normalized volume expansion vs. time optical expandometer and TMA curves we can observe that they are significantly different (Fig. 3a). Maximum expansion values and peak-times, as well as growing/collapse slopes are completely different. However, it is possible to apply a time-normalization to the curves, having as a reference the time of maximum expansion. This normalization should eliminate the heating rate differences between both experiments. Actually, it is important to mention that the normalization factor is similar to the ratio of the heating rates, i.e., 2. Thus, after this normalization (Fig. 3b) both curves are more similar, the growing slopes being parallel. Nevertheless, there are still important differences between both curves regarding characteristics such as the maximum expansion. On the other hand, it can be observed that the TMA volume expansion curve presents a volume reduction before the foam starts to expand. This volume reduction comes from mould filling due to polymer melting, i.e., due to the fact that the sample-mould fitting was not perfect, so when the precursor melts just before ADC's decomposition it starts flowing radially, filling the whole available volume. Therefore it is necessary to apply a volume normalization using as a reference the minimum volume registered for both curves. This procedure only alters TMA's curve. Figure 3c shows the final compared results using both techniques. It can be observed that the maximum volume expansion is almost identical, as well as the expansion onset temperature and growing slope. Nevertheless, differences can be appreciated regarding the collapsing stage, TMA curve showing a considerably smoother decaying slope, presumably due to the friction of the material with the inner walls of the mould.

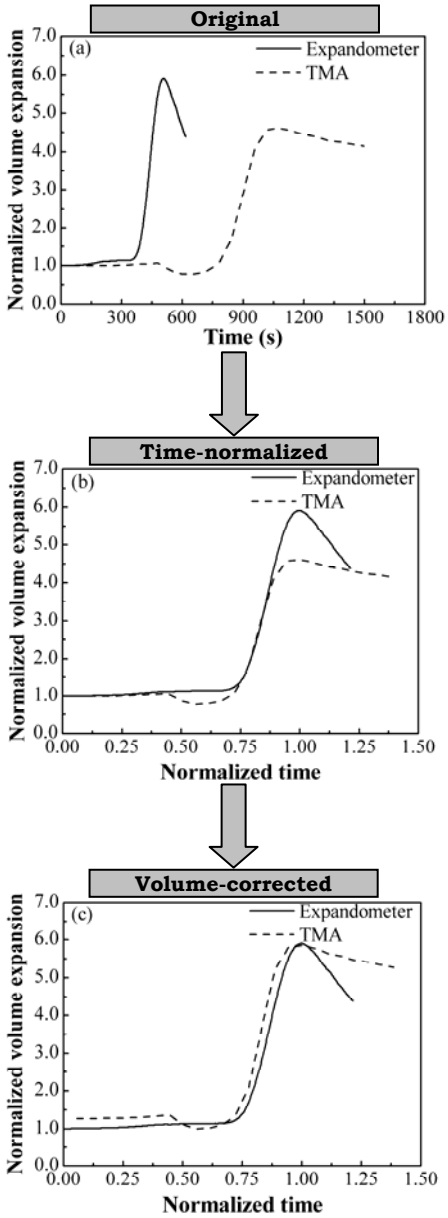

Figure 3. Curve comparison procedure using optical expandometry and TMA: (a) after volume normalization, (b) after volume and time normalizations and (c) final result after normalized volume expansion correction (PP-1.5 ADC, 205 ºC).

In this sense, the experimental expansion ratio determined for the HMS-based formulation was of 5.9, which matches very well the theoretical expected value based on the amount of azodicarbonamide gas yield (6).

It is important to mention that although the accuracy of both methods is different, results can be considered to have the same exactness since the foam expansion is nearly three orders of magnitude higher than the TMA precision.

As a main conclusion of this section it is possible to confirm that the optical expandometry technique is able to characterise the foaming behaviour of thermoplastic systems, with the main advantage of allowing a better measurement of the foam's decay due to unrestricted foaming conditions.

3.2. Influence of the foaming temperature and ADC's content

Different foaming temperatures are expected to alter the onset of expansion, foam stabilization and final collapse. This is shown in fig. 4 by comparing the expansion behaviour of an HMS-based PP formulation containing 1.5 phr of ADC (PP-1.5 ADC) at three different set-point temperatures, 205, 210 and 215 ºC. Being a thermally-activated process, the exothermal decomposition of the ADC is clearly accelerated, even for slight temperature differences. For instance, at 215 ºC, the material starts growing approximately 60 s earlier than at 205 ºC. Maximum expansion is slightly increased with increasing the temperature. It is also important to point out that the temperature is critical for the collapsing stage. For instance, in these experiments the decaying rate is of -0.015, -0.020 and -0.021 NVE/s (Normalized Volume Expansion per second), respectively for 205, 210 and 215 ºC curves, meaning that a 10 ºC temperature difference increases the collapsing speed up to a 40 %.

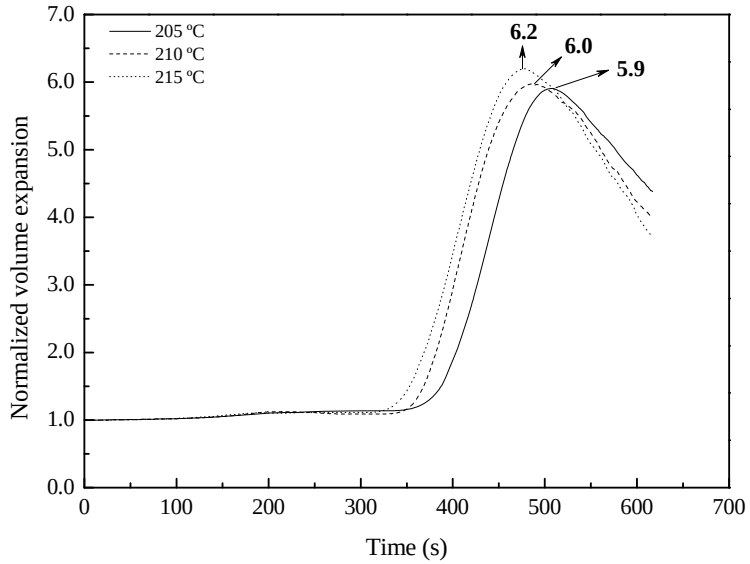

Figure 4. Optical expandometry expansion curves for PP-1.5 ADC at 205, 210 and 215 ºC.

Expandometry may also be used for optimizing the foaming formulation through controlling the amount of ADC required. Comparing the foaming behaviours of two HMS-based PP formulations containing 1.5 and 3.5 phr of the same type of ADC (fig. 5), the one with the higher concentration of ADC (PP-3.5 ADC) not only starts growing earlier (higher cell nucleation rate) but also the growing slope is steeper (0.05 and 0.12 NVE/s for 1.5 and 3.5 phr of ADC respectively), indicating a faster cell growth rate.

In accordance with the expansion, the collapse of this foam also occurs faster, as deduced from the more abrupt decreasing slope after the maximum of the curve. For this particularly case, the collapsing rate is approximately 3 times higher for the foam with the highest ADC content.

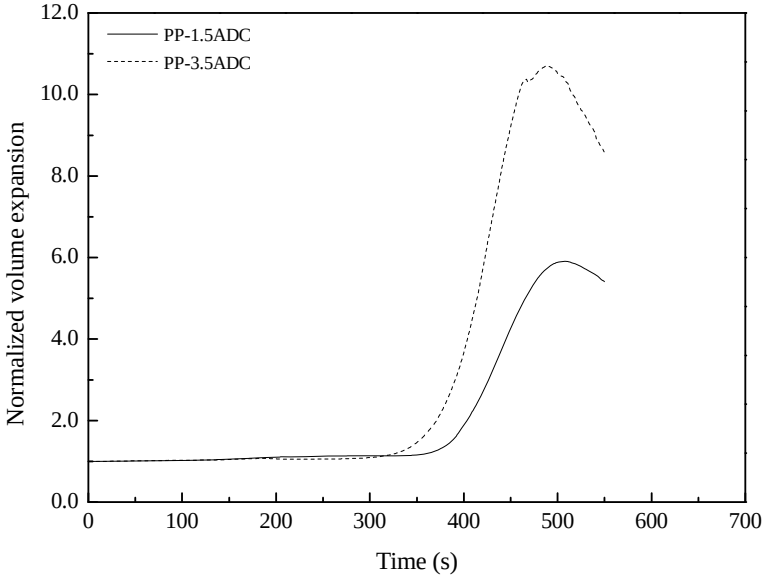

Figure 5. Optical expandometry expansion curves for the PP-1.5 ADC and PP-3.5 ADC.

3.3. Influence of the polymer rheology

If different formulations are compared, it is possible to see, among other effects, how the inner melt strength of the polymer affects the onset of expansion. As displayed in fig. 6, the growing stage starts considerably earlier for the EPR copolymer than for the HMS-based PP formulation, the higher melt strength and extensibility of the HMS blend, alongside its considerably lower melt flow index, clearly restraining the beginning of the expansion.

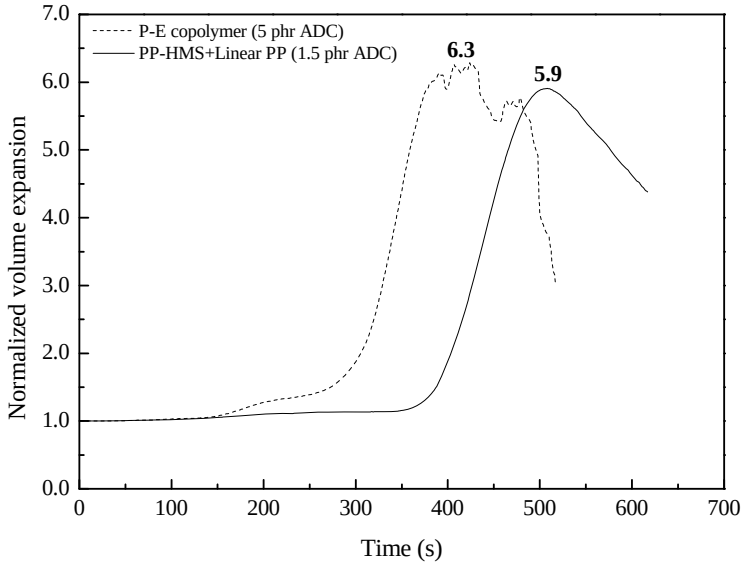

Figure 6. Compared optical expansion curves between the 5.0 phr ADC EPR copolymer and 1.5 phr ADC HMS-based formulations at a set-point temperature of 205 ºC.

Regarding the maximum expansion and expansion rate it is important to remark that although containing different concentrations of the same type of ADC (respectively 5.0 phr for EPR and 1.5 phr for HMS), the values resulted almost the same for both materials, indicating that the rheological characteristics of both base polymers are globally affecting their foamability. Actually, HMS is a special type of PP homopolymer specifically designed for foaming applications, presenting a certain degree of short chain branching that promotes a higher melt resistance and extensibility compared to more conventional linear types of polypropylenes. This is the cause why HMS reaches a similar expansion than the EPR copolymer even using more than 3 times less blowing agent. The somewhat inefficiency of EPR as a foamable system can also be appreciated in fig. 6, exhibiting a considerably less smoother expansion than HMS due to fast pore coarsening and popping. This polymeric system exhibits a considerably higher decay rate and less regular collapsing behaviour. Figure 7 provides a visual observation of the progressive coarsening and collapse of the EPR system. Note that if the surface coalesced cells are thin enough it is possible to approximately determine *in-situ* their cell size.

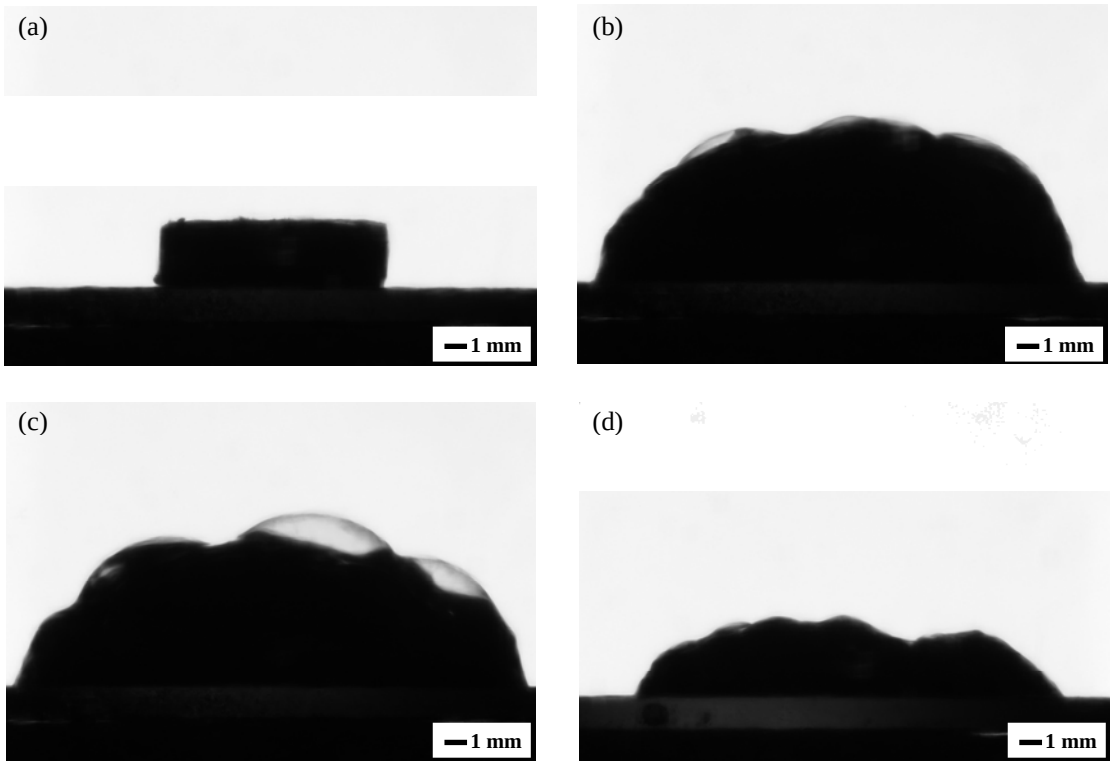

Figure 7. Optical expandometry photos taken at different times for the EPR copolymer: (a) at the beginning; (b) and (c) showing increasingly higher bubble coalescence; (d) after complete collapse.

3.4. Influence of processing on the foaming uniformity

As told in section 2, the optical expandometry technique allows to ascertain the expansion uniformity by examining two different directions during the expansion experiments. In the case of using circular extrusion profiles as pre-forms, it is possible to display how the expansion occurs in the two main directions, radial and axial, of the circular extrusion profile. Figure 8a shows the normalized expansion (NE) vs. time for the two mentioned directions. Significant differences can be assessed between both directions regarding the expansion.

Alongside the important differences that can be registered between both expansions and the visual information that can be gathered *in-situ*, it is possible to calculate the time derivative of the NE in the radial and axial directions, as depicted in fig. 8b. As it is clearly observed, the material shrinks in the axial direction and expands in the radial one during melting, related to the anisotropic crystalline orientation of the material. The

later lower expansion in both radial and axial directions is not only a consequence of the material's anisotropy but also a shape factor effect.

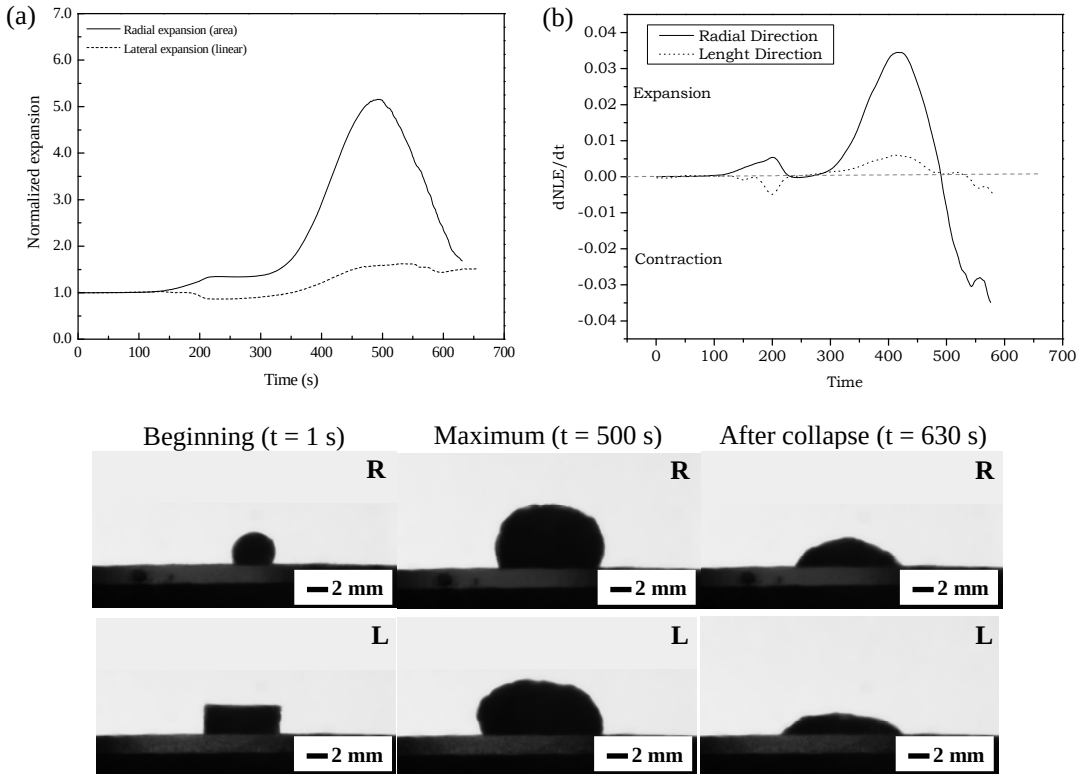

Figure 8. Radial (R) and lateral (L) optical expandometry (a) expansion curves and (b) respective derivatives for the circular extrusion profile and photos taken at the beginning (t = 1 s), maximum (t = 500 s) and after foam collapse (t = 630 s).

4. Conclusions

The novel optical method to determine foam expansion presented in this paper has been demonstrated to give precise reproducible volumetric expansion measurements of chemically foamed thermoplastic polymeric systems.

This technique has several advantages over conventional thermo-mechanical expansion techniques such as:

- Possibility of measuring an accurate volumetric expansion without the need of a mould, eliminating collateral problems that may affect the measurements.

- Since this is a non-contact method it is possible to measure the foam evolution without affecting the material's expansion and collapse. The thermal inertia of the mould is thereby eliminated.
- There is no unidirectional expansion compared to mould foaming. Therefore it is possible to appreciate multidirectional and eventually anisotropic foam expansions in one single experiment.
- It is possible to *in-situ* observe the foam's stability and cell coalescence/coarsening, i.e., apart from the numerical results some visual information can be gathered.
- Measurements can be quicker than those using TMA and although the output is not numerical the image analysis later applied can be done automatically.

In conclusion, a novel optical expandometry technique has been demonstrated to be a very helpful tool for the analysis of the foaming mechanisms of thermoplastic-based materials, ultimately enabling the development of tailor-made improved foaming formulations to be used in the most varied applications.

Acknowledgements

Financial assistance from the Local Government (Junta of Castile and Leon (Project VA047A07 and Excellence Group GR39), Spanish Ministry of Science and Education and FEDER program (project MAT2006 1614-C03-01 and postdoctoral grant 2008-0946) and project MAT2007-62956 is gratefully acknowledged.

References

[1] L.J. Gibson, M.F. Ahsby. Cellular Solids: Structure and Properties. 2nd ed. Pergamon Press, Oxford, 1998.
[2] D. Eaves. Handbook of Polymeric Foams. Rapra Technology, UK, 2004.
[3] S.T. Lee, N.S. Ramesh. Polymeric foams: mechanism and materials. Polymeric Foams Series, CRC Press, USA, 2004.
[4] M.A. Rodríguez-Pérez, J.A. de Saja. Cell Polym 1999;18:1.

[5] C.P. Park. Polyolefin Foams. In: Polymeric Foams and Foam Technology, D. Klempner, V. Sendijarevic. 2nd ed. Hanser, 2004. p. 256-258.

[6] J.A. Martínez-Díez, M.A. Rodríguez-Pérez, J.A. de Saja, L.O. Arcos y Rábago, O.A. Almanza. J Cell Plast 2001;37:21.

[7] M.A. Rodríguez-Pérez. Adv Polym Sci 2005;184:87.

[8] R. Jennings. J Cell Plas 1969;5:159.

[9] R.L. Rowton. J Cell Plas 1980;16:287.

[10] A. Van Thuyne, B.J. Zeegers. J Cell Plas 1978;14:150.

[11] Y. Jianqui, Z. Jianyaun, W. Deniong, H. Chumpu, Y. Shengkang, C. Yiou, C. Yufu, X. Ziquian, S. Jin, W.J. Yin. J Cell Plast 1990;26:39.

[12] L.D. Arteiva, C.W. Mascoko, R.D. Priester, A.K. Schrock, R.B. Turner In: Proceedings of SPI/ISOPA World Congress, 1991. p. 509.

[13] S.A. Baser, D.V. Khakhar. J Cell Plas 1993;29:280.

[14] K. Taki, T. Yanagimoto, E. Funami, M. Okamoto, M. Ohshima. Polym Eng Sci 2004;44:1004.

[15] I. Tsivintzelis, A.G. Angelopolou, C. Panaviotou. Polymer 2007;48:5928.

[16] J.I. Velasco, M. Antunes, O. Ayyad, C. Saiz-Arroyo, M.A. Rodríguez-Pérez, F. Hidalgo, J.A. de Saja. J Appl Polym Sci 2007;105:1658.

[17] J.I. Velasco, M. Antunes, O. Ayyad, J.M. López-Cuesta, P. Gaudon, C. Saiz, M.A. Rodríguez-Pérez, J.A. de Saja. Polymer 2007;48:2098.

[18] J. Banhart. Prog Mat Sci 2001;46:559.

[19] J. Banhart, P. Weigand In: J. Banhart, H. Eifert, Proc. Fraunhofer USA Symposium Metallic Foams, MIT-Verlag, Bremen, 1998. p. 13.

[20] I. Duarte, J. Banhart. Acta Mater 2000;48:2349.

[21] M.A. Rodríguez-Pérez, E. Solórzano, F. García-Moreno, J.A. de Saja In: L.P. Lefebvre, Porous Metals and Metallic Foams: Metfoam, 2007. p. 75.

[22] J. Banhart, H. Stanzick, L. Helfen, T. Baumbach. App Phys Let 2001;78:1152.

[23] A. Rack, F. Garcia-Moreno, T. Baumbach, J. Banhart. J Synch Rad 2009;16:432.

[24] F. García-Moreno, M. Fromme, J. Banhart. Adv Eng Mater 2004;6:416.

[25] H. Hurnik, Chemical Blowing Agents In: H. Zweifel, Plastics Additives Handbook, 5th ed. Hanser, 2001. p. 702-707.

[26] M.D. Abramoff, P.J. Magelhaes, S.J. Ram. Bioph Inter 2004;11:36.

4.7. Referencias.

[1] L.R. Glicksman. Heat transfer in foams. In: N.C. Hilyard, A. Cunningham, Eds. Low Density Cellular Plastics: Physical Basis of Behaviour, 1st edn. Chapman and Hall, London, UK, 1994.

[2] L.J. Gibson, M.F. Ashby. In: Cellular solids, 2nd Ed., Cambridge University Press, Cambridge, 1997, p. 285.

[3] W.M. Rohsenow, J.P. Hartnett, E.N. Ganic. Handbook of Heat Transfer Fundamentals, 2nd edn. McGraw-Hill, New York, 1985.

[4] G.W. Ball, R. Hurd, M.G. Walker, J. Cell. Plast. 1970, 66, 66.

[5] M.A. Shueltz, L.R. Glicksman, J. Cell. Plast. 1984, 20, 114.

[6] H.C. Hottel, A.F. Sarofim. Radiative Transfer. McGraw Hill, New York, 1967.

[7] R. Siegel, J.R. Howell. Thermal Radiation Heat Transfer, Hemisphere Publishing Corporation, Washington DC, 1992.

[8] J. Francl, W.D. Kingery, J. Am. Ceram. Soc. 1954, 37, 99.

[9] A.L. Loeb, J. Amer. Ceram. Soc. 1954, 37, 96.

[10] R.J.J. Williams, C.M. Aldao, Polym. Eng. Sci. 1983, 23, 32.

[11] W.J. Batty, S.D. Probert, P.W. O'Callagham, Appl. Energy, 1984, 18, 117.

[12] R. Boetes, C.J. Hoogendoorn, Proc. Int. Cent. Heat Mass. Trans. 1987, 24, 14.

[13] M.A. Rodríguez-Pérez, Propiedades Térmicas y Mecánicas de Espumas de Poliolefinas, tesis doctoral, Valladolid, 1998.

[14] O.A. Almanza, Modelización de las Propiedades Térmicas y Mecánicas en Espumas de Poliolefinas, tesis doctoral, Valladolid, 2000.

[15] M. Kaviany. Principles of Heat Transfer in Porous Media, Mechanical Engineering Series, 2nd edn. Springer, 1999.

[16] R.M. Felder, G.S. Huvard. Permeation, diffusion, and sorption of gases and vapors. In: Methods of Experimental Physics, Vol. 16: Polymers, Part C: Physical Properties, R.A. Fava, Ed. Academic Press, New York, 1980.

[17] D.H. Weinkauf, R.D. Paul. Effects of structural order on barrier properties. In: Barrier Polymers and Structures, W.J. Koros, Ed. American Chemical Society, Washington DC, 1990.

[18] A.V Nawaby, Z. Zhang. Solubility and diffusivity. In: Thermoplastic Foam Processing: Principles and Development, R. Gendron, Ed. Polymeric Foams Series, CRC Press, 2005, pp. 8-9.

[19] L.J. Lee, C. Zeng, X. Cao, X. Han, J. Shen, G. Xu, Comp. Sci. Tech. 2005, 65, 2344.

[20] [1] L.S. Birnbaum, D.F. Staskal, Environ. Health Persp. 2004, 112, 9.

[21] J. Troitzsch. In: International Plastics Flammability Handbook, Hanser Publishers, Munich, 1990, p. 22.

[22] J.Q. Wang, W.K. Chow, J. Appl. Polym. Sci. 2005, 97, 366.

[23] R.D. Patton, C.U. Pittman, L. Wang, J.R. Hill, Comp. Part A: Appl. Sci. 1999, 30, 1081.

[24] S. Wang, R. Liang, B. Wang, C. Zhang, Carbon 2009, 47, 53.

[25] E.K. Sichel. In *Carbon Black Polymer Composites*, M. Dekker, Ed., Nueva York, 1982.

[26] N. Ryvkina, I. Tchmutina, J. Vilcakova, M. Peliskova, P. Saha, Synth. Met. 2005, 148, 141.

[27] P. Pötschke, S.M. Dudkin, I. Alig, Polymer 2003, 44, 5023.

[28] P. Pötschke, M. Abdel-Goad, I. Alig, S.M. Dudkin, D. Lellinger, Polymer 2004, 45, 8863.

[29] I. Alig, S.M. Dudkin, W. Jenninger, M. Marzantowicz, Polymer 2006, 47, 1722.

[30] I. Alig, D. Lellinger, S.M. Dudkin, P. Pötschke, Polymer 2007, 48, 1020.

[31] M.A. Rodríguez-Pérez, J.A. de Saja, Cell. Polym. 1999, 18, 1.

[32] C.P. Park. Polyolefin Foams. In: Polymeric Foams and Foam Technology, D. Klempner, V. Sendijarevic, Eds., 2nd ed., Hanser, 2004, p. 256.

[33] J.A. Martínez-Díez, M.A. Rodríguez-Pérez, J.A. de Saja, L.O. Arcos y Rábago, O.A. Almanza, J. Cell. Plast. 2001, 37, 21.

Capítulo 5

Discusión, conclusiones y líneas futuras de investigación.

5.1. Discusión general.

Se discuten a continuación los resultados obtenidos en esta investigación de manera agrupada por tipo de material estudiado, particularizando en la microestructura y estructura celular, y en las relaciones existentes entre éstas y las propiedades de las espumas.

a) Espumas entrecruzadas de polietileno de baja densidad reforzado con nanopartículas de hectorita.

La incorporación de nanopartículas de hectorita a la matriz de LDPE, y su posterior entrecruzamiento y espumación resultó en la formación de estructuras celulares más isotrópicas que en las espumas sin nanopartículas a igual grado de expansión, encontrándose diferencias significativas en la estructura celular (por ejemplo una reducción del tamaño celular) al incrementar el porcentaje de hectorita de un 3 a un 7% en peso.

Los nanocompuestos celulares presentaron un comportamiento de colapso más rápido que el de las espumas sin hectorita, resultado directo de un menor grado de entrecruzamiento del LDPE.

Los resultados combinados de difracción de rayos-X (DRX) y TEM permitieron observar que la etapa de mezclado resultó en la intercalación de moléculas entre las láminas de hectorita, alcanzándose un grado de exfoliación parcial de la arcilla durante la pre-espumación, incrementándose así su eficacia.

A pesar de las diferencias microestructurales y a que como esperado la arcilla reduce la expansión volumétrica en los materiales sólidos, no se observaron diferencias muy significativas en el comportamiento de expansión térmica entre los nanocompuestos sólidos y sus respectivas espumas. El hecho se puede explicar sobre la base de que en las espumas el efecto reforzante local de las laminillas en las paredes celulares se ve compensado por el efecto de expansión del gas presente en el interior de las celdas (estructura de celda cerrada) al subir la temperatura. Asimismo, las espumas con y sin hectorita presentaron una expansión volumétrica prácticamente idéntica, con un comportamiento de colapso caracterizado por una superior caída para las espumas con arcilla.

b) Espumas de polipropileno.

Se ha mostrado la posibilidad técnica de preparar espumas rígidas no entrecruzadas en base PP de densidad media-alta para aplicaciones de tipo estructural y con características físicas adicionales de interés, como por ejemplo conducción eléctrica. Con las espumas de PP sin partículas se ha analizado la influencia del proceso de espumación sobre la estructura celular y la microestructura del polímero en las espumas, así como sus propiedades resultantes. Principalmente se ha estudiado la espumación química con ADC y la espumación física por disolución de CO_2.

En el caso de la espumación química fue posible regular la densidad relativa de las espumas a través de la concentración de ADC incorporada a la formulación, y de la relación superficie/volumen del precursor sólido. Una eficaz combinación de las características reológicas de la matriz polimérica, conteniendo una fracción de un PP de alta resistencia en fundido (PP-HMS) optimizada previamente, la proporción del agente espumante, y el ajuste de las variables de espumación (temperaturas y tiempos), resultó en una ventana óptima de espumación para la obtención de espumas rígidas de PP de celda cerrada de densidad media-alta (entre 0.42 y 0.22 g/cm^3).

Dentro de una ventana óptima de espumación se consiguieron espumas isotrópicas con grados de expansión de alrededor de 4 que se acercan a los valores teóricos basados en la cantidad de ADC, demostrando una elevada “espumabilidad” de la matriz polimérica. Para una temperatura de espumación constante, los tiempos de espumación inferiores al intervalo óptimo conducen a menores grados de expansión, mientras que tiempos mayores resultan en estructuras celulares menos finas y más heterogéneas.

La espumación física se estudió mediante un proceso de disolución de CO_2 a elevada presión, controlando las características finales del material celular (grado de expansión y estructura celular) por la caída de presión aplicada y la velocidad de la misma. De esta forma pudimos extender el estudio de la influencia de la estructura celular sobre el comportamiento de las espumas de PP a las espumas microcelulares así obtenidas. Optimizando las variables de espumación fue posible obtener espumas microcelulares isotrópicas de celda cerrada con grados de expansión comprendidos entre 1.4 y 3.0 y tamaños de celda promedio entre 50 y 100 μm, demostrándose la eficacia y posibilidades de este proceso de espumación de PP en estado semi-sólido.

Con relación al PP sólido, las espumas de PP presentaron valores del módulo de almacenamiento (*E'*) determinado a temperatura ambiente por DMTA de ≈ 200 MPa, cerca de 5 veces inferior al módulo de almacenamiento del material sólido. Comparando los valores relativos a la densidad del material (valores específicos, $E'_{esp.}$) la diferencia no es tan pronunciada (≈ 680 $MPa.cm^3.g^{-1}$, 3.5 veces inferior).

El cálculo de un parámetro de anisotropía (*S*), definido como el cociente entre los módulos de almacenamiento medidos en dos direcciones de muestra, permitió tener un conocimiento de las diferencias de comportamiento mecánico debidas a la estructura celular. Para las espumas de PP obtenidas por vía química se obtuvo un valor > 1, indicando que la ligera orientación celular en la dirección de crecimiento de la espuma influye en la respuesta mecánico-dinámica, de tal forma que las espumas presentan valores superiores del módulo de almacenamiento en la dirección del crecimiento respecto a la perpendicular.

La caracterización mecánico-dinámica de las espumas microcelulares preparadas por disolución de CO_2 demostró que las espumas presentan propiedades específicas comparables a las del material sólido de partida, con valores del módulo elástico específico de ≈ 1700 $MPa.cm^3.g^{-1}$.

Se ha obtenido un modelo empírico que relaciona las variables experimentales de caída de presión (ΔP) y por ende de presión residual final con la densidad relativa de la espuma (ρ/ρ_s):

$$\Delta P = 94.7 \times \left(\frac{\rho}{\rho_s}\right)^2 - 310.8 \times \left(\frac{\rho}{\rho_s}\right) + 215.5$$

De manera similar, se consideró el estudio de la eficacia del proceso para conseguir espumas microcelulares usando una relación de escala entre el módulo elástico de la espuma (E_s) y el módulo del sólido (*E*) a través de la densidad relativa (ρ/ρ_s). Aunque el valor del exponente que afecta a la densidad relativa resultó ligeramente superior a la unidad (n = 1.3), valor comúnmente encontrado para espumas microcelulares de celda cerrada, las espumas microcelulares aquí desarrolladas presentan propiedades mecánicas específicas comparables a las del sólido de partida:

$$E = 0.88 \times E_s \left(\frac{\rho}{\rho_s} \right)^{1.3}$$

Se realizó una completa caracterización de la conductividad térmica (λ) de éstas y de otras espumas en base PP producidas por vía química y física mediante procesos de extrusión, inyección y disolución de N_2. La conductividad térmica resultó sobre todo afectada por la densidad relativa final de la espuma. Así, cuanto más elevada es la densidad relativa, más elevado es el valor de la conductividad térmica de la espuma debido a la superior fracción de polímero. Al analizar con detalle, se observan dos ventanas de comportamiento en función de la densidad relativa, el límite encontrándose en torno a un valor de densidad relativa de 0.2, valor a partir del cual la conductividad térmica sube de forma mucho más pronunciada al incrementar la densidad relativa de la espuma.

Para densidades relativas superiores a 0.2, el proceso de espumación y por ende la estructura celular de la espuma apenas afecta al valor absoluto de la conductividad térmica, viniendo su valor determinado por la fracción de sólido y, por tanto, por la densidad relativa de la espuma. La siguiente relación de escala entre la conductividad de la espuma (λ) y la del sólido (λ_s) es la que rige el comportamiento en función de la densidad relativa (ρ/ρ_s) considerando todas las espumas analizadas:

$$\lambda = 0.95 \times \lambda_s \left(\frac{\rho}{\rho_s} \right)^{0.82}$$

Para una densidad relativa > 0.2 la conductividad térmica de la espuma depende casi linealmente con la conductividad del sólido y con la densidad relativa.

Por otra parte, tanto el modelo de Russell como la regla de las mezclas permitieron estimar de forma adecuada los valores de conductividad en este rango. Para el modelo particular de la regla de las mezclas, basado en la conductividad del sólido (λ_{sol}) y del gas (λ_{gas}) y sus respetivas fracciones volumétricas (V_{sol} y V_{gas}) y que considera en primera aproximación un valor del parámetro de tortuosidad ξ igual a 1:

$$\lambda = 0.026 + 0.25 \left(\frac{\rho}{\rho_s} \right)$$

Para densidades relativas inferiores a 0.2 los modelos propuestos estiman a la baja la conductividad térmica de la espuma. El efecto de la estructura celular es más importante en este rango por la superior fracción de gas, aunque sólo se observan efectos importantes para estructuras celulares muy distintas. Así, para densidades relativas similares, las espumas con tamaños de celda más grandes y celdas orientadas en la dirección de aplicación del flujo de calor, en particular las espumas anisotrópicas obtenidas por disolución de CO_2 ($AR \approx 9.4$), presentan una conductividad mayor (0.059 $W.m^{-1}.K^{-1}$) que las espumas más isotrópicas ($AR = 1.4$) y de menor tamaño de celda obtenidas por extrusión (0.054 $W.m^{-1}.K^{-1}$), esto es, un 12% más si se comparan los respectivos valores de la conductividad térmica normalizada.

De manera análoga a la relación de escala encontrada para el rango superior:

$$\lambda = 0.51 \times \lambda_s \left(\frac{\rho}{\rho_s} \right)^{1/3}$$

Para este rango de densidades se obtiene una relación de escala en que la conductividad térmica decrece al reducir la densidad relativa de forma mucho más suave de lo que sucedía en el rango superior. Esto se debe a la importancia creciente de la fracción de gas presente y a su reducida conductividad comparativamente con la del sólido, lo que hace que variaciones ligeras de densidad relativa apenas resulten en cambios apreciables de la conductividad del material. Asimismo, al incrementar la fracción de gas, esto es, al reducir la densidad relativa, empieza a ganar importancia el término de la radiación térmica, que contribuye a incrementar la conductividad total y por ende a acercar los valores de λ de las espumas de menor densidad. Por todo ello, la regla de las mezclas estima a la baja la conductividad térmica de estas espumas ligeras. Por lo tanto, para las espumas de PP preparadas en la presente tesis (densidad relativa > 0.2), la conductividad térmica no se ha visto afectada por el proceso de fabricación y respectivas estructuras celulares desarrolladas, siendo el valor final controlado por la fracción de gas presente.

c) Espumas de polipropileno reforzado con nanopartículas de montmorillonita.

Comparativamente con las espumas de PP sin partículas preparadas por vía química, la incorporación y dispersión de nanopartículas laminares de montmorillonita (MMT)

resultó en intervalos óptimos de espumación más amplios, resultado de una mayor resistencia del polímero fundido por efecto local de las laminillas de silicato, limitando la coalescencia y colapso celulares. Estos efectos se observaron de forma más pronunciada en las espumas más ligeras.

La incorporación de MMT resultó igualmente en estructuras celulares globalmente más isotrópicas y de menor tamaño de celda que las observadas para las espumas de PP, demostrando el efecto nucleante de celdas por parte de las nanopartículas.

La presencia de MMT contribuye a reducir la orientación preferencial del cristal α-monoclínico del PP observada tanto en el sólido sin partículas como en las espumas de PP y promueve una superior perfección cristalina en las espumas, como se demostró por DRX.

Se pudo obtener la siguiente relación entre la conductividad térmica de las espumas de PP con MMT y la conductividad del sólido de referencia y su densidad relativa:

$$\lambda = 1.0 \times \lambda_s \left(\frac{\rho}{\rho_s} \right)^{0.82}$$

Esta relación de escala prácticamente coincide con la encontrada para las espumas de PP en el rango superior de densidades (densidad relativa > 0.2), una vez más indicando que la conductividad de las espumas viene controlada por su densidad relativa.

El ajuste de los valores de la conductividad térmica frente a la densidad relativa condujo a un valor de ξ = 0.92, parámetro relacionado con la tortuosidad del sistema, al aplicar el modelo de dos fases (material compuesto sólido, λ_{comp}, y gas, λ_{gas}):

$$\lambda = 0.026 + \left(0.92 \times \lambda_{comp} - 0.026 \right) \left(\rho / \rho_s \right)$$

La presencia de las partículas de MMT no afectó significativamente el valor de conductividad térmica del nanocompuesto (0.285 $W.m^{-1}.K^{-1}$ frente a 0.26 $W.m^{-1}.K^{-1}$ para el PP). Como consecuencia, las espumas a base de nanocompuestos de PP con MMT presentan conductividades prácticamente idénticas a las espumas de PP sin

partículas de grado de expansión equivalente. Por ello, una regla de mezclas con $\xi = 1$ sirve para estimar satisfactoriamente la conductividad térmica de estas espumas.

Un modelo de tres fases, que considera un único valor del parámetro ξ asociado a una fracción sólida formada por dos fases (PP y MMT), estima los valores de conductividad de las espumas de forma prácticamente idéntica al modelo de dos fases ($\xi = 0.92$).

Con respecto al comportamiento mecánico-dinámico de las espumas de PP-MMT, aún presentando un módulo de almacenamiento similar al de las respectivas espumas de PP sin partículas para grados de expansión equivalentes (≈ 250 MPa), si se comparan los módulos de almacenamiento específicos se aprecia el efecto de refuerzo de las laminillas de MMT, con incrementos superiores al 20% (≈ 830 $MPa.cm^3.g^{-1}$ frente a 680 $MPa.cm^3.g^{-1}$).

El parámetro de anisotropía *S* resulta en un valor próximo a 1 para las espumas de PP con MMT, relacionado con una estructura celular geométricamente más regular que en las espumas de PP sin partículas, en particular con menores tamaños de celda, lo que redunda en un comportamiento mecánico similar en todas las direcciones.

Las espumas de PP-MMT presentaron valores del factor de pérdidas (tan δ) mayores que las espumas de PP sin partículas. Estas diferencias fueron relacionadas con la diferente microestructura del polímero presente en las paredes celulares en base a interacciones de éste con las laminillas del silicato y menor movilidad molecular, apreciable debido al incremento de la relajación α. Así, en lo que toca a la transición vítrea del PP, ésta se hace más definida, intensa y se desplaza hacia temperaturas superiores, incluso observándose la presencia de un doble pico a mayor temperatura, relacionado con una inmovilización adicional de la fase amorfa del PP sobre/entre las laminillas del silicato. La relajación α, que depende de la morfología cristalina, aparece también de forma más marcada, como consecuencia de un estado microestructural más inestable y sensible a las condiciones termo-mecánicas del ensayo, que resultaría por interferencia física de las nanopartículas durante la cristalización del PP en las espumas.

d) Espumas de polipropileno cargado con hidróxido de magnesio.

Las espumas preparadas a base de PP con 70% en peso de hidróxido de magnesio presentaron tamaños de celda considerablemente más pequeños (> 180 μm) que las del

50% (> 750 μm), y una estructura celular casi isotrópica (*AR* ≈ 1) e independiente del grado de expansión. Por su parte, la estructura celular de las espumas con 50% de hidróxido resultó más anisotrópica al aumentar el grado de expansión, alcanzándose valores de *AR* > 3 para las espumas de menor densidad relativa.

A nivel microestructural, las espumas con $Mg(OH)_2$, tanto si se considera la orientación de las partículas de hidróxido como la del cristal α-PP del polímero, presentan anisotropías crecientes, con una orientación preferencial en la dirección de crecimiento de la espuma al introducir superiores fracciones de gas (orientación perpendicular a la superficie). Un análisis cuantitativo de la orientación de las partículas y de los cristales de PP a partir de datos de DRX, indicó valores crecientes del parámetro de anisotropía al reducir la densidad relativa, alcanzándose valores de hasta un 60%. Se ha concluído que estas elevadas anisotropías microestructurales resultan en general de una marcada orientación preferencial de la estructura celular en estas espumas en la dirección del espesor, que orientan las partículas de $Mg(OH)_2$ preferencialmente en esa dirección, y éstas por su parte influyen en la orientación del cristal α-PP del polímero.

Con respecto al comportamiento térmico-mecánico-dinámico, tanto las espumas de PP con 50% de $Mg(OH)_2$ como las del 70% presentaron valores del módulo de almacenamiento específico a temperatura ambiente comparables al módulo específico del PP sólido, lo que indica que los elevados porcentajes de carga mineral actúan reforzando mecánicamente las espumas.

La elevada anisotropía microestructural presente en estas espumas resultó en propiedades mecánico-dinámicas dependientes de la dirección, incrementándose la diferencia entre ambas direcciones consideradas al aumentar el grado de anisotropía celular.

En estas espumas se observaron efectos interesantes en su comportamiento frente a la llama, siendo significativa la reducción en los valores de los tiempos de combustión. Esto indica un superior carácter de auto-extinción de las espumas frente a los respectivos sólidos. Aunque no se observaron incrementos significativos en los valores de LOI al incorporar un 50% de hidróxido, tanto espumas como sólidos mostraron valores similares y muy ligeramente superiores a los del PP. Los materiales con 70%, sin embargo, presentaron valores de LOI muy superiores, en particular las

espumas, con un incremento de más del 100% comparado con el PP y de más del 50% con respecto a los compuestos del 50% de $Mg(OH)_2$. Estos materiales mostraron una más rápida auto-extinción de la llama, junto a una superior consistencia de sus residuos de combustión, resultado de combinar una elevada cantidad de una fase mineral que descompone endotérmicamente con una estructura celular que permanece en parte durante la combustión y que aisla de la fuente de ignición.

En este sentido, se pudo observar una diferencia remarcable en el comportamiento de descomposición termo-oxidativa (combustión) en las dos direcciones consideradas, con las espumas con estructura celular marcadamente orientada en la dirección de crecimiento presentando mayor estabilidad térmica en esa dirección.

En lo relativo al comportamiento de estas espumas frente al flujo de calor, se obtuvieron respectivamente para las espumas con 50 y 70% de $Mg(OH)_2$, las siguientes relaciones de escala para la conductividad térmica:

$$\lambda = 0.98 \times \lambda_s \left(\frac{\rho}{\rho_s} \right)^{0.82}$$

$$\lambda = 1.0 \times \lambda_s \left(\frac{\rho}{\rho_s} \right)^{1.1}$$

Así, las espumas de ambos materiales compuestos presentaron un comportamiento frente al flujo de calor que se relaciona de forma prácticamente lineal con la conductividad térmica del compuesto sólido respectivo y con la densidad relativa.

Cabe destacar el elevado valor absoluto de la conductividad térmica obtenido para estos materiales celulares, si se compara con las conductividades de las espumas de PP de similar densidad relativa. Así, para las espumas de 50% de $Mg(OH)_2$ la conductividad térmica resulta el doble que la de las respectivas espumas de PP, incluso para una densidad relativa de 0.3, comparables a la conductividad del PP sólido. Las espumas de 70% de hidróxido tienen una conductividad térmica de aproximadamente 0.50 $W.m^{-1}.K^{-1}$, quedando demostrada así la influencia que altos porcentajes de un refuerzo mineral puede tener sobre la conductividad térmica de este tipo de espumas de PP.

Aplicando dos modelos a la conductividad térmica, uno considerando un sistema de dos fases y otro de tres fases, se obtuvieron respectivamente valores del parámetro de tortuosidad (ξ) de 0.94 y 0.98, lo que indica que la combinación de la estructura celular desarrollada y los elevados porcentajes de carga mineral hace con que la conductividad térmica se desvíe ligeramente del valor predicho por la regla de las mezclas ($\xi = 1$), demostrando la importancia que tienen la estructura celular y microestructura en la conductividad térmica de estos compuestos celulares.

Así, aunque el comportamiento global de conducción térmica de las espumas con un 50% de hidróxido pudo ser analizado considerando tanto un modelo de relación de escala como modelos basados en la conductividad de los distintos componentes, se observaron diferencias para las espumas de menor densidad relativa. Las medidas de la conductividad térmica de las componentes axial (λ_{axial}) y radial (λ_{radial}) resultaron en diferencias crecientes entre ambas al reducir la densidad relativa, como resultado de una superior anisotropía celular y microestructural, que induce orientación de las partículas paralela a la dirección axial y por ende superior conducción térmica en esa dirección. De este modo, para las espumas de menor densidad relativa se alcanzó una anisotropía térmica ($\lambda_{axial}/\lambda_{radial}$) superior a 2.5. Es de destacar que la conductividad térmica medida en modo convencional (conductividad térmica global) resulta prácticamente idéntica al promedio aritmético de las componentes axial y radial.

Por tanto, y aunque el comportamiento global de conducción térmica de las espumas de PP con hidróxido de magnesio dependa fundamentalmente de la densidad relativa, al contrario de lo que sucedía para las espumas de PP de densidad relativa > 0.2 sí que se observan efectos importantes derivados de la estructura celular y de la microestructura de la fracción sólida. La estructura celular tiene consecuencias en la generación de una orientación preferencial de las partículas de hidróxido paralelas a la dirección del crecimiento, de esa manera induciendo una superior conductividad térmica en esa dirección. Se demuestra así que, pese a que las medidas globales de conductividad de las espumas siga la tendencia típica para espumas poliméricas de densidad media-alta, la estructura celular y la microestructura desarrolladas durante la espumación condiciona sus propiedades de conducción térmica.

e) Espumas de polipropileno reforzado con nanofibras de carbono.

La incorporación de porcentajes crecientes de nanofibras de carbono (entre 5 y 20% en peso) resulta en estructuras celulares crecientemente isotrópicas y de menor tamaño de celda a igualdad de densidad relativa ($ER \approx 3$), asociado a un efecto nucleante de celdas inducido por dichas nanofibras, además de a la limitación del movimiento molecular del PP en el plano del molde.

Se ha probado que las nanofibras de carbono (CNF) inducen un incremento en la temperatura de transición vítrea y en la cristalinidad del PP, siendo estos efectos más notables al incrementar el porcentaje de las mismas en el material.

Las nanofibras de carbono contribuyen a limitar la orientación preferencial cristalina del PP tanto en los sólidos como en las espumas. Además, inducen una superior perfección cristalina en el PP al espumar.

En lo relativo a su comportamiento térmico-mecánico-dinámico, y para grados de expansión similares, las espumas de PP-CNF presentan módulos de almacenamiento absolutos crecientes con el porcentaje de nanofibras, comparables a los del PP sólido en lo que toca a valores específicos, demostrando la eficacia de estas nanofibras como refuerzo mecánico.

Tanto los nanocompuestos PP-CNF sólidos como las espumas preparadas a partir de los mismos no muestran incrementos importantes en la conductividad térmica con relación a los valores del PP, hecho que se asocia a la rotura parcial de las nanofibras durante la etapa de composición en fundido, así como a una insuficiente dispersión, necesaria para la conducción térmica. Así, se obtiene un valor prácticamente constante de la conductividad térmica para los nanocompuestos sólidos independientemente de la concentración de nanofibras de carbono: 0.3 $W.m^{-1}.K^{-1}$, indicativo de que éstas no contribuyen a mejorar la transferencia térmica. A partir de este valor constante de conductividad se encuentra una relación de escala para todas las espumas de PP con nanofibras de carbono:

$$\lambda = 1.0 \times \lambda_s \left(\frac{\rho}{\rho_s} \right)^{0.86}$$

Contrariamente a los nanocompuestos sólidos, la conductividad térmica de las espumas se vio incrementada de forma lineal, para grados de expansión similares, al

aumentar el porcentaje de nanofibras. Este comportamiento es semejante al de otros sistemas al añadir concentraciones crecientes de partículas térmicamente conductoras. Por tanto, cabe decir que la espumación induce una mejor dispersión de las nanofibras, mejorando de esa manera la eficacia de las mismas en la transmisión de calor.

El valor teórico de la conductividad térmica del nanocompuesto que se obtiene con un modelo de dos fases (ξ = 1) coincide con el valor determinado experimentalmente (0.3 $W.m^{-1}.K^{-1}$).

Aún así, para las espumas de PP-CNF el comportamiento global de conducción térmica sigue siendo regulado por la fracción de gas presente en el material, ya que las espumas presentan un comportamiento y valores de conductividad térmica semejantes al de las espumas de PP sin partículas.

En lo tocante a la conductividad eléctrica de estos materiales, se analizó la posible sinergia existente entre la estructura celular y el efecto de distintas concentraciones de nanofibras de carbono. Para concentraciones de nanofibras < 5% en peso las propiedades eléctricas de los compuestos y respectivas espumas resultaron controladas por la matriz de PP, esto es, un comportamiento marcadamente aislante, con una conductividad en torno a los 10^{-6} $S.cm^{-1}$. A porcentajes superiores sí se observó un comportamiento de conducción eléctrica, tanto en los sólidos como en las espumas. Las conductividades eléctricas alcanzadas fueron considerablemente inferiores a las esperables de una hipotética red conductora por contacto directo entre las nanofibras y del valor teórico de conductividad eléctrica de las nanofibras. Estos valores inferiores de conductividad eléctrica se explican por un mecanismo de transporte eléctrico por efecto túnel, asociado al transporte de los electrones por una nanofibra y salto a la siguiente a través de la matriz polimérica. Este mecanismo permite explicar igualmente el alcance de un valor límite para la conductividad eléctrica por encima de una concentración crítica, ya que una mayor concentración de nanofibras sube localmente la cristalinidad y por tanto disminuye la conducción eléctrica entre las nanofibras.

Es de resaltar que las espumas presentaron un valor de la concentración crítica de nanofibras para la conducción eléctrica por efecto túnel inferior al de los respectivos compuestos sólidos, indicando así un comportamiento más parecido al de un sistema formado por una red conductora de fibras dispuestas al azar, frente al de los sólidos, que se muestra más parecido al de un sistema a base de partículas esféricas conductoras.

Esta diferencia la hemos asociado con el nivel de aglomeración de las nanofibras en el material, el cuál se ve reducido en las espumas con respecto a los sólidos por el efecto de la expansión.

Se ha demostrado que la estructura celular de la espuma afecta enormemente a sus propiedades eléctricas. Así, medidas de la conductividad eléctrica realizadas en la dirección del espesor y en el plano opuesto sobre espumas altamente anisotrópicas de PP con 20% de CNF preparadas por espumación física con CO_2 demostraron que tal anisotropía celular conlleva superiores conductividades eléctricas en la dirección del espesor. Dichos valores resultan superiores a los de los sólidos y a los de las espumas preparadas químicamente por compresión. La estructura celular altamente orientada induce una reorientación de las nanofibras de carbono en la dirección de crecimiento de la espuma (perpendiculares a la superficie), de esa manera resultando en valores más elevados de la conductividad en esa dirección. Recordemos que la orientación de las nanofibras es preferencialmente paralela a la superficie en los precursores sólidos y en menor medida en las espumas obtenidas por vía química.

f) Análisis *in-situ* del proceso de espumación y optimización de formulaciones poliméricas para espumación.

Se ha aplicado la nueva técnica de expandometría óptica y se ha contribuído a poner a punto una metodología de análisis de imagen para el seguimiento del proceso de espumación química en compuestos poliolefínicos, basada en la representación de la expansión volumétrica normalizada frente al tiempo de ensayo normalizado (curvas de expandometría).

Este método presenta ventajas frente a otros sistemas de contacto empleados para el análisis *in-situ* del proceso de espumación. A saber, posibilidad de medir de forma precisa la expansión volumétrica sin necesidad de un molde, eliminando los problemas de la limitación de crecimiento en su interior, así como los derivados del contacto de la muestra con el analizador; eliminación de los problemas de crecimiento unidireccional relacionados con las dimensiones del molde; posibilidad de analizar anisotropías de expansión en un único experimento; o visualización *in-situ* de la espumación.

Con varios ejemplos se han ilustrado las posibilidades de la expandometría óptica como técnica para la determinación de la espumabilidad de formulaciones poliolefínicas: influencia de los parámetros de espumación (temperatura); importancia de los componentes de la formulación (cantidad de espumante y características reológicas de la matriz polimérica); influencia del procesado y preparación de los precursores sólidos en el comportamiento de expansión; influencia de la incorporación de partículas de dimensión micrométrica o nanométrica. En particular, se puso de manifiesto cómo la incorporación de una pequeña cantidad de partículas de MMT disminuye considerablemente el tiempo de inicio de la espumación y su velocidad de crecimiento, como consecuencia respectivamente del efecto nucleante de las celdas (menores tiempos de inicio de espumación) y del incremento local de la resistencia en fundido por efecto de las laminillas exfoliadas de silicato (pico de expansión más ancho). Aunque no tan pronunciadamente, se observó también un efecto similar en el comportamiento de espumación al incorporar nanofibras de carbono al PP.

5.2. Conclusiones.

Considerando los objetivos inicialmente planteados en esta investigación, a continuación se enumeran las conclusiones principales que se extraen de ella:

1. La incorporación de nanoarcillas y nanofibras de carbono al PP y LDPE resulta en espumas con estructuras celulares más finas e isotrópicas, y con superiores densidades celulares (> nº de celdas/cm^3), demostrando su efecto sobre la nucleación celular.

2. Las nanopartículas ejercen un efecto de refuerzo de la resistencia y/o viscosidad de la matriz polimérica en el estado fundido, ampliando así el intervalo práctico de espumación.

3. En general, las nanopartículas estudiadas limitan la orientación cristalina preferencial del PP paralela a la superficie observada en los precursores sólidos al espumar el material.

4. La incorporación de los refuerzos nanométricos resulta en espumas con superiores módulos elásticos específicos, demostrando la eficacia de los mismos como elementos de refuerzo mecánico para las espumas.

5. La incorporación de las nanopartículas resulta en espumas de PP con menor anisotropía mecánica, resultado de una estructura celular más fina y homogénea.

6. Se ha puesto a punto y optimizado un método para preparar espumas microcelulares de PP con grados de expansión de hasta 3, por disolución de CO_2 supercrítico en PP en estado semi-sólido y posterior caída de presión en una única etapa. Se obtiene una relación prácticamente lineal entre el módulo de almacenamiento de estas espumas microcelulares y el producto del módulo del sólido por la densidad relativa de la espuma, lo que demuestra la eficacia del proceso.

7. La espumación de compuestos muy cargados de PP con $Mg(OH)_2$ por vía química permite la obtención de espumas, bien con una estructura celular isotrópica y reducido tamaño de celda, o bien de espumas con una estructura celular orientada en la dirección del crecimiento, dependiendo de la composición y la densidad relativa. La anisotropía celular contribuye a "modular" la anisotropía microestructural del polímero, a través de la orientación de las partículas de $Mg(OH)_2$.

8. La conductividad térmica de las espumas de PP viene controlada por su densidad relativa, siendo su valor poco dependiente de la estructura celular. La conductividad de estas espumas (ρ > 180 kg/m^3) se puede estimar como el producto de la conductividad del sólido por la densidad relativa.

9. La incorporación de 5% de nanopartículas de MMT al PP no afecta significativamente a la conductividad térmica del sólido ni a la de las espumas, resultando su valor absoluto y relación de escala prácticamente idénticos a las de las respectivas espumas sin refuerzos.

10. Se encuentra un valor constante de la conductividad térmica de los nanocompuestos de PP con nanofibras de carbono independientemente de su concentración (entre 5 y 20%), indicativo de que éstas no contribuyen a mejorar el mecanismo de transferencia térmica en el sólido. Por el contrario, se observa un incremento lineal de conductividad térmica en las espumas para grados de expansión similares al incrementar el porcentaje de nanofibras, demostrando la eficacia de la espumación en mejorar la transferencia térmica en este tipo de materiales celulares.

11. Pese a que la conductividad térmica global de las espumas de PP con $Mg(OH)_2$ sigue la tendencia esperable para espumas de densidad media-alta, su estructura celular anisotrópica promueve una mayor conductividad térmica en la dirección de crecimiento de la espuma.

12. Las propiedades eléctricas de los compuestos y espumas con bajos porcentajes de nanofibras de carbono están controladas por el carácter aislante del PP. Sin embargo, a porcentajes superiores al 10% se observa un comportamiento de conducción eléctrica por efecto túnel. Las espumas presentan una concentración crítica de nanofibras para conducción eléctrica inferior a la de los sólidos, debido a una dispersión y/o distribución más eficaz de las mismas por efecto de la expansión.

13. La estructura celular y la microestructura del PP en las espumas PP-CNF afecta en gran medida a sus propiedades eléctricas. La anisotropía celular que se genera en las espumas producidas por disolución de CO_2 supone una reorientación parcial de las nanofibras en la dirección del crecimiento, y conlleva como resultado superiores valores de conductividad eléctrica en esa dirección.

14. Las espumas a base de compuestos de PP con $Mg(OH)_2$ muestran reducciones importantes en los tiempos de combustión respecto a los sólidos, y valores superiores de LOI, indicando una mayor auto-extinguibilidad en el material celular.

5.3. Líneas futuras de investigación.

A lo largo de esta memoria se ha podido constatar cómo el elevado número de materiales preparados y analizados, por un lado, ha permitido tener una primera visión de las posibles estrategias existentes para la producción de espumas multifuncionales rígidas a base de nanocompuestos de poliolefinas, en particular PP, pero también ha dejado abiertas muchas posibles vías de investigación. En particular, queremos destacar las siguientes:

- Futuros experimentos deberán considerar más detenidamente la influencia de los parámetros de espumación en la estructura celular de las espumas preparadas por disolución de CO_2, permitiendo establecer las mejores condiciones experimentales para la obtención de espumas rígidas de PP de densidad media-alta con estructuras celulares que se podrían decir “a la carta”, desde las espumas isotrópicas microcelulares hasta las altamente expandidas con estructuras celulares de tipo nido de abeja.

- Análisis sistemático de las condiciones idóneas de espumación para obtención de una morfología de nanopartículas exfoliadas en la espuma producida. Extensión de la espumación de estos materiales al proceso de disolución de CO_2 para el estudio de la sinergia existente entre las láminas de MMT y la espumación para preparación de espumas rígidas a base de nanocompuestos de PP con propiedades mejoradas.

- Extensión del estudio a la incorporación de otras nanopartículas de estructura laminar como los hidróxidos dobles laminares. Este tipo de arcilla se caracteriza por la flexibilidad de sus laminillas constituyentes, siendo interesante poder analizar el efecto de incorporar estructuras nanométricas laminares más flexibles en las propiedades finales de las espumas.

- Optimización de la formulación y condiciones de espumación de cara a conseguir materiales ligeros ignífugos para aplicaciones estructurales. Estudio más exhaustivo de la influencia de la anisotropía celular y orientación de las partículas de $Mg(OH)_2$ en las propiedades mecánicas, de conducción térmica y en el comportamiento

al fuego de las espumas producidas. En particular, extensión del análisis del comportamiento al fuego de estas espumas a la calorimetría de cono.

- Combinación de elevadas cantidades de cargas minerales con pequeños porcentajes de arcillas laminares nanométricas de cara a conseguir materiales celulares ignífugos en base PP. Optimización de los componentes para obtención de características ignífugas a menores porcentajes totales de carga mineral.

- Profundizar para elucidar las causas y fenomenología asociada con la presencia de una doble temperatura de transición vítrea (T_g) y de fases o poblaciones cristalinas de alta estabilidad térmica en el PP de determinadas espumas microcelulares.

- Empleo de agentes compatibilizantes para mejorar la interacción entre la matriz polimérica y las nanofibras de carbono, limitando su posible reagregación. Optimización de las condiciones de mezclado y espumación, y caracterización de las espumas resultantes, por forma a conseguir la máxima funcionalidad de las nanofibras.

- Estudio más exhaustivo de la influencia de la estructura celular, en particular de parámetros relacionados con la anisotropía geométrica y tortuosidad, en las propiedades eléctricas de las espumas.

- Influencia de las nanofibras de carbono en la pendiente de comportamiento de la conductividad eléctrica a altas frecuencias (corriente alterna, ac) para los materiales espumados.

- Optimización de las condiciones de ensayo, tanto de parámetros como de dimensiones de la muestra, y de análisis de las imágenes obtenidas, de cara a un análisis más sistemático del comportamiento de espumación de distintas formulaciones poliolefínicas por expandometría óptica. Posibilidad de acoplar otras técnicas de análisis de imagen, como la microtomografía de rayos-X para la visualización *in-situ* de la evolución de la estructura celular durante la etapa de crecimiento.

Además de las posibles líneas de trabajo asociadas a puntos concretos de cada una de las espumas producidas, hay que añadir el interés en extender el concepto de tortuosidad como parámetro relacionado con la complejidad intrínseca de estos materiales multifásicos para la modelización de las propiedades mecánicas y de transporte.

UNIVERSITAT POLITÈCNICA
DE CATALUNYA